



UNIVERSITÀ
DEGLI STUDI
DI PADOVA

Sede Amministrativa: Università degli Studi di Padova

Dipartimento di *Scienze Chimiche*, via F. Marzolo, 1 – 35131 Padova (Italia)

SCUOLA DI DOTTORATO DI RICERCA IN: SCIENZE MOLECOLARI

INDIRIZZO: SCIENZE CHIMICHE

XXVII CICLO

**MOLECULAR CATALYSIS
TOWARDS ARTIFICIAL PHOTOSYNTHESIS**

Direttore della Scuola: Ch.mo Prof. Antonino Polimeno

Supervisore: Ch.mo Dr. Andrea Sartorel

Dottoranda: Irene Bazzan

“...e mi parve che il trattare dell'utilizzazione dell'energia solare dal punto di vista fotochimico, poteva costituire argomento di generale interesse ... chè la vita e la civiltà dureranno finchè splende il sole.”

“... and I thought that exploiting sun light from a photochemical point of view, could be a general interest topic ... since life and civilization will last as long as the sun shines”

Bologna, 1912

G. Ciamician

“...<< Donna, chi cerchi? >>...la definizione stessa dell'uomo è: un essere di ricerca, con un punto di domanda piantato in fondo al cuore...”

“...<< woman, who you are looking for? >> ...indeed, the definition of human being is: a being in research, with a question mark set deep in his heart..”

Alla mia stupenda e forte mamma

Molecular catalysis towards artificial photosynthesis

Ph.D. Thesis, Irene Bazzan, Università degli studi di Padova, Italy

The 21st century is a time of unprecedented uncertainty for the energy sector: a secure, clean, continuous and equally distributed source of energy is fundamental to global economic growth and human development. Nowadays, being able to find a real substitute to fossil fuels represents a fascinating challenge. Among possible alternatives, renewable sources seems to better fit the energetic demand and solar energy is by far the largest exploitable. However, it has to be captured, converted and conveniently stored. Inspired by Nature, artificial photosynthesis is a process aimed at efficiently converting sunlight energy into alternative fuels such as hydrogen or other different reduced form of carbon. This artificial system is characterized by an articulate scheme of events, terminating with redox reactions that need to be efficiently catalysed.

The project of this thesis aims to study the development of new catalytic, molecular and Earth-abundant based systems for redox processes in artificial photosynthesis. For our goals, photo-activated systems are preferred in order to better mimic the light-driven activation in an ideal artificial device. Moreover, multi and mono metallic active sites in catalysts structure are considered, inspired by several efficient examples in literature. The work is mainly focused on water oxidation reaction, being still considered the bottleneck of artificial photosynthesis; however also preliminary studies on CO₂ reduction have been examined.

First, a Cobalt-based oxo cluster, [Co₄(μ₃-O)₄(μ-O₂CCH₃)₄(pyridine)₄] has been studied as a molecular catalyst for water oxidation in a light activated system with Ru(bpy)₃²⁺ as photosensitizer and S₂O₈²⁻ as sacrificial donor. The species has been characterized through different analytic techniques and tuning electronic substituents properties, structure-activity correlations have been investigated by cyclic voltammetry and laser flash photolysis. Moreover, a synthetic approach to modify the structure of the species has been evaluated in order to design no covalent dyads between the catalyst and the photosensitizer exploiting π-π interactions.

Other Cobalt-based species with high nuclearity and totally inorganic ligands (polyoxometalates, POMs) have been studied in water oxidation catalysis. In particular, complexes $[\text{Co}_9(\text{H}_2\text{O})_6(\text{OH})_3(\text{PW}_9\text{O}_{34})_3]^{16-}$, $[\text{Co}_6(\text{H}_2\text{O})_{30}\{\text{Co}_9\text{Cl}_2(\text{OH})_3(\text{H}_2\text{O})_9(\text{SiW}_8\text{O}_{31})_3\}]^{5-}$ and $[\{\text{Co}_4(\text{OH})_3\text{PO}_4\}_4(\text{PW}_9\text{O}_{34})_4]^{16-}$ have been investigated with laser flash photolysis and in the photo-activated system. Interesting mechanistic insights have been reached thanks to the analysis of these species.

Moreover, during the thesis work a novel single site Copper-based compound with a tetraazacyclotetradecane ligand has been proposed as water oxidation catalyst. In particular, the species has been characterized among the electrochemical system and the catalytic behaviour has been explored by means cyclic voltammetry, electrolysis and photoelectrochemical experiments. With the aim of the development of a sunlight activated water splitting device, for the first time in this thesis work a Copper molecular species has been examined in combination with light. Results seem to be preliminary interesting for further studies on azamacrocyclic Copper-based molecular species.

Finally, dealing with the catalysis of CO_2 reduction some studies have been performed with a POM-based complex, $[\text{Cu}(\text{SiW}_{11}\text{O}_{39})]^{6-}$. Cyclic voltammetry experiments have been run in order to evaluate the possible catalytic activity of the compound in CO_2 reduction.

The aim of this thesis work is to suggest a method to achieve a better understanding of the analysed topic through optimized experimental conditions and mechanistic insights.

Catalisi molecolare per fotosintesi artificiale

Tesi di dottorato, Irene Bazzan, Università degli studi di Padova, Italia

Il 21° secolo appare come un momento di enorme incertezza per il settore energetico: un'energia sicura, pulita, continua ed equamente distribuita risulta necessaria per la crescita economica e lo sviluppo della società umana. Riuscire a trovare un'adatta alternativa ai combustibili fossili costituisce una sfida affascinante per l'avanzamento scientifico. Considerando diverse possibilità, le risorse rinnovabili sembrano essere in grado di rispondere meglio alla richiesta energetica e fra queste, l'energia solare è sicuramente la più sfruttabile, però deve essere raccolta, convertita e conservata. Ispirandosi alla Natura, la fotosintesi artificiale è una soluzione in grado di convertire efficientemente l'energia derivante dalla luce solare in combustibili alternativi come idrogeno o altre forme ridotte di carbonio. Questo sistema artificiale presenta una struttura articolata di eventi, che terminano con reazioni di ossidoriduzione che necessitano un'efficiente catalisi.

All'interno del panorama descritto, questo progetto di tesi è quindi focalizzato nello sviluppo di nuovi sistemi molecolari basati su metalli abbondanti sulla superficie terrestre in grado di catalizzare processi redox coinvolti nella fotosintesi artificiale. Lo studio di sistemi foto indotti è stato privilegiato, poiché si avvicina maggiormente all'attivazione da parte della luce di un ideale sistema artificiale. Inoltre, ispirandosi ai numerosi esempi presenti in letteratura, i catalizzatori considerati sono basati su strutture con centri attivi sia multi che mono metallici. Il lavoro è maggiormente focalizzato sulla reazione di ossidazione dell'acqua, considerata ancora la problematica maggiore nel processo di fotosintesi artificiale, ma sono stati presi in considerazione anche studi preliminari per la catalisi della reazione di riduzione di CO₂.

Inizialmente, un osso cluster di Cobalto, [Co₄(μ₃-O)₄(μ-O₂CCH₃)₄(pyridine)₄] è stato esaminato come catalizzatore molecolare in un sistema foto attivato con Ru(bpy)₃²⁺ come fotosensibilizzatore e S₂O₈²⁻ come donatore sacrificale. La specie è stata caratterizzata mediante diverse tecniche analitiche e variando le proprietà elettroniche dei sostituenti, correlazioni fra la struttura e l'attività sono state investigate con voltammetria ciclica e laser flash fotolisi. Inoltre, un

approccio sintetico volto alla modifica strutturale del catalizzatore è stato valutato per progettare diadi non covalenti tra la specie stessa e il fotosensibilizzatore sfruttando interazioni $\pi-\pi$.

Altre specie ad alta nuclearità, contenenti Cobalto e con leganti totalmente inorganici (poliossometallati, POMs) sono stati valutati per la catalisi di ossidazione dell'acqua. In particolare i complessi $[\text{Co}_9(\text{H}_2\text{O})_6(\text{OH})_3(\text{PW}_9\text{O}_{34})_3]^{16-}$, $[\text{Co}_6(\text{H}_2\text{O})_{30}\{\text{Co}_9\text{Cl}_2(\text{OH})_3(\text{H}_2\text{O})_9(\text{SiW}_8\text{O}_{31})_3\}]^{5-}$ e $[\{\text{Co}_4(\text{OH})_3\text{PO}_4\}_4(\text{PW}_9\text{O}_{34})_4]^{16-}$ sono stati investigati nel sistema foto attivato e con laser flash fotolisi. Interessanti informazioni di meccanismo sono state ottenute grazie allo studio di questi composti.

Inoltre, durante il lavoro di tesi un nuovo composto basato su un unico atomo di Rame e un legante tetraazaciclotetradecano è stato proposto come catalizzatore per ossidazione dell'acqua. In particolare, la specie è stata caratterizzata nel sistema elettrochimico e la sua attività catalitica è stata valutata mediante voltammetria ciclica, elettrolisi ed esperimenti fotoelettrochimici. Con lo sguardo volto allo sviluppo di un dispositivo per *water splitting* attivato dalla luce solare, in questa tesi per la prima volta è stata esaminata una specie molecolare di Rame in combinazione con la luce. I risultati ottenuti sembrano aprire la strada a nuove linee di ricerca legate a specie molecolari di Rame con leganti macrociclici azotati.

Infine, per quanto riguarda la catalisi della reazione di riduzione di CO_2 , un complesso di Rame con legante POM è stato selezionato, $[\text{Cu}(\text{SiW}_{11}\text{O}_{39})]^{6-}$, ed esperimenti di voltammetria ciclica sono stati effettuati per valutarne l'attività catalitica.

Questo lavoro di tesi si propone di indicare un metodo di lavoro per ottenere una migliore comprensione dell'argomento trattato, attraverso l'ottimizzazione delle condizioni sperimentali e approfondimenti riguardanti il meccanismo dei processi in esame.

INDEX

| | |
|---|-----------|
| 1. CHAPTER General introduction | 1 |
| 1.1 Energy issue: a general overview | 1 |
| 1.2 Natural photosynthesis | 4 |
| 1.2.1 Water splitting | 5 |
| 1.3 A step forward: the artificial system | 7 |
| 1.4 Water oxidation and CO₂ reduction | 9 |
| 1.4.1 Water Oxidation reaction..... | 9 |
| 1.4.2 CO ₂ reduction..... | 10 |
| 1.5 Overview of common catalytic systems | 10 |
| 1.5.1 Electrochemical system..... | 11 |
| 1.5.2 Chemical agent system..... | 12 |
| 1.5.3 Photo-catalytic system..... | 13 |
| 1.5.4 Evaluation parameters for catalysts performance..... | 14 |
| 1.6 WOCs: state of the art | 15 |
| 1.6.1 Oxides as WOCs..... | 16 |
| 1.6.2 Molecular WOCs..... | 22 |
| 1.6.2.1 Ruthenium..... | 23 |
| 1.6.2.2 Iridium..... | 27 |
| 1.6.2.3 Earth abundant metals..... | 28 |
| 1.7 State of the art: CO₂ reduction catalysts | 41 |
| 1.7.1 Noble metals-based catalysts..... | 41 |
| 1.7.2 Earth-abundant catalysts..... | 42 |
| 1.8 Aim of this thesis | 44 |
| 1.9 References | 44 |
| | |
| 2. CHAPTER Cobalt molecular species | 53 |
| 2.1 Introduction | 53 |
| 2.2 A Cobalt-based cubane as WOC | 53 |
| 2.3 Structure-activity correlation | 59 |
| 2.3.1 Electrochemical potentials..... | 60 |
| 2.3.2 ET constant rate..... | 61 |
| 2.3.3 Photo induced kinetic experiments..... | 63 |
| 2.4 An open question: is cubane 1 a real molecular catalyst for water oxidation?.. | 64 |
| 2.5 Dyads photosensitizer-catalyst | 68 |
| 2.5.1 Dyads: no covalent interactions..... | 69 |
| 2.5.2 Photosensitizer-Catalyst dyads: the synthetic approach..... | 71 |
| 2.6 A brief conclusion | 74 |
| 2.7 References | 75 |

| | |
|---|------------|
| 3. CHAPTER Cobalt Polyoxommetalates as molecular WOC..... | 77 |
| 3.1 The first example of a Cobalt-based POM as molecular WOC..... | 78 |
| 3.2 High nuclearity Cobalt based polyoxometalates..... | 76 |
| 3.3 Conclusions and Perspectives..... | 85 |
| 3.4 References..... | 85 |
| 4. CHAPTER A novel Copper catalyst for Water Oxidation..... | 87 |
| 4.1 Introduction..... | 87 |
| 4.2 Results and discussion..... | 87 |
| 4.2.1 Synthesis and characterization..... | 87 |
| 4.2.2 Cyclic Voltammetry..... | 89 |
| 4.2.3 Photoelectrochemical experiments..... | 94 |
| 4.2.4 A limit of this system: stability..... | 97 |
| 4.3 Conclusions and Perspectives..... | 98 |
| 4.4 References..... | 99 |
| 5. CHAPTER Polyoxometalates in CO₂ reduction catalysis..... | 101 |
| 5.1 Introduction..... | 101 |
| 5.2 Results and Discussion..... | 101 |
| 5.3 Conclusions and Perspectives..... | 105 |
| 5.4 References..... | 106 |
| 6. CHAPTER Experimental Section..... | 107 |
| 6.1 Synthesis..... | 107 |
| 6.1.1 Synthesis of Co ₄ (μ ₃ -O) ₄ (μ-O ₂ CMe) ₄ (py) ₄ , (1)..... | 107 |
| 6.1.2 Synthesis of Co ₄ (μ ₃ -O) ₄ (μ-O ₂ CMe) ₄ (p-NC ₅ H ₄ X ₄), (1-X) (X = Me, t-Bu, OMe, Br, COOMe, CN)..... | 108 |
| 6.1.3 Synthesis of 4-(pyren-1-yl)-N-(pyridin-4-yl)butanamide and 4-(pyren-1-il)-N-(pyridin-3-yl)butanamide compounds (2_m e 2_p)..... | 112 |
| 6.1.4 Synthesis of Co ₄ (μ ₃ -O) ₄ (μ-O ₂ CCH ₃) ₄ (4-(pyren-1-yl)-N-(pyridin-4-yl)butanamide) ₄ and Co ₄ (μ ₃ -O) ₄ (μ-O ₂ CCH ₃) ₄ (4-(pyren-1-yl)-N-(pyridin-3-yl)butanamide) ₄ compounds (3_p e 3_m)..... | 113 |
| 6.1.5 Synthesis of Co ₄ (μ ₃ -O) ₄ (4-(pyren-1-yl)butanoate) ₄ (py) ₄ (4)..... | 114 |
| 6.1.6 Synthesis of [Co ₆ (H ₂ O) ₃₀ {Co ₉ Cl ₂ (OH) ₃ (H ₂ O) ₉ (SiW ₈ O ₃₁) ₃ }] ⁵⁻ (Co₁₅)..... | 115 |
| 6.1.7 Synthesis of [Cu(1,4,8,11-Tetraazacyclotetradecane)](ClO ₄) ₂ (Cu-Cyclam)..... | 116 |
| 6.2 Instrumentation..... | 116 |
| 7. CHAPTER Conclusions and Perspectives: an overview..... | 119 |

1. CHAPTER

General introduction

1.1 Energy issue: a general overview

This is a time of unprecedented uncertainty for the energy sector: a secure, reliable, affordable, clean and equitable energy supply is fundamental to global economic growth and human development and presents a real challenge. ⁽¹⁾

During the 20th century fossil fuels offered great opportunities to technological innovation and to the energetic market and they are still the most important present energy source. Even though all the success they have brought to our modern society, their exploitation caused new energetic issues.

1) During this century, humanity will face the problem of fossil fuel harmful effects, such as **pollution** that threatens human health and greenhouse gases (in particular carbon dioxide, CO₂) associated with global warming. ⁽²⁾

2) In addition, **world energy demand** is expected to increase every year: as reported by the Eurostat agency, between 2005 and 2011 global energetic consumption passed from 11 billions toe (tons of oil equivalent; about 16 TW per year) to 13 billions toe (about 20 TW per year), among which 82% was provided by fossil fuels, Fig. 1.1. In this time frame China showed an increased consumption by more than a half, while Japan, Canada, USA and EU-28 recorded lower values, due to the concurrent global financial and economic crisis. ⁽³⁾

| | Consumption (million toe) | | Analysis by energy type, 2011 (%) | | | | | |
|---------------|---------------------------|----------|-----------------------------------|----------------------------|------|----------------|----------------------|--------------------------|
| | 2005 | 2011 | Coal and lignite | Crude oil and oil products | Gas | Nuclear energy | Renewables and waste | Electricity and heat (*) |
| EU-28 | 1 833.8 | 1 706.2 | 16.8 | 35.3 | 23.5 | 13.7 | 10.8 | 0.0 |
| Argentina | 67.0 | 80.1 | 1.5 | 37.7 | 50.5 | 2.1 | 7.2 | 1.0 |
| Australia | 113.5 | 122.9 | 39.2 | 33.7 | 22.0 | 0.0 | 5.2 | 0.0 |
| Brazil | 215.3 | 270.0 | 5.7 | 40.4 | 8.5 | 1.5 | 42.7 | 1.2 |
| Canada | 272.2 | 251.8 | 7.8 | 32.5 | 33.2 | 9.7 | 18.1 | -1.2 |
| China | 1 775.7 | 2 727.7 | 68.1 | 16.2 | 4.0 | 0.8 | 10.9 | 0.0 |
| India | 539.4 | 749.4 | 43.5 | 22.1 | 6.7 | 1.2 | 26.5 | 0.1 |
| Indonesia | 179.5 | 209.0 | 15.1 | 34.7 | 16.6 | 0.0 | 33.6 | 0.0 |
| Japan | 520.5 | 461.5 | 23.3 | 44.7 | 21.7 | 5.7 | 4.6 | 0.0 |
| Mexico | 170.3 | 186.2 | 5.4 | 53.8 | 30.2 | 1.4 | 9.3 | 0.0 |
| Russia | 651.7 | 731.0 | 15.9 | 21.7 | 53.5 | 6.2 | 3.0 | -0.3 |
| Saudi Arabia | 145.54 | 187.0 | 0.0 | 62.6 | 37.4 | 0.0 | 0.0 | 0.0 |
| South Africa | 128.2 | 141.4 | 69.7 | 14.9 | 2.7 | 2.5 | 10.5 | -0.2 |
| South Korea | 210.2 | 260.4 | 30.8 | 36.0 | 16.0 | 15.5 | 1.7 | 0.0 |
| Turkey | 84.4 | 112.5 | 30.2 | 27.0 | 32.7 | 0.0 | 10.0 | 0.1 |
| United States | 2 318.9 | 2 191.2 | 21.9 | 35.9 | 26.0 | 9.8 | 6.4 | 0.1 |
| World | 11 532.0 | 13 113.4 | 28.8 | 31.5 | 21.3 | 5.1 | 13.3 | 0.0 |

(*) Gross inland consumption of electricity and heat is equal to electricity net imports.

Fig. 1.1: A table resuming the global gross inland consumption between 2005 and 2011 ⁽³⁾

3) As visible in details for 2011, the ***distribution of energy production*** doesn't match with its gross in land consumption. The energy prices and its high associated volatility have become the most critical uncertainty for energy leaders.

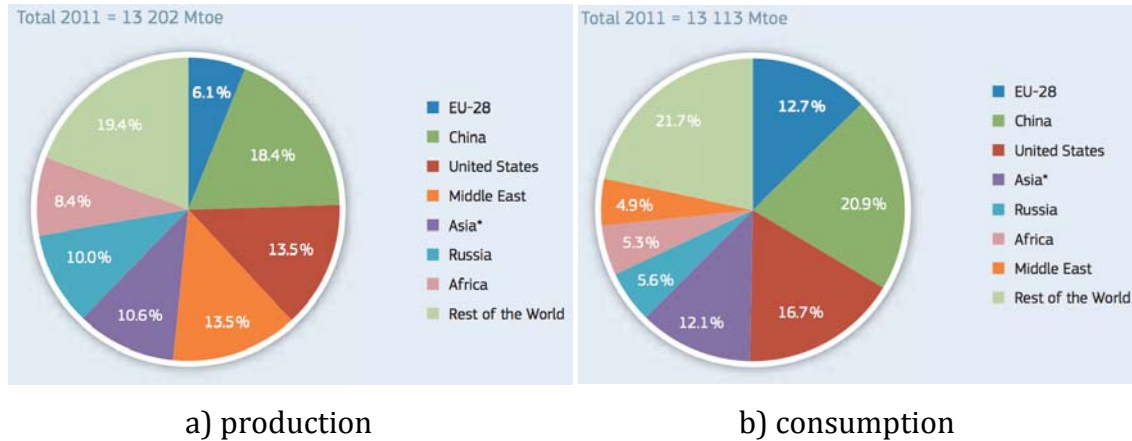
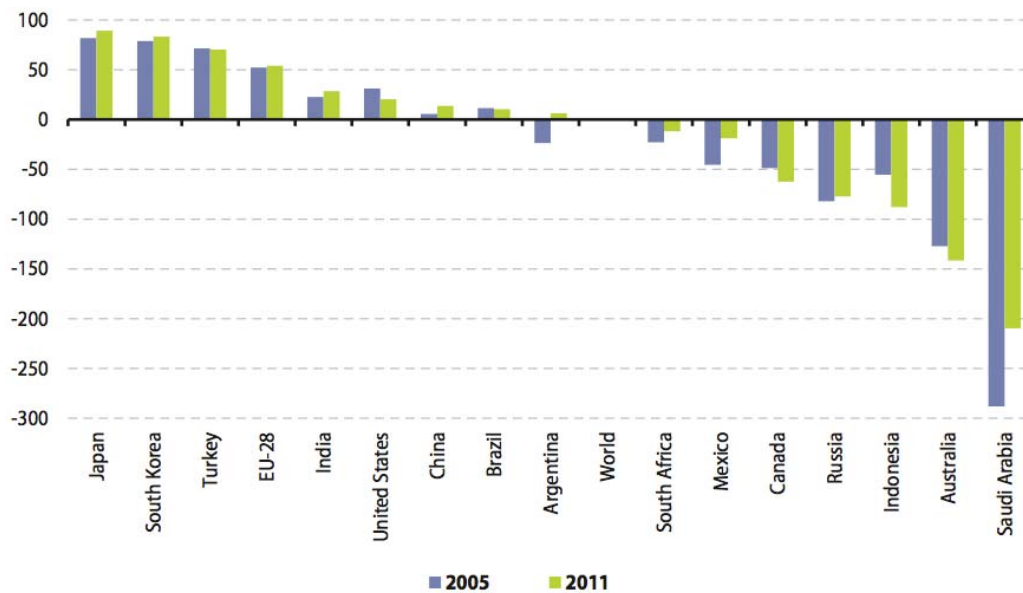


Fig. 1.2: Parallel representation in pie charts of **a)** world energy production divided by region and **b)** world gross inland consumption by region ⁽⁴⁾

In Fig. 1.3 the energy dependency indicator reveals the countries that were net exporters in the period from 2005 to 2011. Japan, South Korea, Turkey and the EU-28 had energy dependency ratios in excess of 50 % in 2011, indicating that more than half of their gross inland consumption was met by imports. Australia's net exports exceeded its consumption resulting in an energy dependency ratio that was below -100 %, while Saudi Arabia's net exports were more than twice as high as its gross inland consumption. ⁽³⁾ It is easy to conclude that this energy source distribution can let to peculiar politic and economic issues. Holding most of the energy sources, few countries nowadays have already a crucial power in global affaires.



(1) Net imports divided by the sum of gross inland energy consumption plus bunkers, expressed as a percentage.

Fig. 1.3: Comparison of different countries energy dependency between 2005 and 2011 ⁽³⁾

4) On the **fossil fuels availability**, sources are divided in two major schools of thoughts: some assure that fossil energy reserves are still present in different forms and available to supply the future energy demand for several centuries. ⁽⁶⁾ Others state that the fossil fuels reserves will not more be able to satisfy the increasing request in terms of oil and natural gas and humanity has to face the problem of found alternative energetic sources. ^(2, 5)

However, even if there are still fossil energy reserves available, without a change of direction, on timescale CO₂ anthropogenic emissions will cumulate in the atmosphere letting to climate, environmental and human health issues. ⁽⁶⁾

In a world becoming more interconnected, where new technologies foster faster innovations, we need additional investments and incentives. Not only for the growing population ⁽⁷⁾ but also for the developing countries that grow more and more energetic demand to satisfy their advancement and progress. Any long-term solution relies on the identification and exploitation of alternative energy sources, ideally abundant, cheap, clean and widespread on Earth.

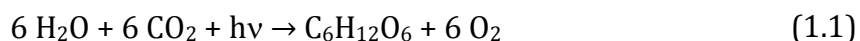
Among possible alternatives, renewable energies seem to be the most interesting approach and solar energy is by far the largest exploitable resource. The sun continuously irradiates the Earth with a huge amount of energy in form of

electromagnetic radiation equal to 1.2×10^5 TW per year, four orders of magnitude higher than the current globally required quantity. ^(8, 9)

Solar energy has an important role to play in reducing future carbon emission and ensuring a suitable energy future but since it is diffuse and intermittent it requires to be captured, converted and stored. The most attractive way to energy conversion and storage is in the form of chemical bonds as Nature has acted for million of years with photosynthesis.

1.2 Natural photosynthesis

In natural photosynthesis a complex reactions scheme converts H_2O and CO_2 in O_2 and sugars through sun light.



Even if the absorbed light by photosynthetic organism belongs to the whole visible solar radiation, the wavelengths actually used for this conversion dwells only the red region of the spectrum. The energy of two “red” photons (800 nm, energy ca 1.55 eV) ⁽¹⁰⁾ is needed for every electron/proton extraction from water and CO_2 reduction. These tasks are accomplished by two different photosystems: *i)* photosystem II (PSII) able to exploit light to permit the extraction of electrons/protons from water and *ii)* photosystem I (PSI) which uses light to provide additional energy in order to drive the CO_2 fixation process.

Natural photosynthesis shows the possibility to convert sunlight into chemical fuels; this means absorption of the light, transfer the energy and store it in the form of chemical bonds. In green plants chlorophyll and other pigments, which lie in the chloroplasts of leaves, absorb solar light, which is then efficiently transferred to the enzyme PSII. The latter is a multi subunit complex able to carry out the catalytic conversion of water into oxygen, protons and reducing electrons, the so called “water splitting reaction”. The PSII complex combines different components and it is the reaction centre where the charge separation happens. Its units are able to separate and stabilize electrons and holes produced during this initial process where the light energy is converted into an electrochemical potential. ^(8, 9) The P_{680} , a chlorophyll molecule, is turned into P_{680}^{*+} a species with a high oxidizing power, while the reducing equivalent is

transferred along an electron transport chain to PSI where it is excited by the second “red” photon absorbed. Thus, Nature is able to accumulate enough energy to drive also the fixation of CO₂ through this organized scheme.

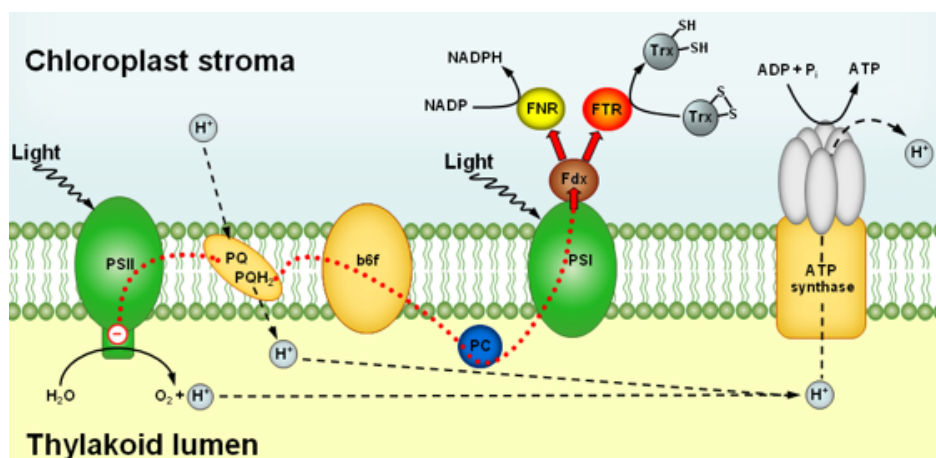


Fig. 1.4: Schematic representation of the membrane inside chloroplasts showing the four protein complexes involved in the photosynthetic light reactions among which PSII and PSI are described in this work ⁽¹¹⁾

These natural photosystems are efficient molecular photovoltaic nanomachines, since the light-driven electron/proton transfer from H₂O to CO₂ involves a great number of cofactors both in PSII and PSI proteins. ⁽⁹⁾ Natural strategy and organization could be incorporate into the design of an “artificial device”, it may be possible to develop an artificial, efficient and molecular-based solar energy converting technology. ⁽¹²⁾

1.2.1 Water splitting

Compared to other photosystems, PSII turns out to be unique for its redox skills: indeed it carries out the water splitting, which is the most appealing reaction for scientists in order to mimic nature and design an artificial device.

Therefore, many research groups ^(8, 13, 14, 15, 16, 17) have been studying the way in which Nature approaches this issue because better understanding can help developing of more appropriated bioinspired systems. In particular, the identification of PSII structural details has provided information about the involvement of supramolecular architectures with a perfect organization in spaces (Fig. 1.5), energy and time, useful for the sequential processes involved.

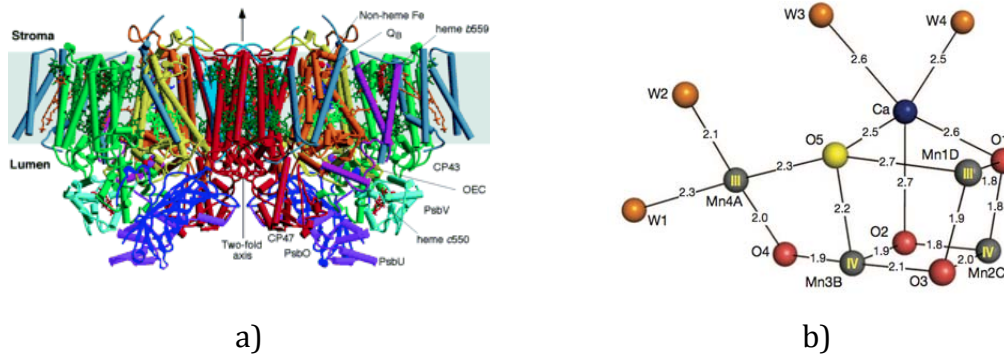


Fig. 1.5: Pictures showing **a)** PSII structure complexity, ⁽¹³⁾ **b)** OEC spatial arrangement ⁽¹⁷⁾

The major actors in natural water splitting consist in *i)* a multimer of chlorophyll, P_{680} , *ii)* a redox active tyrosine aminoacid, Tyr_Z , and *iii)* the oxygen-evolving center (OEC) a cluster with four Mn atoms and a Ca atom connected in a cubane-like structure through μ -oxo bridges (Fig. 1.5 b)). ^(16, 17)

The main events involve:

- 1) P_{680} after absorption of a photon, directly transferred by the antenna units of the chlorophyll, changes to its P_{680}^+ form, one of the most oxidizing species present in Nature, (reduction potential of ca +1.2 V vs NHE).
- 2) P_{680}^+ is then reduced by a Tyr_Z residue, forming a tyrosine based radical; as the Tyr_Z is linked with an histidine through a hydrogen bond, the oxidation of Tyr_Z and deprotonation occur at the same time, with release of the proton to the His residue.
- 3) the tyrosine radical oxidizes the OEC.
- 4) steps 1-3 are cyclically repeated four times in order to allow the OEC to reach its active state, that performs water oxidation and the release of molecular oxygen; this process is known as the Kok cycle, Fig. 1.6. ⁽¹⁸⁾ The OEC undergoes to five oxidation states, labelled S_i ($i= 0-4$), where the suffix i indicates the level of oxidation of the OEC, and S_4 being the active intermediate needed for the one-step, four-electron oxidation of water leading to oxygen evolution.

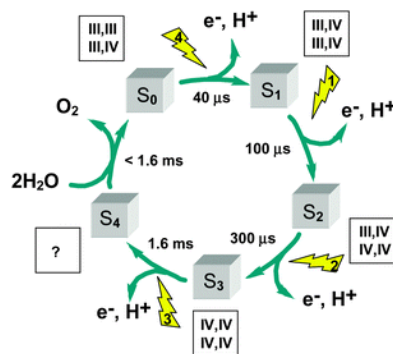


Fig. 1.6: Classical S-state cycle of photosynthetic ⁽¹⁰⁾ (Kok cycle)

The OEC has been hardly studied and the structure is now well elucidated ^(15, 16, 17, 19) in the cubane-like structure of Mn and Ca atoms and the protein entourage. It is a quite perfect result of natural evolution where the number and the setting of metal centres can be connected with the multielectron processes. However the precise natural mechanism is still quite blurred and other deeper future studies could give useful insights for the design of nature mimic devices. Moreover, the harsh oxidizing conditions under which the OEC works are quite demanding in terms of chemical resistance of the molecular components involved. To bypass the inevitable long-term oxidative degradation of organic molecules, Nature devised a strategy of continuous replacement and repair of the molecular machinery of the OEC: the catalytic centre is resynthesized every thirty minutes to compensate the self-caused oxidation damage. ⁽²⁰⁾

1.3 A step forward: the artificial system

"...the solar energy that reaches a small tropic country...is equal annually to the energy produced by the entire amount of coal mined in the world! For our purposes the fundamental problem from the technical point of view is how to fix the solar energy through suitable photochemical reactions...By using suitable catalysts, it should be possible to transform the mixture of water and carbon dioxide into oxygen and methane, or to cause other endo-energetic processes..."

(G. Ciamician, 1912)

Being inspired by Nature, we can think to an artificial system able to efficiently converting sunlight energy in alternative fuels such as hydrogen or other different reduced form of carbon (from the fixation of atmospheric CO₂): **artificial photosynthesis.**

In order to design an artificial device able to mimic natural photosynthesis, research has to consider all the functional steps involved, such as light absorption, energy transfer, electron transfer and redox catalysis with the aim to assemble them in the most efficient way.

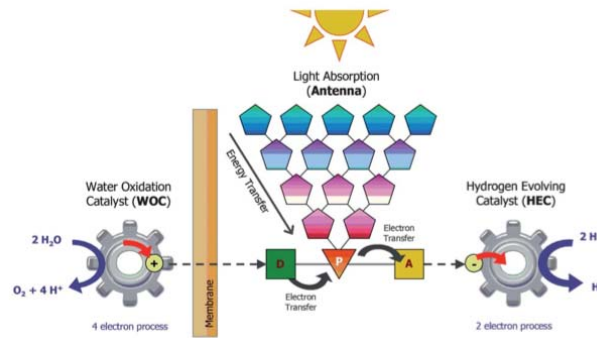
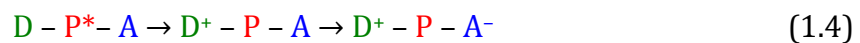
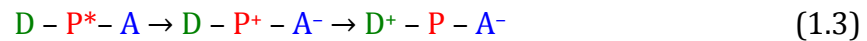
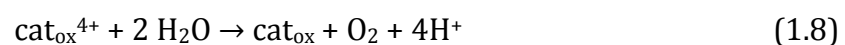


Fig. 1.7: Schematic representation of artificial photosynthesis architecture

A possible, articulate architecture of tasks with their related assembly for artificial photosynthesis is illustrated in Fig. 1.7. The first of these steps is light absorption by an antenna complex and energy transfer to a photosensitizer (**P**, Eq. 1.2). In its excited state, **P** induces an electron transfer from a suitable donor (**D**) to an acceptor (**A**), leading to an overall charge separation (Eq. 1.3-4).



Once charge separation is reached, it is important to preserve it as long as possible in order to enable electron transfer and activate the redox systems. ⁽²¹⁾ Electrons related to A^- are transferred to a reduction catalyst cat_{red} which promotes a reductive process for protons or CO_2 (Eq. 1.5-6), while holes (electrons lacks) in D^+ are transferred to an oxidation catalyst cat_{ox} able to extract electrons from water leading oxygen (Eq. 1.7-8).



Thus, the presence of good catalysts is required for both oxidation and reduction reactions: catalysts can assist the electrons and holes transfer from D/A moieties to avoid recombination, which brings to deactivation of the system. In section 1.4 the issues related to the redox reaction involving water oxidation and CO₂ reduction will be presented in more details.

1.4 Water oxidation and CO₂ reduction

As already pointed out in the section before, artificial photosynthesis is characterized by an articulate reactions scheme, terminating with redox reactions. In particular, two of them display a major interest: water oxidation and CO₂ reduction. This work will focus on the better understanding and investigation of the catalysis of such reactions. Therefore, a brief presentation of these redox reactions will be given in this section; section 1.5 will be dedicated to the analytical techniques and the parameters to evaluate catalysts; finally, in section 1.6 and 1.7 the state of the art of water oxidation and CO₂ reduction catalysts will be presented.

1.4.1 Water Oxidation

At present water oxidation is considered the bottleneck of artificial photosynthesis because it is a very complex process. It deals with issues of:

- thermodynamic: the semi reaction (Eq. 1.9) exhibits a standard potential of 1.23 V vs NHE (at pH = 0);



- kinetic: it is a complex process involving multi electrons and protons transfer with breaking bonds and formation of new ones, implying high activation barriers and slow reactions.

Therefore an ideal artificial devices tightly requires a Water Oxidation Catalyst (WOC). The WOC can be design to supply the oxidative equivalents and to

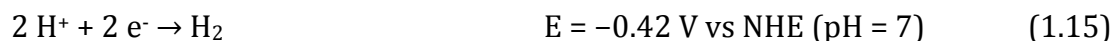
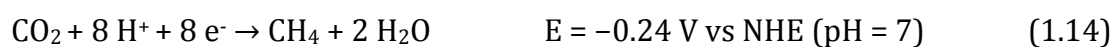
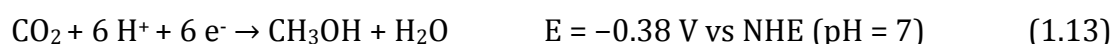
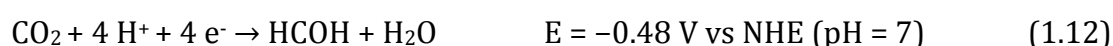
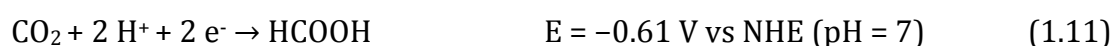
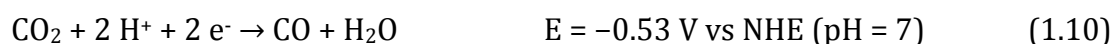
control the neutrality of charge in the system with simultaneous electron and proton transfer (PCET), requiring less energy than the usual single electron transfer.

1.4.2 CO₂ reduction

A principal issue in CO₂ reduction is that the first one-electron reduction of CO₂ to CO₂^{•-} is highly unfavourable, which occurs at a very negative potential E⁰ = -1.90 V vs NHE. ⁽²²⁾ In addition, there is a large kinetic issue for the one-electron reduction because of the structural changes that the linear CO₂ molecule has to overcome to transform in its reduction products. ⁽²³⁾

On the other hand, multi electron reductions (Eq. 1.10-14) are thermodynamically more favoured but these reactions increase the activation energy cost and usually do not take place in the absence of catalysts.

A second major issue in CO₂ reduction is its selectivity: the reduction of CO₂ may lead to CO, HCOOH, HCOH, CH₃OH, CH₄, or higher hydrocarbons (Eq. 1.10-14). Furthermore, in protic solvents, hydrogen evolution (Eq. 1.15) is often competitive and favored over CO₂ reduction. ⁽²⁴⁾



1.5 Overview of common catalytic systems

A huge amount of compounds have been considered in literature for water oxidation or CO₂ reduction catalysis, with the aim to find best components for artificial photosynthesis devices. Some of these catalysts will be introduced and described in sections 1.6 and 1.7.

In order to evaluate these species, different systems are exploited where water oxidation or CO₂ are studied separately. Although this does not exactly mimic the conditions employed in a potential artificial photosynthesis cell, using these different approaches enables rapid screening and tuning of catalysts. ⁽²⁵⁾

1.5.1 Electrochemical system

Electrochemical methods are among the most employed for screening catalysts activity. There are different useful techniques such as cyclic voltammetry (CV) and electrolysis to obtain performance catalysts parameters moreover, photo-electrochemistry, which matches the interaction of light with electrochemical systems.

CV is the most commonly employed electroanalytical technique for studying molecular electrocatalysts: at a working electrode (WE), the potential is ramped linearly versus time. Unlike linear voltammetry, after the set potential is reached in a cyclic experiment, the working electrode potential is ramped in the opposite direction to return to the starting value. The current recorded at the working electrode is plotted versus the value of the potential, reported versus a standard reference. Instead, electrolysis experiments provide an applied constant potential to a solution over time in order to record the value of the current passed at the WE and simultaneously the charge obtained during the process. Finally, during a photoelectrochemical experiment at the working electrode, a semiconductor (SC), is recorded the current due to a charge separation induced by the absorption of light among the suitable band gap of the employed SC.

The catalysts can be studied in solution or assembled onto a conducting material. The first method is simpler than the second, which requires considerable expertise and equipment, which explains the limited number of examples where catalysts have been functionalized on a conducting surface for electrochemical or photo-electrochemical H₂O oxidation and CO₂ reduction. ⁽²⁶⁾

The catalyst of interest can be assembled on the conducting surface by different methods, such as physic-sorption or covalent attachment. The functional groups that have been used for covalently interfacing the catalyst with different

conducting materials are either carboxylate ($-\text{COO}^-$) or phosphonate ($-\text{PO}_3^-$).^(27, 28)

1.5.2 Chemical agent system

Another method to evaluate the activity of potential catalysts, which is particularly exploited for water oxidation, is the employment of chemical redox agents. In particular, for testing WOCs a widely used method is the addition of an oxidant in an aqueous solution containing the metal complex. One of the oxidant prerequisite is to display a higher redox potential than the $\text{O}_2/\text{H}_2\text{O}$ couple (Eq. 1.9) and a higher redox potential than the active form of the investigated WOC.⁽²⁹⁾

A widely used oxidant in catalysts screening is ceric ammonium nitrate (CAN, $\text{Ce}(\text{NH}_4)_2(\text{NO}_3)_6$, CeIV).⁽³⁰⁾ This strong one-electron oxidant has a redox potential of about +1.70 V vs NHE⁽³¹⁾ and weak absorption in the UV-Vis region hence exploitable in various spectroscopic techniques for mechanistic studies. Moreover, it is a suitable candidate to study WOCs activity because it is commercially available and stable in aqueous acidic solutions.



However, CAN presents some disadvantages: it requires strong acidic solution ($\text{pH} < 1$), not a suitable condition for all catalysts. Furthermore, recently some studies underlined that the nitrate anion in CAN can be involved in promotion oxygen atom transfer.⁽³²⁾ CAN showed to be not innocent in the O_2 evolution mechanism because one of the oxygen atoms may originate from the nitrate instead of H_2O , precluding real water oxidation.

Potassium peroxymonosulfate (Oxone) is another powerful oxidant with +1.82 V vs NHE as oxidation potential.⁽³³⁾ Otherwise from CAN, Oxone is stable in solution up to about pH 6 and it is able to act as two-electron oxidant.^(29, 34)

WOCs activity has been analysed also with sodium periodate, NaIO_4 , a two-electron oxidant with an oxidation potential of +1.6 V vs NHE at pH 1, potentially exploitable in solutions up to neutral pH.⁽³⁵⁾

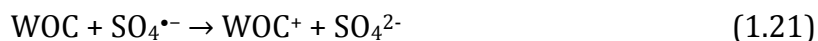
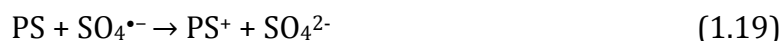
Other different peroxides have been employed to drive water oxidation, as sodium hypochlorite under alkaline conditions, ⁽²⁹⁾ although some care needs to be considered, concerning the origin of the evolved O₂ and the ambiguity of their benefit in the evaluation of a potential WOC. ⁽²⁵⁾

Among other possibilities, [Ru(bpy)₃]³⁺ has been explored as one electron oxidant. It exhibits a potential of +1.26 V vs NHE and it can run in neutral conditions. The low redox potential makes it still uncommon because it cannot permit to activate the majority of developed WOCs. Moreover, the compound is more expensive if compared with other oxidants and it slowly decomposes at pH > 4. ⁽³⁶⁾

1.5.3 Photo-catalytic system

In a photo-catalytic system, the oxidant or reducing agent is formed in situ, after light absorption by a suitable photosensitizer. A common set up foresees the involvement of a three components system: catalyst/ photosensitizer (PS)/ sacrificial electron acceptor for water oxidation, catalyst/photosensitizer (PS)/ sacrificial electron donor for CO₂ reduction. Adding a sacrificial electron acceptor for WO or donor for CO₂, this light-driven system with a multi component scheme lets to allow the catalytic cycle removing or providing electrons to the catalyst.

For WOCs screening, the photosensitizer [Ru(bpy)₃]²⁺ is largely exploited in combination with sodium persulfate (Na₂S₂O₈) as sacrificial electron acceptor. ⁽³⁷⁾ After light excitation (Eq. 1.17), this system proceeds via an oxidative quenching of the photoexcited state [Ru(bpy)₃]^{2+*} by S₂O₈²⁻ (Eq. 1.18) , to produce [Ru(bpy)₃]³⁺, sulfate, and a sulfate radical (SO₄^{•-}). The sulfate radical is a strong oxidant by itself and has sufficient potential (E° > 2.40 V vs NHE) ⁽³⁸⁾ to directly oxidize [Ru(bpy)₃]²⁺ to generate a second equivalent of [Ru(bpy)₃]³⁺ (Eq. 1.19). Four equivalents of the photogenerated [Ru(bpy)₃]³⁺, oxidizes then the WOC (Eq. 1.20) although, it is important to note that direct oxidation of the WOC by sulfate radical may occur (Eq. 1.21). After accumulation of four holes, the WOC oxidizes water (Eq. 1.22).



To ensure that the sulfate radical preferentially reacts with $[\text{Ru}(\text{bpy})_3]^{2+}$, it is vital to conduct the photocatalytic H_2O oxidation experiments with a significantly higher concentration of the photosensitizer than the WOC being studied. ^(10, 25) As an alternative to using persulfate in similar system, as electron acceptor Co^{III} has also been explored. ⁽³⁹⁾

The photoactivated cycles for CO_2 reduction operate with a similar scheme, where a sacrificial electron donor is used instead of the sacrificial electron acceptor. The sacrificial electron donors usually employed are amines, or ascorbic acid.

1.5.4 Evaluation parameters for catalysts performance

From the systems described above, several parameters describing catalyst performance can be extracted. Direct comparison between different systems is often difficult because of the large variety of experimental conditions; hence, it is very important to reports catalytic performances together with details of reaction conditions and analysis methods employed in order to more readily compare catalysts. ⁽⁴⁰⁾

Regarding electrochemical methods useful parameters to consider are:

- the *overpotential* (η): this indicates the additional potential needed to drive a redox reaction at a specific rate, beyond the thermodynamic requirement. ⁽⁴¹⁾ It is also described as the difference between the applied potential and the standard potential for the examined reaction.
- the *turnover frequency* (TOF) ⁽⁴²⁾ is the number of moles of product evolved per unit of time per mole of catalyst, and quantifies the rate of catalytic activity. In electrochemical experiments the TOF depends on the

applied potential, while recently the TOF_0 , defined as the TOF extrapolated at overpotential = 0, has been proposed as universal parameter to compare different catalysts. ⁽⁴³⁾

- the *Faradaic efficiency* in bulk electrolysis, is defined as the ratio between the moles of product and the total charge transferred at the electrode, multiplied by the number of electrons involved in the reaction.

Concerning homogeneous solution systems (oxidant agent and photo-activated systems) the parameters more evaluated are:

- the *turnover number* (TON) refers to the ratio between the moles of the product per mole of catalyst used.
- the *TOF* is the number of TON per time.
- the *chemical yield* is obtained by the ratio between moles of product and moles of sacrificial agent. This parameter is useful since the quantity of this species is limiting for the whole efficiency of the system.
- the electron-transfer rate constant, in particular for water oxidation the *constant rate of hole scavenging* between the active photosensitizer and the catalyst. This is an important parameter affecting the total light-driven system, the faster is the electron transfer the higher efficiency and stability.
- the *quantum yield* is the ratio between the molar concentration of the products and the photons flux

1.6 WOCs: state of the art

Water oxidation requires the removal of four electrons from two water molecules, and rearrangement of bonds, breaking the four O-H bonds and forming a O-O bond: these tasks are definitely not easily accomplished. The high activation barrier requires the involvement of catalysts capable of accumulating four oxidizing equivalents and ideally operating close to the thermodynamic potential of H₂O oxidation. An ideal WOC should be fast, amenable to interfacing with photosensitizing materials, and stable to oxidative, hydrolytic, and thermal

degradation during turnover. ⁽⁴⁴⁾ The search for novel and improved WOCs has led to the development of a number of homogeneous and heterogeneous WOCs. In fact, it is possible to classify two different families of WOCs: *i)* heterogeneous systems (usually derivatives of metal oxides), which provide low cost and easy synthesis process and *ii)* homogeneous, molecular catalysts, which enhance the activity and allow deeper mechanistic understanding. Since this work will deal with molecular WOCs, the state-of-the-art for this class of catalyst will be presented in detail; heterogeneous catalysts, such as metal oxide-based WOCs will be also briefly introduced in section 1.6.1.

1.6.1 Oxides as WOCs

Even if this work will not concern heterogeneous matter, the state of the art of metal oxides will be briefly describe since literature reports several examples of such catalytic species for water oxidation.

In particular, Iridium and Ruthenium oxides (IrO_2 and RuO_2) represent so far the most efficient species in this field. Moreover, their performances have been improved within nanoparticles system in order to maximize the active surface and therefore the efficiency. ^(45, 46)

Iridium: Nowadays, some remarkable examples for light-induced water oxidation system are present: a combination of citrate stabilized IrO_2 colloids with $\text{Ru}(\text{bpy})_3^{2+}$ in aqueous buffer at $\text{pH} = 5$ reached the value of $\text{TON} = 100$. ⁽⁴⁷⁾ Afterwards, the polymerization of the sensitizer promoted the heterogeneity of the system yielding to a $\text{TOF} = 160 \text{ s}^{-1}$ per surface of Iridium atom. ^(48, 49) Further improvements have been obtained reducing the dimensions of colloids and promoting electron transfer in a covalently assembled sensitizer-catalyst system. ⁽⁵⁰⁾ Indeed, ET from catalyst Ir^{IV} to Ru^{III} sensitizer occurred with a first rate constant of $8 \times 10^2 \text{ s}^{-1}$ with O_2 releasing.

These achievements gave the access to the developement of a photoelectrochemical cell for water splitting using low applied voltage. ⁽⁵¹⁾ In such system, Fig. 1.8, IrO_2 nanoparticles are covalently bound to a nanostructured TiO_2 film, through a Ru^{II} bipyridine derivative used as dye.

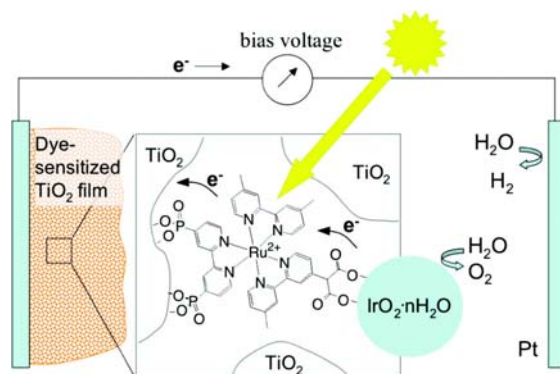


Fig. 1.8: Pictures showing a schematic representation of the water splitting dye sensitized solar cell. ⁽⁵¹⁾

Despite the covalent linkage upgrade of the system, there is no improvement in the photoinduced ET rate between the catalyst IrO_2 and Ru-based dye, remaining the limiting factor of the process and curbing the quantum efficiency of the system to 1-2%. Considering this low value, further advances can be proposed in the molecular components targets. Puntoriero et al. combined IrO_2 nanoparticles with a dendrimeric tetranuclear $\text{Ru}\{(\mu\text{-dpp})\text{Ru}(\text{bpy})_2\}_3^{8+}$ (dpp = diphenylphosphinate anion, bpy = 2,2'-bipyridine) as the sensitizer in order to maximize the absorption of solar radiation with better fitting in oxidation potentials for faster photoinduced ET. ^(52, 53) This system achieved an overall quantum efficiency of 3%, preserving the sensitizer from irreversible degradation thus gaining more long-term activity and efficiency. Another step forward deals with the use of nanostructured hematite $\alpha\text{-Fe}_2\text{O}_3$ with IrO_2 nanoparticles deposited by electrophoresis. ⁽⁵⁴⁾

Ruthenium: The catalytic activity of RuO_2 in water oxidation was first reported by Grätzel et al. in 1979: ⁽⁵⁵⁾ the colloidal nanoparticles were active in presence of Ce^{IV} as oxidant enhancing the performance of bulk RuO_2 powder by two order of magnitude the oxidation rate. These were then tested in a photo-induced system using $\text{Ru}(\text{bpy})_3^{2+}$ as sensitizer and dimethylviologen as sacrificial oxidant. ⁽⁵⁶⁾ Other studies on the integration of RuO_2 within light activated systems have been achieved both in homogeneous solution and by devising a photoactive heterogeneous material. ^(57, 58) Interestingly, a photo-driven oxygenic-gel was generated upon assembling nano- RuO_2 particles, with a cross-linked polycationic matrix incorporating the ruthenium sensitizer. A different strategy involves the

use of a Nafion film embedding a RuO₂/Ru(bpy)₃²⁺ composite, which was then screened for electrocatalytic water oxidation. ⁽⁵⁸⁾

Earth-abundant metal oxides constitute an attractive alternative to IrO₂ and RuO₂, due to their abundance and limited cost. While their activity was known already from the eighties, ^(59, 60) they have regained new interest in the last few years compared with their noble metals analogs. ⁽⁶¹⁾

A brief summary of these oxides is presented in Tab. 1.1, indicating the systems where they are analyzed and a short overview of their properties.

| catalyst | system | properties | ref. |
|---|--|---|-------------|
| Mn | | | |
| Mn ^{III} oxides | electrochemical | onset electrolysis +1.35 V, overpotential 590 mV | (64) |
| CaMnO _x , amorphous | sacrificial oxidant (Ce ^{IV}) | TOF = 2×10 ⁻³ s ⁻¹ | (65) |
| LiMn ₂ O ₄ , spinel | light-driven, ([Ru(bpy) ₃] ²⁺ /NaS ₂ O ₈) | TOF = 3×10 ⁻⁵ s ⁻¹ | (67) |
| nano Mn oxide clusters@mesoporous silica | light-driven, ([Ru(bpy) ₃] ²⁺ /NaS ₂ O ₈) | TOF up to 3330 s ⁻¹ , overpotential 350 mV | (68) |
| Fe | | | |
| Ta/Al-Fe ₂ O ₃ | photoelectrochemical | Ta doping increases the Al-Fe ₂ O ₃ performance, pH = 9.3-13.3 | (78) |
| Co | | | |
| Co-P oxide | electrochemical | overpotential 280 mV, pH = 7 | (70- 75) |
| Ni | | | |
| Ni-B oxide | electrochemical | overpotential 425 mV, pH = 9.2 | (77) |
| Cu | | | |
| Cu ^{II} oxide film from CuSO ₄ | electrochemical | overpotential 700 mV, pH = 10.8 | (79) |

Tab. 1.1: Overview on oxides catalyst and their properties, potentials are reported vs Normal Hydrogen Electrode (NHE)

Manganese oxides have been widely investigated in water oxidation for their close structural similarities with the natural OEC. Electrochemical studies were performed with different Manganese oxides, in particular in alkaline media, to investigate water oxidation catalytic activity. ⁽⁶²⁾ The different activity with pH

values is related to the instability of Mn^{3+} , active as precursor for the water oxidation, which is stabilized in alkaline conditions by a comproportionation reaction. In acidic/neutral media, Mn^{3+} ions are unstable due to their disproportionation into Mn^{2+} and Mn^{4+} .⁽⁶³⁾

Dau et al. developed further studies at neutral pH, where they were able to control the nature of the electrodeposited material changing the voltage protocol obtaining an active species different from an initially inactive Mn oxide.⁽⁶⁴⁾ This catalyst consists of nanoparticles with a complex fine-structure. The characterization of this material and comparison with inactive species enabled to identify some pivotal skills linking structure and activity. Dau and coworkers suggested that the voltage-cycling protocol resulted in the formation of Mn^{III} sites preventing formation of ordered and unreactive $\text{Mn}^{\text{IV}}\text{O}_2$. The O_2 evolution was detected at a potential of +1.35 V vs NHE, while a TOF = 0.01 s^{-1} per deposited Mn ion was reported. The electrodes showed an overpotential of 590 mV to reach a current density of $1 \text{ mA}\cdot\text{cm}^{-2}$.

Catalytic water oxidation was tested by Najafpour et al. with CaMnO_x in the presence of Ce^{IV} as the sacrificial oxidant: the observed TOF (mol O_2 per mol Mn per second) was about $2\times 10^{-3} \text{ s}^{-1}$, four times higher than the best turnover frequency reported for a manganese compound.⁽⁶⁵⁾ These achievements were functional for the design of Mn oxide monosheets forming layers in the presence of 4-aminophenol. These aggregates represent the first attempt to synthesize a self-assembled layered hybrid of phenol and $\text{Mn}^{\text{III, IV}}$ to mimic the oxygen evolving center of Photosystem II.⁽⁶⁶⁾ Regarding light-induced systems with $\text{Ru}(\text{bpy})_3^{2+}$ as sensitizer and $\text{Na}_2\text{S}_2\text{O}_8$ as electron acceptor some studies were published. Dismukes et al. reported a MnO_x active water oxidation catalyst rising from treatments of a nanocrystalline spinel LiMn_2O_4 precursor.⁽⁶⁷⁾ Maintaining the spinel structure, the cubical cores become active at pH = 5.8 upon loss of the Lithium atoms, displaying a TOF = $3\times 10^{-5} \text{ s}^{-1}$ per Mn centre. At the same pH conditions (pH = 5) Frei et al. obtained good results synthesizing nanostructured Manganese oxide clusters supported on mesoporous silica. This scaffold protects the active Mn centres from deactivation and assures stable dispersion of the catalyst maximizing activity.⁽⁶⁸⁾ The system reached a TOF 3330 s^{-1} per catalyst cluster with a modest overpotential of 350 mV. Moreover, the group of Kurz

investigated in light-driven water oxidation the calcium Mn^{III} oxide hydrates, CaMn₂O₄·xH₂O, using the [Ru^{II}(bpy)₃]²⁺/[Co^{III}(NH₃)₅Cl]²⁺ system. ⁽⁶⁹⁾ Even though they were able to record O₂ evolution during the first three minutes, they could not quantify the gas with GC analysis due to irreproducible long-term experiments.

An important breakthrough in Cobalt-based water oxidation catalysis was achieved by Matthew Kanan and Daniel Nocera, at the Massachusetts Institute of Technology (Boston, U.S.A.). They obtained an active film, a mixture of Co^{III} phosphates, ⁽⁷⁰⁾ hydroxides and oxides by electrodeposition onto conductive glass slides of a neutral aqueous solution containing Co^{II} and phosphate ions ^(71, 72, 73). Self-assembling is one of the novel and attractive skill of this film, prepared under mild conditions with control of the control of the thickness by tuning the electrodeposition time.



Fig. 1.9: a) Scanning electron microscopy (SEM) image of a cobalt phosphate (Co-Pi) film for electrocatalytic water oxidation; ⁽⁷²⁾ **b)** edge-sharing molecular cobaltate cluster as the proposed model for the surface catalyst ⁽⁷³⁾

Water oxidation catalysis on this film occurs electrochemically at neutral pH and at a modest 280 mV overpotential, and bulk electrolysis at +1.29 V vs NHE leads to prolonged oxygen evolution. Exploiting Electron Paramagnetic Resonance (EPR) some insights into the catalytic mechanism were reached. The evidence of low-spin Co^{IV} formation during the electro-preparation of the film allows considering the involvement of proton-coupled oxidation to form Co^{IV} oxo units responsible for Oxygen generation, with phosphate residues as proton acceptors. ^(74, 75) The long-term film stability is guaranteed by self-repairing of the mixed oxide.

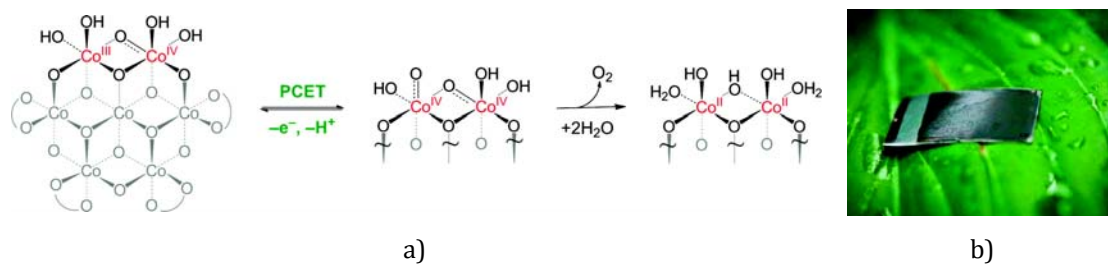


Fig. 1.10: **a)** Representation of the catalytic scheme involving a $\text{Co}^{\text{II/III/IV}}$ manifold, ⁽⁷⁵⁾ **b)** picture of the “artificial leaf” ⁽⁷³⁾

Nocera’s cobalt oxide had been proposed for the design of the so-called “*artificial leaf*”. The device is realized interfacing the Co mixed oxide and a Ni-Mo-Zn composed with a triple junction amorphous Si solar cell, ⁽⁷⁶⁾ and was proposed as a first step in low-cost system engineering and manufacturing. ⁽⁷³⁾

With similar approach Nocera et al. proposed a Nickel based oxide with similar properties to those of the Cobalt based one, by electrodeposition from dilute Ni^{2+} solutions in borate electrolyte at pH 9.2. ⁽⁷⁷⁾ A current density of 1 mAcm^{-2} was recorded for the Ni-B oxide at an overpotential of about 425 mV. The long-term stability and the absence of corrosion make this catalyst a valid alternative to the Cobalt film.

Recently, Iron and Copper oxides have been considered in catalytic water oxidation although studies are so far developed only in alkaline media.

A new type of ternary iron oxides, Ta/Al- Fe_2O_3 has been employed as photoanode for solar water splitting on FTO substrate. ⁽⁷⁸⁾ Using visible light the photocurrent of the (0.25 %)Ta/(10 %)Al- Fe_2O_3 film increases by 15 times at +0.55 V vs NHE in aqueous NaOH. The result is attributed to catalytic water oxidation occurring at the doped electrode, which shows also a shift to lower energy band value of about 50 mV and a reduced anodic overpotential comparing with the corresponding no Ta-doped photoanode.

Studying electrochemical activity of Cu^{II} salts, Meyer et al. observed the formation of a solid at the surface of ITO electrodes, ⁽⁷⁹⁾ in the presence of high concentration of Cu^{II} ions in carbonate solutions (pH = 10.8) when an anodic bias was applied to the electrode. This material was electrochemically active in water oxidation to O_2 ; electrolysis experiments at the onset of +1.30 V vs NHE, with CuSO_4 3 mM in Na_2CO_3 solution reported an overpotential of about 700 mV. After

6 hours of stable current the scanning electron microscopy (SEM) and X-ray photoelectron spectroscopy (XPS) measurements confirmed the presence of an amorphous solid containing Copper and Oxygen.

1.6.2 Molecular WOCs

Molecular WOCs are particularly appealing for some important reasons. 1) The properties of a molecular WOC are potentially tunable by molecular design, ⁽¹⁰⁾ 2) they can reach outstanding reactivity, overcoming metal oxides. 3) The mechanistic understanding of the catalytic reaction is facilitated by the molecular system, potentially enabling the development of more efficient catalysts. 4) In a light-driven process, molecular WOCs allow a more controlled interface between the photosensitizer and the catalyst, ^(80, 81, 82) thus boosting the kinetic of the involved electron transfers. ⁽⁵¹⁾

In molecular catalysis, a complicated and frequent issue is whether the primary compound is the actual catalyst or it is just a precursor of the real active species. In fact, as a consequence of strongly oxidative experimental conditions often catalysts are susceptible to, generally irreversible, transformations. ^(61, 83) This is a fundamental key to understand the catalytic process and a prerequisite for further improvement of the real catalyst itself. The evolution of the system can concern small amount of the pristine species, involving formation of coordination polymer, metal or metal-oxide particles, in the form of colloids, films or powders. Thus, the development of molecular catalysts requires an accurate study and a careful characterization of the species during the catalytic process.

As already anticipated above, this work will deal in particular with molecular WOCs, therefore an ample state-of-the-art will be presented. For easiness of reading, species will be classified considering the nature of the catalytic metal, and an excursus of the most attractive examples will be illustrated in order to give an overview of the domain where this work is placed.

1.6.2.1 Ruthenium

Although Ruthenium is not present in the active site of the natural OEC, its versatile redox and coordination chemistry lead to the particular interest in this metal, and indeed several studies have been conducted, reporting the development of molecular catalysts for water oxidation based on mononuclear, dinuclear and multinuclear Ruthenium complexes.

Concerning such species, a milestone consists in the $[(\text{bpy})_2(\text{H}_2\text{O})\text{-Ru-O-Ru}(\text{H}_2\text{O})(\text{bpy})_2]^{4+}$ (bpy = bipyridine), the first molecular water oxidation catalyst, known as “*blue dimer*” and reported by Meyer et al. in 1982. ⁽⁸⁴⁾

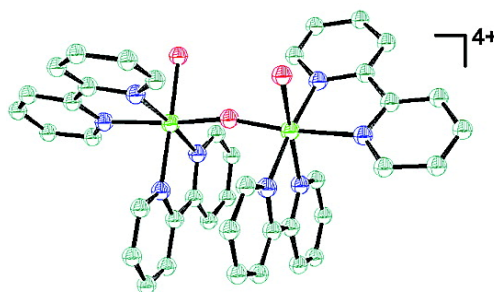


Fig. 1.11: Structure of the Ruthenium “blue dimer” as perchlorate, dehydrate salt: $[(\text{bpy})_2(\text{H}_2\text{O})\text{-Ru}^{\text{III}}\text{-O-Ru}^{\text{III}}(\text{OH}_2)(\text{bpy})_2](\text{ClO}_4)_4 \cdot 2\text{H}_2\text{O}$ ⁽⁸⁵⁾

This compound is able to catalyse water oxidation in presence of an sacrificial electron acceptor such as Ce^{IV} or via electrochemical process. Although the modest turnover number (TON) of 13.2, ⁽⁸⁶⁾ and turnover frequency (TOF) of $4.2 \times 10^{-3} \text{ s}^{-1}$, ⁽⁸⁷⁾ these results proved that the difficult multielectron oxidation of H_2O to O_2 was indeed possible.

After the “*blue dimer*”, several efforts have been dedicated to improve the activity and stability of this dinuclear species intervening on ligand environment; this is indeed a definite proof of the potential of molecular Llobet et al. proposed in 2004 the $[\text{Ru}^{\text{II}}(\text{tpy})(\text{H}_2\text{O})]_2(\mu\text{-bpp})]^{3+}$ complex (tpy = 2,2':6',2''-terpyridine; bpp = bis(2-pyridyl)-3,5-pyrazolate) as molecular WOC, Fig. 1.12 a). ⁽⁸⁸⁾ The catalytic activity was tested with Ce^{IV} as sacrificial oxidant in triflic acid and a TON of about 18.6 and TOF of $1.4 \times 10^{-2} \text{ s}^{-1}$ was obtained. However, even if this system enhanced the “*blue dimer*” activity, the low performance was alleviated

by supporting the catalyst onto a solid phase. The anchoring highly improved the species capability to oxidize water to oxygen achieving a TON of 250.

Later, in 2012 Sun, Llobet and coworkers published a novel, single site Ruthenium-based WOC, achieving high TOF comparable with OEC values. ⁽⁸⁹⁾ The $[\text{Ru}(\text{bda})(\text{isoq})_2]$ (H_2bda = 2,2'-bipyridine-6,6'-dicarboxylic acid; isoq = isoquinoline), Fig. 1.12 b), shows a TOF of 303 s^{-1} combined with a high chemical stability (TON = 8360) for water oxidation with Ce^{IV} as sacrificial oxidant. This study enlightened some insights of the mechanism, especially in the formation of the O-O bond, which requires a bimolecular event involving two catalyst molecules.

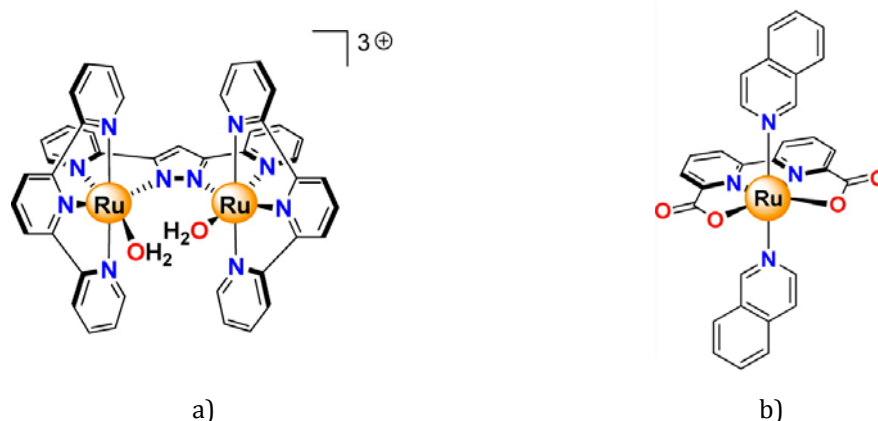


Fig. 1.12: Structure of **a)** $[\text{Ru}^{\text{II}}(\text{tpy})(\text{H}_2\text{O})]_2(\mu\text{-bpp})]^{3+}$ complex and **b)** the mononuclear Ruthenium complex $[\text{Ru}(\text{bda})(\text{isoq})_2]$ ⁽²⁴⁾

Although organic ligands give the possibility of a fine catalyst tuning, they can be limitedly robust in the harsh, oxidative conditions required for water oxidation, compromising their long-term performance. Indeed, alternative ligand families were considered, and in particular a class of totally inorganic ligands: the polyoxometallates (POMs). These are polyanionic molecular oxo-clusters formed by the condensation of oxo groups and early transition metals, in their highest oxidation state (V^{V} , Nb^{V} , Ta^{V} , Mo^{VI} , W^{VI}). Thanks to their properties, POMs have applications in several research fields including medicine, magnetism, high performance materials and catalysis. ⁽⁹⁰⁾ In particular, they can act as ligands towards a variety of other transition metals, often showing catalytic activities: ⁽⁹¹⁾ in Fig. 1.13 some relevant structures of POM ligands are introduced. ⁽¹⁰⁾

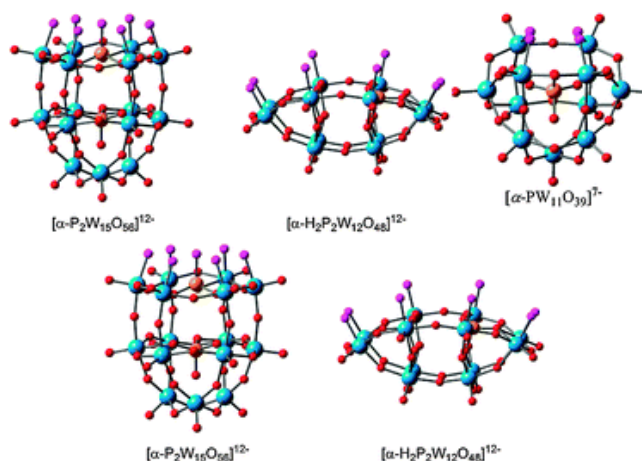


Fig. 1.13: Relevant structures of polyoxometallate (POM) ligands. Light blue: tungsten; red: oxygen; purple: oxygen atoms of the coordination site ⁽¹⁰⁾

The great stability of POMs ligands and of their transition metal complexes towards oxidizing conditions is related to their structure, since the transition metals that constitute the POM architecture are usually in their highest oxidation states (d^0 electronic configuration, i.e. W^{VI} , Mo^{VI} or V^V), and therefore inert to oxidation. However POMs may be sensitive to pH conditions, that need to be optimized in order to avoid hydrolytic degradation, especially favored in alkaline, aqueous solution. A careful control of the ionic strength and counter-ion nature is usually required for boosting the catalytic efficiency. Another important property of POMs ligands, particularly relevant for water oxidation chemistry, is their capability of coordinating multimetal cores. ^(92, 93) Indeed, lacunary POMs can coordinate several transition metal centers, according to the size of the lacunary site and to the number of available nucleophilic oxygens.

In 2008, a breakthrough was achieved in the field of water oxidation catalysis, employing POM ligands: at the same time, following different synthetic strategies, two different research groups reported a tetra-ruthenium compound obtained from the lacunary POM $[\gamma-SiW_{10}O_{36}]^{8-}$. ^(94, 95) The resulting species $\{Ru_4(\mu-O)_4(\mu-OH)_2(H_2O)_4[\gamma-SiW_{10}O_{36}]_2\}^{10-}$ (Ru_4POM), Fig. 1.14, presents an adamantane-like structural motif of the ruthenium-oxo core, that can be reminiscent of the natural OEC in PSII.

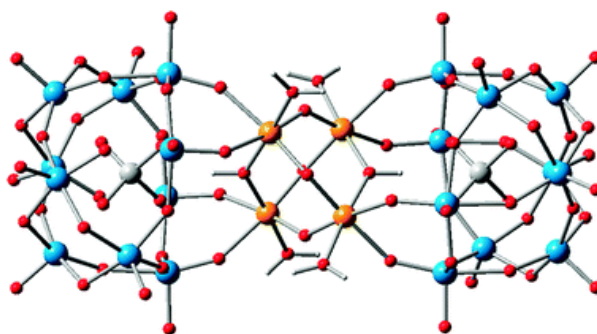


Fig. 1.14: Structure of $\{\text{Ru}_4(\mu\text{-OH})_2(\mu\text{-O})_4(\text{H}_2\text{O})_4[\gamma\text{-SiW}_{10}\text{O}_{36}]\}^{10-}$, Ru_4POM . Light blue: tungsten; orange: ruthenium; gray: silicon; red: oxygen.

Ru_4POM turned out to evolve oxygen from water in the presence of a chemical oxidant such as Ce^{IV} with up to 500 turnover and a TOF of $1.25 \times 10^{-1} \text{ s}^{-1}$. Moreover, at neutral pH and with the photogenerated oxidant $\text{Ru}(\text{bpy})_3^{3+}$, Ru_4POM reaches 350 TONs and the oxygen evolution is limited only by the oxidative instability of the sensitizer. ^(96, 97, 98) As observed in cyclic voltammetry (CV) experiments, ^(99, 100) Ru_4POM undergoes several redox events associated to oxidation of the Ru^{IV} centres to higher oxidation states, until the species reaches the active form capable of oxidizing water. In such kind of processes, the Oxygen-Oxygen bond formation is often recognized as the rate limiting step. ⁽¹⁰¹⁾ Concerning Ru_4POM , the most plausible proposed mechanism foresees a water nucleophilic attack to a high valent Ruthenium-oxo (or hydroxo) moiety, resulting in a metal hydroperoxo formation. ⁽⁹⁹⁾

Exploiting its polyanionic nature, Ru_4POM has been supported onto different nanostructured materials ^(102, 103, 104) where it retains its activity even in heterogeneous conditions.

Finally, it is interesting to note that the tetraruthenate core can be considered a minimal, optimized fragment of a ruthenium oxide phase. Indeed, it presents structural and functional properties that can be associated to a metal oxide fragment. Suchlike relationship between molecular and extended species, still scarcely investigated in literature, has a powerful potential, since it demonstrates that knowledge on molecular species can be transferred to metal oxide systems.

1.6.2.2 Iridium

The first example of Iridium based, molecular WOCs was reported by Bernhard et al. who identified a family of cyclometalated Iridium complexes, composed by bis-phenylpyridines groups, $[\text{Ir}(\text{phenylpyridine})_2(\text{H}_2\text{O})_2]$, Fig. 1.15. ⁽¹⁰⁵⁾ Such catalysts, using Ce^{IV} as oxidant, reach TOF of $1.5 \times 10^{-3} \text{ s}^{-1}$ and TON of 2500.

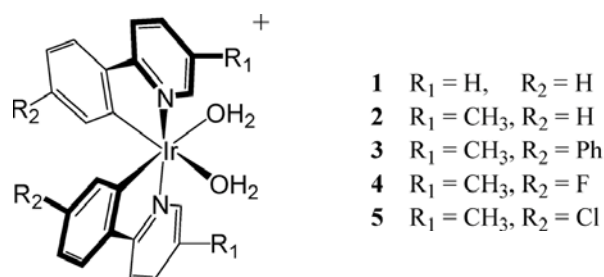


Fig. 1.15: Structure of the described oxidation catalyst, $[\text{Ir}(5\text{-}R_1,4'\text{-}R_2,2\text{-phenylpyridine})_2(\text{OH}_2)_2]^+$
⁽¹⁰⁵⁾

The nature and behavior of catalyst ligands is fundamental for the catalysis because *i)* they give access to multi-redox states, which can be promoted within a stable molecular entourage, ⁽¹⁰⁶⁾ *ii)* they can prevent the formation of Iridium oxide colloids, which competes for water oxidation. ⁽¹⁰⁷⁾ After Bernhard's report, different groups considered Iridium complexes with several classes of ligands such as: substituted bipyridine, ⁽¹⁰⁸⁾ 2-phenylpyridine and pentamethylcyclopentadienyl (Cp^*), ⁽¹⁰⁹⁾ substituted pyridine, ⁽¹¹⁰⁾ ethylenediaminetetraacetate (EDTA), ⁽¹¹¹⁾ polyoxometallates ⁽¹¹²⁾ and carbenes. ⁽¹¹³⁾ Nowadays, Iridium species retain great interest due to the high turnover numbers (upto 10^4) and turnover frequencies (upto 1.5 s^{-1}). ^(113a) Very recently, they have been also used within the $\text{Ru}(\text{bpy})_3^{2+}/\text{Na}_2\text{S}_2\text{O}_8$ light-driven system reaching a TON of 9.3 and TOF of $4.85 \times 10^{-3} \text{ s}^{-1}$. ^(113g)

Following studies from Brudvig's group showed that molecular species were precursors of the real catalyst, upon electrochemical oxidation. $[\text{Cp}^*\text{Ir}(\text{H}_2\text{O})_3]\text{SO}_4$ and $[(\text{Cp}^*\text{Ir})_2(\text{OH})_3]\text{-OH}$ complexes deposit onto the anode an amorphous robust Iridium oxide significantly more active as WOC than crystalline IrO_2 . No deactivation or significant corrosion of the new species were observed for at least 70 h. Further studies will underline the pivotal starting molecular nature of

the catalyst precursor. ⁽¹¹⁴⁾ A major concern in the use of Iridium based molecular WOC was indeed the nature of the actual species carrying on the catalysis. Recently, Brudvig et al. proposed a common, active intermediate in chemical or electrochemical water oxidation starting with Iridium precursors, bases on a dinuclear core where the two Iridium atoms are connected via two μ -oxo bridges. ⁽¹¹⁵⁾ A bis μ -oxo iridium dimer was considered as the active species by Hetterscheid, Koper et al. in electrochemical water oxidation on gold surfaces by an Iridium-N-dimethylimidazolin-2-ylidene species, by surface enhanced raman spectroscopy. ⁽¹¹⁶⁾

1.6.2.3 Earth abundant metals

Although the high performance of noble metal-based WOCs, their limited abundance on the Earth's crust, their high price and toxicity confine them to the use on a large scale. Thus, the development of WOCs based on first-row transition metals is particularly appealing.

Some examples of catalysts with Manganese, Iron, Cobalt, Nickel and Copper will be presented, lingering on different kinds of ligands and metal nuclearity. In particular, in order to further outline the specific subjects related to this work, Co and Cu based catalysts will be highlighted.

Manganese

In Nature, the Mn cluster in the OEC is kept together by several bridging μ -oxo ligands, and is further stabilized by surrounding amino acids containing imidazole and tyrosine functionalities. This efficient stabilization allows the cluster to cycle up to 10^6 times between the five oxidation states of the Kok cycle during the oxidation of H_2O , reaching an outstanding TOF of $400\ s^{-1}$ (see 1.3). However, due to the presence of highly oxidizing species throughout this cycle, damage is regularly inflicted on the surrounding peptide structures. ⁽¹¹⁷⁾

In order to mimic structure, activity of the PSII-OEC and inspired by Nature, researchers have dedicated major efforts toward the synthesis of Mn-based WOCs. Besides its natural abundance, Manganese has a low cost, and is also environmentally benign. Furthermore, it has a large redox chemistry, with access

to a wide range of oxidation states with strong oxidizing power. Unfortunately, this involves an intrinsic instability of these high-valent species, which require for effective ligand stabilization to prevent them from decomposing. In addition, the strongly oxidizing property of such Manganese species requires robust and stable ligand scaffolds against oxidative degradation. ⁽²⁵⁾ Indeed, Mn-based molecular WOCs are confined to few examples.

The first functional model with di- μ -oxo Mn units able to catalyse homogeneous O₂ evolution is the dimer [H₂O(terpy)Mn(μ -O₂)Mn(terpy)OH₂](NO₃)₃, (terpy = 2,2',6,2''-terpyridine) presented by Limburg et al. ⁽¹¹⁸⁾ The conditions involved the use of sacrificial donors as NaOCl or KaHSO₅ in aqueous solution at pH = 8.6 and 4.5 respectively, while decomposition to MnO₄⁻ was observed in the presence of Ce^{IV}. However, recently Dau and coworkers have questioned on the molecular nature of the catalytic species, ascribing the activity to the transformation into layered type Mn oxide particles, on the basis of EXAFS experiments. ⁽¹¹⁹⁾

One elaborate dimeric complex was reported by the group of Åkermark as the most stable WOC based on Manganese. ⁽¹²⁰⁾ Such species consists of imidazole, carboxylate and Oxygen ligands bridging two metal centers. Catalytic water oxidation was observed with photogenerated [Ru(bpy)₃]³⁺ as oxidant at neutral pH. Anyway, the system presented quite low efficiency with a TOF of 0.03 s⁻¹ and TON = 25.

A tetrametallic complex was introduced by Dismukes and coworkers, who described a cubane like [Mn₄O₄(dpp)₆] and [Mn₄O₄(Me-dpp)₆], (dpp = diphenylphosphinate anion; Me-dpp = bis(tolyl)phosphinate) releasing molecular oxygen in gas phase upon UV light absorption. ^(121,122) Further studies enabled to overcome the poor solubility of such cubane derivatives: they were supported onto conducting fluorinated membranes that could be used as heterogeneous catalytic materials. As a Nafion composite [Mn₄O₄(MeO-dpp)₆]⁺ (MeO-dpp = bis(4-methoxyphenyl)phosphinate), Fig. 1.16 a) is proposed to drive oxygen evolution under white light and applied potential. ⁽¹²³⁾ An initial photocurrent density of 9 μ Acm⁻² is reported at pH 11 and at an applied potential of +1.2 V vs NHE, when the electrode is illuminated with > 275 nm white light. The photocurrent was accompanied by oxygen evolution with almost

quantitative Faradaic efficiency and about 1000 TON per Mn_4O_4 after 65 hours electrolysis.

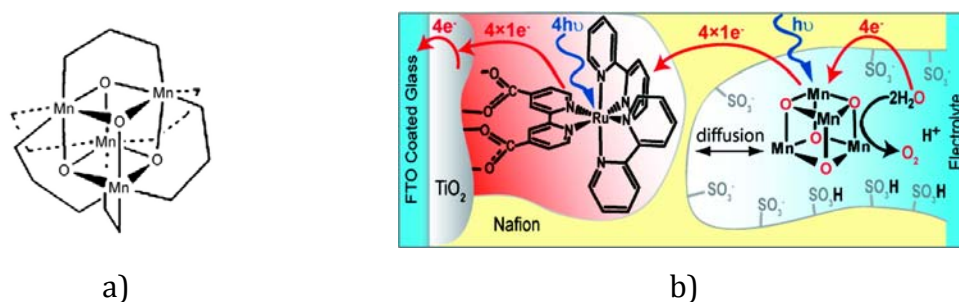


Fig. 1.16: Schematic representation of **a)** $[\text{Mn}_4\text{O}_4(\text{MeO-dpp})_6]^+$ species ⁽¹²³⁾ and **b)** the photoanode showing the proposed operations of the device ⁽¹²⁴⁾

Moreover, the hybrid nafion- $[\text{Mn}_4\text{O}_4(\text{MeO-dpp})_6]^+$ was used to develop a photoanode where solar power promotes the ET from the catalyst to the electrode, avoiding the application of an external bias (Fig. 1.16 b)). ⁽¹²⁴⁾ Such system is constituted by a conductive fluorine tin oxide (FTO) coated glass, where a titania layer sensitized with $\text{Ru}(\text{bpy})_2(\text{bpy}(\text{COO})_2)$, ($\text{bpy} = 2,2'$ bipyridine; $\text{bpy}(\text{COO})_2 = 4,4'$ -dicarboxy-2,2'-bipyridine), is deposited and finally coated with nafion- $[\text{Mn}_4\text{O}_4(\text{MeO-dpp})_6]^+$ material. The molecular nature of the catalyst was subsequently questioned by Spiccia et al., who reported in situ X-ray absorption experiments and transmission electron microscopy (TEM) studies demonstrating dissociation of the Mn cubane cluster in Mn^{II} compounds in the Nafion membrane, which are reoxidized in dispersed nanoparticles of a Mn^{III/IV} oxide phase. ⁽¹²⁵⁾ The Mn cubane turned out to be the precursor of the actual WOC.

Very recently Bonchio et al. published new interesting results on a tetramanganese species stabilized by a hybrid organic-inorganic set of ligands, the $[\text{Mn}^{\text{III}}_3\text{Mn}^{\text{IV}}\text{O}_3(\text{CH}_3\text{COO})_3(\text{A-}\alpha\text{-SiW}_9\text{O}_{34})]^{6-}$ (Mn_4POM), Fig. 1.17. ⁽¹²⁶⁾

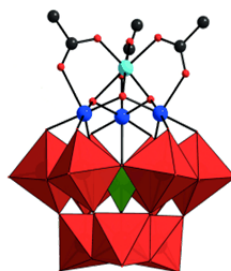


Fig. 1.17: Structure of Mn_4POM , Balls: calcium yellow, carbon dark grey, manganese(III) blue, manganese(IV) light blue, oxygen red; polyhedra : SiO_4 green, WO_6 red ⁽¹²⁶⁾

This species states an unprecedented structural mimic of the OEC in its reduced S_0 state. The ligands entourage helps the access of Mn high oxidation states needed for the catalysis and oxygen evolving. CV experiments showed in the oxidative scan an anodic wave at +1.07 V vs NHE ascribable to a multi-electron oxidation of the Mn core, followed by an intense catalytic wave due to water oxidation at +1.45 V vs NHE with an overpotential of 530 mV. Moreover, Mn₄POM was investigated in a light activated cycle, with Ru(bpy)₃²⁺ as the photosensitizer and S₂O₈²⁻ as the sacrificial electron acceptor. Laser flash photolysis studies evidenced the occurrence of three fast electron transfers (within 50 ms) from Mn₄POM to photogenerated Ru^{III}(bpy)₃³⁺, leading to the formation of the three-oxidized species of Mn₄POM. This was a further similarity to the natural OEC, where three fast oxidations during the Kok cycle transform the S_0 into the S_3 state. Finally, in such photo activated system, in NaHCO₃/Na₂SiF₆ buffer (pH = 5.2) and using the system Ru(bpy)₃²⁺/S₂O₈²⁻ the catalyst evolves oxygen showing per Mn₄POM a TOF up to 2.84×10⁻³ s⁻¹, a TON of ca 5.2 and a quantum efficiency of 1.7%.

Iron

Because of its low cost, low toxicity, and high natural availability, Iron has also been considered as a promising metal for the construction of artificial WOCs.

In 2010, the group of Bernhard and Collins reported different Iron macrocyclic complexes, [Fe^{III}(taml)]⁻ (taml = tetra amido macrocyclic ligand), among which some of them were able to act as WOCs using Ce^{IV} as sacrificial oxidant. ⁽¹²⁷⁾ The best values of TOF obtained is 1.3 s⁻¹ and TON = 16, however the species decomposes rapidly, most likely due to ligand oxidation.

Another important example of Iron based WOC tested with Ce^{IV} or NaIO₄ as sacrificial oxidants was published by Costas et al. ⁽¹²⁸⁾ The Fe complex *cis*-Fe(mcp)OTf₂ (mcp = N,N'-dimethyl-N,N'-bis(2-pyridylmethyl)-cyclohexane-1,2-diamine; OTf = trifluoromethanesulfonate) achieved TON of 1000 and TOF of 0.23 s⁻¹. Lau et al. confirmed the molecular nature of the catalytic species in acidic conditions, while at higher pH values they showed the formation of Fe₂O₃, after hydrolysis acting as real catalyst for water oxidation. ⁽¹²⁹⁾

Cobalt

Although Co^{II} aquo ions have been known to catalyze water oxidation since the 1980s, ^(35, 59, 60) the interest in molecular cobalt-based WOCs was quite low until when Nocera and co-workers showed that an in situ generated cobalt-based WOC oxide was capable of operating under neutral conditions.

Since then, the development of molecular cobalt-based WOCs has progressed very rapidly, with respect to other first-row transition metals.

The group of Berlinguette reported in 2011 the first example of a well-defined and stable coordination compound: the $[\text{Co}(\text{PY5})(\text{OH}_2)](\text{ClO}_4)_2$, Fig. 1.18, a single site Co^{II} molecular complex bearing a pentadentate ligand able to catalyse water oxidation. ^(130, 131)



Fig. 1.18: Molecular representation of $[\text{Co}(\text{PY5})(\text{OH}_2)](\text{ClO}_4)_2$, counteranion and hydrogen atoms are omitted for clarity ⁽¹³⁰⁾

The catalyst stability has been investigated in electrochemical process, where Oxygen evolution was confirmed at an applied potential of +1.59 V vs NHE over 10 minutes and a TOF of 79 s^{-1} was reported.

Another interesting and bifunctional Cobalt corrole complex $[\text{Co}(\text{tpfc})(\text{pyr})_2]$, (tpfc = 5,10,15-tris-(pentafluorophenyl)corrole; pyr = pyridine) for both electrochemical O_2 evolution and H_2 production was very recently reported by Lei et al. ⁽¹³²⁾ The electrochemical results confirmed that this species possessed sufficient oxidizing power to function as a potential WOC. In aqueous solution, the catalyst was deposited on an ITO-coated glass electrode giving a film, the electrode was subsequently immersed into a phosphate buffer solution (0.1 M, pH = 7.0). A rise of the current began at +1.36 V vs NHE, attributed to catalytic H_2O oxidation, with an overpotential of 540 mV. The TOF of the process was determined at +1.61 V vs NHE to be 0.20 s^{-1} .

Recently, the group of Groves reported on a series of single-site cobalt porphyrin complexes functioning as electrochemical WOCs in neutral pH. ⁽¹³³⁾ Co^{III} -

5,10,15,20-tetrakis(1,3-dimethylimidazolium-2-yl)porphyrin with a highly electron-deficient ligand structure showed to be the most active catalyst, reaching a Faradaic efficiency of about 90% and TOF = $1.4 \times 10^3 \text{ s}^{-1}$. Electrochemical experiments conducted in a 0.2 M aqueous sodium phosphate solution at pH 7 gave rise to a strong catalytic current with an onset potential of +1.41 V vs NHE and high O₂ evolution over several hours without any loss of catalytic current.

Similar complexes capable of catalyzing light-driven WO are the cobalt–porphyrin species recently reported by the group of Sakai. ⁽¹³⁴⁾ These catalysts are similar in structure, containing a Co^{III} center stabilized by a porphyrin ligand that varies only in the aryl groups (N-methylpyridine, benzoic acid, benzenesulfonic acid) located at the four meso-positions. The catalysis was performed at pH 11, in phosphate buffer, with [Ru(bpy)₃]²⁺ as photosensitizer and Na₂S₂O₈ as sacrificial electron acceptor, which resulted in TOFs between 0.118 and 0.170 s⁻¹ and TONs between 89 and 122.

So far, another molecular cobalt-based species was reported by the group of Lau to catalyze both water reduction and oxidation without the need of electrochemical conditions. ⁽¹³⁵⁾ The trans-[Co(qpy)(OH₂)₂]²⁺ complex (qpy = 2,2':6',2'':6'',2'''-quaterpyridine) species proved to be compatible with the mild system [Ru(bpy)₃]²⁺/S₂O₈²⁻, allowing H₂O oxidation to be driven in borate buffer (pH = 8). Measurements of O₂ evolution recorded a TON of 335, obtained after irradiating the reaction (λ = 457 nm) for about 90 minutes.

Concerning a different ligand environment, the [Co₄(H₂O)₂(α-PW₉O₃₄)₂]¹⁰⁻ (Co₄POM), Fig. 1.19, was introduced by Hill and co-workers as the first carbon-free homogeneous WOC containing abundant metals. ⁽¹³⁶⁾

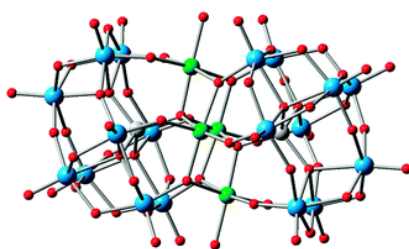


Fig. 1.19: Structure of [Co₄(H₂O)₂(α-PW₉O₃₄)₂]¹⁰⁻, Co₄POM. Light blue: tungsten; green: cobalt; gray: phosphorous; red: oxygen ⁽¹⁰⁾

The four central Co atoms are bridged by oxo-groups, sandwiched between two lacunary $PW_9O_{34}^{9-}$ fragments and the unshared vertices of two Co ions are occupied by coordinated water molecules. CV of Co_4POM showed an intense catalytic current at +1.3 V vs NHE and pH = 8. Further, using $Ru(bpy)_3^{3+}$ as chemical oxidant in large concentration, oxygen evolution was observed at pH = 8 with maximum values of TON of 1000 over 3 minutes, and TOF of $5\ s^{-1}$. The Co_4POM catalyst had been tested also in the photoactivated $[Ru(bpy)_3]^{2+}/Na_2S_2O_8$ system obtaining a TON of about 220. ⁽¹³⁷⁾ The authors provided different points of evidence for the stability of the species during the catalytic activity. Otherwise later, two different groups have been advanced a concern regarding the nature of the real WOC. Stracke and Finke found out that this tetra cobalt POM decomposes during electrocatalytic water oxidation to generate a CoO_x film, which becomes the major catalyst. ⁽¹³⁸⁾ Natali et al. analysed the same photocatalytic conditions reported by Hill and co-workers taking advantage of laser flash photolysis technique. The study evidenced that the rate of electron transfer from Co_4POM to photogenerated $Ru^{III}(bpy)_3^{3+}$ increases upon aging the Co_4POM in aqueous buffer for some minutes. The initial, negligible rate of electron transfer suggests that pristine Co_4POM cannot be operative in the photocatalytic cycle, while its transformation leads to a more active species. ⁽¹³⁹⁾ Very recently Hill et al. reported another Co_4POM WOC based on vanadates: the $Na_{10}[Co_4(H_2O)_2(VW_9O_{34})_2]\cdot 35\ H_2O$. ⁽¹⁴⁰⁾ This species is able to perform catalytic water oxidation both in dark and in light-driven system. Using $Ru(bpy)_3^{3+}$ as stoichiometric oxidant in dark high TOFs in the range of $1.6-2.2\times 10^3\ s^{-1}$ were founded, in the photo-induced catalytic process a quantum yield of oxygen formation of about 68% was achieved. Several proofs were collected in order to attest the molecular nature of the active WOC.

As a final remark, the question about the actual nature of the catalyst is of particular relevance for Cobalt based water oxidation catalyst, since Cobalt based oxides are very efficient WOC. Therefore, the possible presence of active CoO_x phases upon transformation of the molecular active species needs to be carefully investigated. Oxidative decomposition of the organic ligands, ⁽¹⁴¹⁾ or solution

equilibria liberating Co^{2+} ions could be the primary events, yielding Cobalt oxide formation. ⁽¹³⁶⁾

As a consequence: 1) it is important to screen different experimental conditions for each catalytic reaction. Indeed, a process for the same molecular catalyst can be homogeneous in a particular set of conditions and heterogeneous for another one. Furthermore, 2) even if the molecular starting compound is transformed into a solid-state or colloidal catalyst, the ligands of the precursor may influence the formation and the nature of the final catalyst. This could allow for a selective tuning of the structure and the activity of the heterogeneous system. 3) The stability of molecular compounds can be enhanced through interactions with surfaces, through covalent bonds or simple adsorption. Sometimes this stabilizing effect is only partial, retaining some of the structural features of the precursor but can lead to a total different and enhanced activity. 4) The characterization of the catalytic process, homogeneous or heterogeneous, requires a complete set of experimental evidences: the full investigation of the catalytically active species is the only way for a rational optimization of the systems. ⁽⁶¹⁾

Nickel

Very recently a study on a Ni^{II} based WOC has been published by Zhang and coworkers. The catalyst, based on the macrocyclic ligand 5,5,7,12,12,14-hexamethyl-1,4,8,11-tetraazacyclotetradecane, which already showed ability of electrochemically reducing water to H_2 , was observed also to oxidize water at neutral pH. ⁽¹⁴²⁾ The overpotential obtained is 170 mV, much lower than the typical values for many homogeneous WOCs (300-600 mV). After 6 hours of controlled potential electrolysis at +1.55 V vs NHE, the current reaches 0.9 mAcm^{-2} and $73 \mu\text{mols}$ of O_2 were detected, with a Faradaic efficiency of 97.5% and 15 TON. The authors noted that after the experiments the catalyst integrity was confirmed with different techniques and supported their mechanistic hypothesis with DFT calculations, that support formation of the O-O bond from the cis-isomer of the catalyst through a water nucleophilic attack.

Copper

The investigation of copper-based WOCs is emerging as a novel research area showing a promising potential. So far, studies are dealing with electrochemical activation of the catalysts.

The group of Mayer reported the first example of a homogeneous WOC Copper catalyst in 2012. ⁽¹⁴³⁾ The (bpy)Cu(OH)₂ (bpy = 2,2'-bipyridine) complex could self-assemble in aqueous solutions, giving rise to an active WOC, Fig. 1.20 a). CV measurements of the Copper-bpy revealed that it exhibited a large, pH-dependent, and irreversible wave at +1.30–1.50 V vs NHE. Bubbles formation was observed at the electrode surface over multiple scans. With electrolysis experiments on the basis of the Faradaic efficiency, the authors concluded that 30 equivalents of O₂ were generated based on the total amount of Cu, with a calculated TOF up to 100 s⁻¹. However, it was assumed that only the Copper species in close proximity of the electrode surface were catalytically active. The linear dependence of catalytic current on the Cu concentration proved the molecular nature of the electrocatalyst and a single site mechanism.

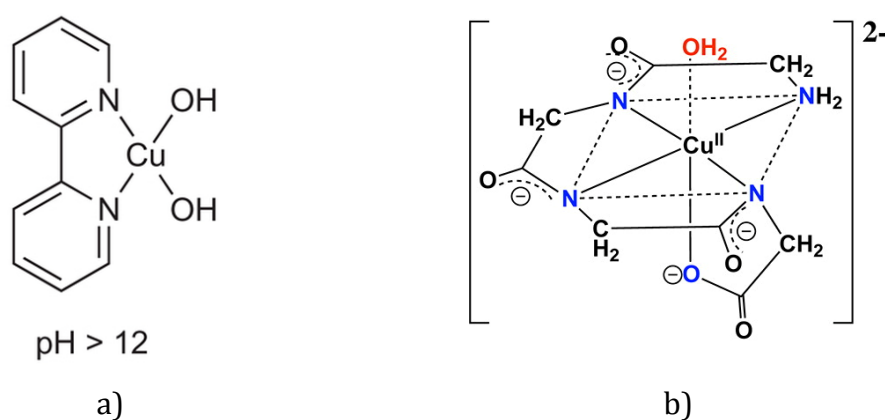


Fig. 1.20: Structure of catalysts **a)** (bpy)Cu(OH)₂ at cited pH ⁽¹⁴³⁾ and **b)** [(TGG⁴⁻)Cu^{II}-OH₂]²⁻ ⁽¹⁴⁵⁾



More recently, Chen and Meyer published that simple Cu salts were electrochemically active WOCs. ⁽¹⁴⁴⁾ Cu^{II} salts in aqueous buffered solutions dramatically enhanced the current at the onset potential for the catalytic process of +1.05 V vs NHE at pH 10.8, with an overpotential of 450 mV. The catalytic current was second order in Cu concentration and stable for at least 6 hours.

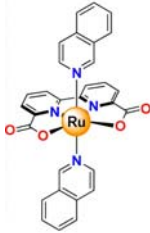
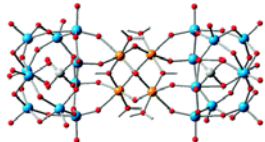
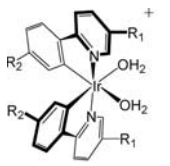

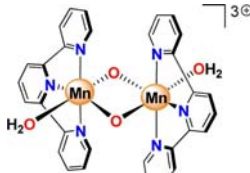

Later, the group of Meyer studied also the water oxidation catalyzed by a Copper complex containing a triglycylglycine macrocyclic ligand (TGG⁴⁻), [(TGG⁴⁻)Cu^{II}-

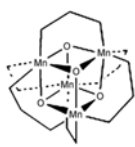
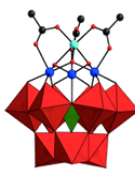

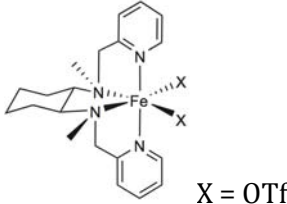
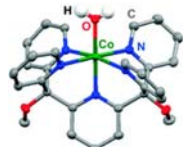
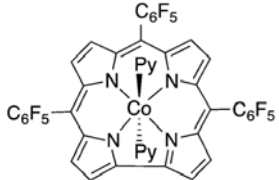
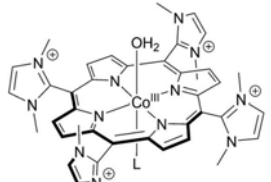
$\text{OH}_2]^{2-}$ Fig. 1.20 b).⁽¹⁴⁵⁾ The species was isolated and demonstrated ability to self-assemble in solution at $\text{pH} = 11$ from $\text{Cu}(\text{OH})_2$ and the macrocyclic ligand. In same conditions the CV of the catalyst showed a well-defined and reversible wave at $+0.58 \text{ V vs NHE}$, more the onset potential for electrochemical oxidation occurred at $+1.10 \text{ V vs NHE}$, corresponding to an overpotential of 520 mV . Upon electrolysis over a period of 8 hours, the total oxygen evolved was measured by gas chromatography giving $39 \mu\text{mol}$, a Faradaic efficiency of 99% and a $\text{TON} = 13$. The TOF was then calculated to be 33 s^{-1} .

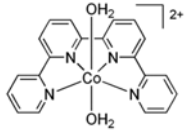
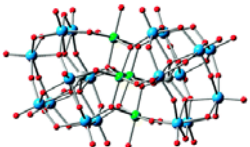
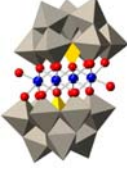
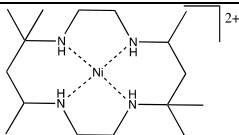
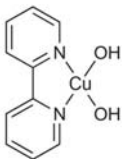
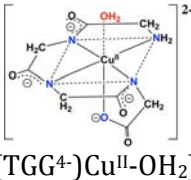
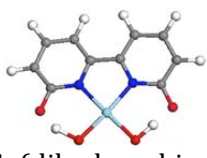
Finally, starting from Mayer's catalyst but following a biomimetic approach, Lin et al. developed a WOC designed with a particular ligand, which should provide a non-innocent redox environment.⁽¹⁴⁶⁾ CVs of CuL ($\text{L} = 6,6'$ -dihydroxy-2,2'-bipyridine) show irreversible catalytic current, occurring with an onset potential of $+0.8 \text{ V vs NHE}$ at $\text{pH} = 12\text{--}14$ and low overpotential of $510\text{--}560 \text{ mV}$. Thus, the new ligand stabilizes high-valent intermediates, lowering the overpotential for the reaction of water oxidation. Lin and coworkers demonstrated that incorporation of redox-accessible ligand frameworks into metal complexes could be a viable strategy for constructing efficient WOCs.

In Tab. 1.2 the molecular WOC are briefly summarized as well as the conditions of studies and particular skills.

| catalyst | system | properties | ref |
|---|--|--|---------|
| Ru | | | |
|  $[(\text{bpy})_2(\text{H}_2\text{O})\text{-Ru-O-Ru}(\text{H}_2\text{O})(\text{bpy})_2]^{4+}$ | sacrificial oxidant (Ce^{IV}) | $\text{TON} = 13.2,$ $\text{TOF} = 4.2 \times 10^{-3} \text{ s}^{-1}$ | (85-87) |
|  $[\text{Ru}^{\text{II}}(\text{tpy})(\text{H}_2\text{O})]_2(\mu\text{-bpp})]^{3+}$ | sacrificial oxidant (Ce^{IV}) | $\text{TON} = 18.6,$ $\text{TOF} = 1.4 \times 10^{-2} \text{ s}^{-1}$ | (88) |

| | | | |
|--|--|--|---------|
|  <p>[Ru(bda)(isoq)₂]</p> | sacrificial oxidant (Ce ^{IV}) | TON = 8.4, TOF = 303 s ⁻¹ | (89) |
|  <p>{Ru₄(μ-O)₄(μ-OH)₂(H₂O)₄[γ-SiW₁₀O₃₆]₂}¹⁰⁻</p> | sacrificial oxidant (Ce ^{IV}) | TOF = 1.25×10 ⁻¹ s ⁻¹ | (94-98) |
| | light-driven, ([Ru(bpy) ₃] ²⁺ /NaS ₂ O ₈) | TON = 350 | |
| Ir | | | |
|  <p>[Ir(5-R₁,4'-R₂,2-phenylpyridine)₂(OH₂)₂]⁺</p> | sacrificial oxidant (Ce ^{IV}) | TON = 2500, TOF = 1.5×10 ⁻³ s ⁻¹ | (105) |
|  <p>N-heterocyclic dicarbene Ir^{III}</p> | sacrificial oxidant (Ce ^{IV}) | TON = 2800, TOF = 0.20 s ⁻¹ | (113) |
| | light-driven, ([Ru(bpy) ₃] ²⁺ /NaS ₂ O ₈) | TON = 9.3, TOF = 4.85×10 ⁻³ s ⁻¹ | |
| Mn | | | |
|  <p>[H₂O(terpy)Mn(μ-O₂)Mn(terpy)OH₂](NO₃)₃</p> | sacrificial oxidant (NaOCl or KaHSO ₅) | pH = 8.6 and 4.5 respectively but molecular nature doubted by Dau | (118) |
|  <p>[Mn₂^{II,III}(H₂L)(OAc)(OCH₃)]</p> | light-driven, ([Ru(bpy) ₃] ²⁺ /NaS ₂ O ₈) | TON = 25, TOF = 0.03 s ⁻¹ | (120) |

| | | | |
|--|--|---|-----------|
|  <p>$[\text{Mn}_4\text{O}_4(\text{MeO-dpp})_6]^+$</p> | photoelectrochemical | pH = 11, applied potential of +1.2 V; TON = 1000, 65 h electrolysis | (123) |
|  <p>$[\text{Mn}^{\text{III}}_3\text{Mn}^{\text{IV}}\text{O}_3(\text{CH}_3\text{COO})_3(\text{A-}\alpha\text{-SiW}_9\text{O}_{34})]^{6-}$</p> | electrochemical | overpotential 530 mV | (126) |
| | light-driven, ([Ru(bpy) ₃] ²⁺ /NaS ₂ O ₈) | pH = 5.2 TOF = $0.71 \times 10^{-3} \text{ s}^{-1}$ quantum efficiency = 1.7% | |
| Fe | | | |
|  <p>$[\text{Fe}^{\text{III}}(\text{taml})]^-$</p> | sacrificial oxidant (Ce ^{IV}) | TON = 16, TOF = 1.3 s^{-1} | (127) |
|  <p>X = OTf $[\text{Fe}(\text{OTf})_2(\text{mcp})]$</p> | sacrificial oxidant (Ce ^{IV} and NaIO ₄) | TON = 1050 with NaIO ₄ , TOF = 0.23 s^{-1} with Ce ^{IV} molecular nature at low pH confirmed by Lau | (128) |
| Co | | | |
|  <p>$[\text{Co}(\text{PY5})(\text{OH}_2)](\text{ClO}_4)_2$</p> | electrochemical | TOF = 79 s^{-1} | (130-131) |
|  <p>$[\text{Co}(\text{tpfc})(\text{pyr})_2]$</p> | electrochemical | TOF = 0.20 s^{-1} overpotential = 540 mV | (132) |
|  <p>Co^{III}-5,10,15,20-tetrakis(1,3-dimethylimidazolium-2-yl)porphyrin</p> | electrochemical | TOF = $1.4 \times 10^3 \text{ s}^{-1}$, pH = 7, Faradaic efficiency = 90 % | (133) |

| | | | |
|---|--|---|---------------|
| cobalt-porphyrin species with different aryl groups | light-driven, ([Ru(bpy) ₃] ²⁺ /NaS ₂ O ₈) | TON = 89-122 after 30 min, TOF = 0.118- 0.170 s ⁻¹ , pH = 11 | (134) |
|  trans-[Co(qpy)(OH ₂) ₂] ²⁺ | light-driven, ([Ru(bpy) ₃] ²⁺ /NaS ₂ O ₈) | TON = 335, pH = 8 | (135) |
|  [Co ₄ (H ₂ O) ₂ (α-PW ₉ O ₃₄) ₂] ¹⁰⁻ | sacrificial oxidant (Ru(bpy) ₃ ³⁺) | (at high conc of oxidant) TON = 1000, TOF = 5 s ⁻¹ , pH = 8 | (136- 137) |
| | light-driven, ([Ru(bpy) ₃] ²⁺ /NaS ₂ O ₈) | TON = 220, pH = 8 | |
| | molecular nature denied by Strake, Finke, Natali et al. | | |
|  Na ₁₀ [Co ₄ (H ₂ O) ₂ (VW ₉ O ₃₄) ₂].35 H ₂ O | sacrificial oxidant (Ru(bpy) ₃ ³⁺) | TOF = 1.6-2.2×10 ³ s ⁻¹ | (140) |
| Ni | | | |
|  Ni ^{II} macrocyclic ligand | electrochemical | TON = 15, overpotential = 170 mV, pH = 7, Faradaic efficiency = 97.5 % | (142) |
| Cu | | | |
|  (bpy)Cu(OH) ₂ | electrochemical | TOF = 100 s ⁻¹ , pH > 12 | (143) |
|  [(TGG ⁴⁻)Cu ^{II} -OH ₂] ²⁻ | electrochemical | TON = 13, TOF 33 s ⁻¹ , overpotential 520 mV, self-assembling at pH = 11, Faradaic efficiency = 99% | (145) |
|  Cu(dihydroxybipy) | electrochemical | overpotential 510- 560 mV, pH = 12-14 | (146) |

Tab. 1.2: Overview on oxides catalyst and their properties, potentials are reported vs Normal Hydrogen Electrode (NHE)

1.7 State of the art: CO₂ reduction catalysts

Among the analysis of the catalysed CO₂ reduction, the state of the art will be focused on molecular species. Indeed, this work aims to be a preliminary approach to this articulate and wide area of artificial photosynthesis. As our laboratory skills and knowledge highlight molecular compounds the study was addressed to this direction.

The catalysts will be presented dividing complexes on the nature of the metal on which they are based: noble and Earth-abundant metals.

1.7.1 Noble metals-based catalysts

The tricarbonyl Rhenium complexes are a big group of catalysts having received great attention for both photochemical and electrochemical CO₂ catalytic reduction. Lehn et al. first analysed the [Re^I(bpy)(CO)₃Cl] species ⁽¹⁴⁷⁾ in homogeneous conditions, achieving quantum yield of 14% and Faradaic efficiency of 98%. Then Ishitani's group analysed similar catalyst, the [Re(bpy)(CO)₃{P(OEt)₃}]⁺, achieving a quantum yield of 0.38. ⁽¹⁴⁸⁾ Moreover, among different mechanistic insights a systematic study of electrochemical CO₂ reduction catalysed by Re(CO)₃LCl (L = bpy, dcbpy, dmbpy, 4,4'-di-*tert*-butyl-bpy, or 4,4'-dimethoxy-bpy) underlined the relevant effect of electron donating or withdrawing nature of 4,4' positioned bipyridine ligands. ⁽¹⁴⁹⁾ Furthermore, in the photochemical system these catalysts have been addressed to the design of dyads where the Rhenium complex is covalently linked to a photosensitizer, generally derivatives of Ru(bpy)₃²⁺. The goal of this approach consists in enhancing the ET rate from the sensitizer to the catalyst in order to promote the entire process and maximize the quantum yield.

Another noble metal-based catalyst is the [Ir^{III}(tpy)(ppy)Cl]⁺ (tpy = terpyridine, ppy = 2-phenylpyridine) proposed by Ishitani et al. ⁽¹⁵⁰⁾ The compound catalyses selectively the reduction of CO₂ to CO under visible light at 480 nm in the presence of a sacrificial electron donor, no additional photosensitizer is needed. In particular, the modified [Ir^{III}(tpy)(Me-ppy)Cl]⁺ reported a quantum yield of

0.21, which is the best value present in literature for homogeneous photocatalytic system using low-energy visible light.

In the class of CO₂ reduction catalysts, there are some other few examples of polypyridyl complexes with Ruthenium and Osmium. The [Ru(bpy)₂(CO)₂]²⁺ is used in protic solvents to obtain carbon monoxide and formic acid from the electro or photochemical activation of CO₂.⁽¹⁵¹⁾ From the dicationic species in CV experiments the neutral [Ru(bpy)₂(CO)] is formed with an irreversible two electrons process at -0.76 V vs NHE and evolution of CO.

In addition, *cis*-[Os(bpy)₂(CO)H]⁺ has been studied for the activation of CO₂ to CO as major product and formate.⁽¹⁵²⁾

Du Bois et al. showed other organic ligands as phosphine exploitable in the synthesis of Pt complexes generally represented as [Pd^{II}(PR₃)(CH₃CN)](BF₄)₂.⁽¹⁵³⁾ The phosphine potential is the control on the number and position of solvent molecules able to coordinate on the metallic centre, while the CO₂ is linked when the Pd^{II} is reduced to Pd^I. This class of catalysts is highly selective for the production of CO, more the dimeric complexes turned out to enhance the catalytic reaction.

Regarding Ruthenium, Neumann et al. reported the POM species [Ru^{III}(H₂O)(SiW₁₁O₃₉)]⁵⁻,⁽¹⁵⁴⁾ which catalyses the reduction of CO₂, after its coordination, in the presence of amines as electron donors in a photoactivated system. The system presents low efficiency but opened the perspective to a new class of totally inorganic catalysts.

1.7.2 Earth-abundant catalysts

Among tricarbonyl bipyridyl complexes seen above, there is an interesting example also with an Earth-abundant metal: the Mn^I(bpy)(CO)₃Br is reported to be the precursor of an active species able to electrocatalyse CO₂ reduction.⁽¹⁵⁵⁾ The Mn^I complex yields CO as major product with a TON of 13, the value is highly enhanced in the photocatalytic system in presence of mixed solvent N,N'-dimethylformamide and triethanolamine and [Ru(dmb)₃]²⁺/1-benzyl-1,4-dihydronicotinamide as photosensitizer/reductant. The formic acid is produced with great selectivity achieving a TON of 149 irradiating with monochromatic

light ($\lambda = 480 \text{ nm}$) and under CO_2 atmosphere. ⁽¹⁵⁶⁾ In both cases the formation of a dimeric species is the key of the process, even if the identification of the real catalyst is still in progress since the major product changes according with the system studied.

Porphyrin metal complexes occupy large space in literature, in particular Iron and Cobalt species are widely studied. It has been reported that Fe^{II} porphyrin, when reduced to Fe^0 , yields to a durable, efficient and CO -selective CO_2 electroreduction. However, a real breakthrough was introduced by the group of Savéant with the modified Fe-tetracarboxyphenyl porphyrine (Fe-TPP). ⁽¹⁵⁷⁾ The modification consists in adding phenolic groups in all *ortho* and *ortho'* position of the phenyl groups of TPP Fig. 1.21 a). They were able to reach a Faradaic yield of 90% in CO , a TON = 50×10^6 over 4 hours of electrolysis at a low overpotential of 465 mV, without catalyst degradation. The high performance is reasonably ascribed to the introduced local concentration of protons due to the phenolic substituents.

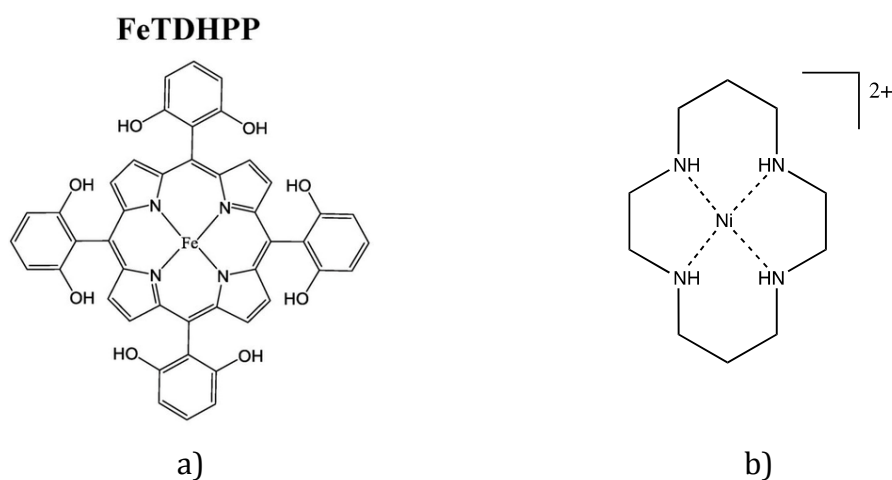


Fig. 1.21: Structure of **a)** the Iron 5, 10, 15, 20-tetrakis(2',6'-dihydroxyphenyl)-porphyrin ⁽¹⁵⁷⁾ and **b)** the $\text{Ni}(\text{cyclam})^{2+}$ catalyst

Another example of highly selective- CO and stable catalyst for the electroreduction of CO_2 is $\text{Ni}(\text{cyclam})^{2+}$ (cyclam = 1,4,8,11-tetraazatetradecane), Fig. 1.21 b). ⁽¹⁵⁸⁾ No relevant deactivation was observed after thousands of catalytic cycles and later different groups reported observations on the mechanistic pathways. ⁽¹⁵⁹⁾ Abba et al. also suggested that the cyclam and azacyclam framework is fundamental to enhance the efficiency of $\text{Ni}(\text{cyclam})^{2+}$

catalyst and its structural derivatives. ⁽¹⁶⁰⁾ They found out that even small geometrical variations of the ligands can inhibit the electrocatalytic activity.

Other examples of catalysts are based on tetraazamacrocycles, phtalocyanine and corroles but they are reported to be less active towards CO₂ electroreduction than their porphyrine analogues. ⁽¹⁶¹⁾

Nowadays the development of CO₂ reduction catalysts seems to be still far from the commercialization of devices; literature suggests some possible ideas for new progress focus on 1) the enhance of the catalytic activity and stability, 2) the implement of the understanding through experiments and theoretical modelling, 3) the improvement of electrodes, reactors, and system designs for practical applications. ⁽¹⁶¹⁾

1.8 Aim of this thesis

The main goal of this thesis is the development and the study of catalytic redox processes involved in artificial photosynthesis. Both water oxidation and CO₂ reduction have been treated with a particular care for “*green*” solution. This work is particularly focused on Earth-abundant metals, and on light activated catalysis.

The final purpose is not only present unique solutions to the energy issue but rather a method to reach a better understanding through optimized experimental conditions and mechanistic insights. Indeed with these instruments in our hands we can think how to evolve the direction of the research.

1.9 References

¹ World Energy Council, 2014, World Energy Issues Monitor

² N. Armaroli, V. Balzani *Angew Chem Int Ed*, **2007**, *46*, 52

³ *The EU in the world 2012, A statistical portrait*, Eurostat Statistical books, **2014**

⁴ *EU energy in figures, Statistical pocketbook*, 2014, European Commission

-
- ⁵ G. Ciamician, from general speech *La Fotochimica dell'avvenire*, New York, 1912, Zanichelli, 1913
- ⁶ N. S. Lewis, D. G. Nocera *Proc Natl Acad Sci USA*, **2006**, *103* (43), 15729
- ⁷ Data from *United Nation, Department of Economic and Social Affairs, Population division*, <http://www.un.org>
- ⁸ V. Balzani, A. Credi, M. Venturi *ChemSusChem*, **2008**, *1*, 26
- ⁹ J. Barber *Chem Soc Rev*, **2009**, *38*, 185
- ¹⁰ A. Sartorel, M. Bonchio, S. Campagna, F. Scandola *Chem Soc Rev*, **2013**, *42*, 2262
- ¹¹ Figure modified by P. Schürmann, **2010**, from Y. Meyer, B.B. Buchanan, F. Vignols, J. P. Reichheld *Thioredoxins and Glutaredoxins: Unifying Elements in Redox Biology*, *Annu Rev Genet*, **2009**, *43*, 335
- ¹² H. van Amerongen, L. Valkunas, R. van Grondelle *Photosynthetic Excitons*, World Scientific, Singapore, **2000**
- ¹³ K. N. Ferreira, T. M. Iverson, K. Maghlaoui, J. Barber, S. Iwata *Science*, **2004**, *303*, 1831
- ¹⁴ B. Loll, J. Kern, W. Saenger, A. Zouni, J. Biesiadka *Nature*, **2005**, *438*, 1040
- ¹⁵ J. Barber *Inorg Chem*, **2008**, *47*, 1700
- ¹⁶ Y. Umena, K. Kawakami, J.-R. Shen, N. Kamiya *Nature*, **2011**, *473*, 55
- ¹⁷ M. Suga, F. Akita, K. Hirata, G. Ueno, H. Murakami, Y. Nakajima, T. Shimizu, K. Yamashita, M. Yamamoto, H. Ago, J.-R. Shen *Nature*, **2014**, DOI: 10.1038/nature13991
- ¹⁸ B. Kok, B. Forbush, M. McGloin *Photochem Photobiol*, **1970**, *11*, 457
- ¹⁹ J. P. McEvoy, G. W. Brudvig *Chem Rev*, **2006**, *106*, 4455
- ²⁰ T.J. Meyer *Nature*, **2008**, *451*, 778
- ²¹ J. H. Alstrum-Acevedo, M. K. Brennaman, T. J. Meyer *Inorg Chem*, **2005**, *44*, 6082
- ²² Y. Oh, X. Hu *Chem Soc Rev*, **2013**, *42*, 2253
- ²³ E. Fujita *Coord Chem Rev*, **1999**, *185-186*, 373
- ²⁴ J. Schneider, H. Jia, J. T. Muckerman, E. *Chem Soc Rev*, **2012**, *41*, 2036
- ²⁵ M. D. Kärkäs, O. Verho, E. V. Johnston, B. Åkermark *Chem Rev*, **2014**, DOI: [dx.doi.org/10.1021/cr400572f](https://doi.org/10.1021/cr400572f)
- ²⁶ K. S. Joya, Y. F. Joya, K. Ocaoglu, R. van de Krol *Angew Chem Int Ed*, **2013**, *52*, 10426
- ²⁷ J. R. Swierk, T. E. Mallouk *Chem Soc Rev*, **2013**, *42*, 2357
- ²⁸ K. S. Joya, J. L. Valleś-Pardo, Y. F. Joya, T. Eisenmayer, B. Thomas, F. Buda, H. J. M. de Groot *ChemPlusChem*, **2013**, *78*, 35
- ²⁹ A. R. Parent, R. H. Crabtree, G. W. Brudvig *Chem Soc Rev*, **2013**, *42*, 2247
- ³⁰ V. Nair, A. Deepthi *Chem Rev*, **2007**, *107*, 1862
- ³¹ E. Wadsworth, F. R. Duke, C. A. Goetz *Anal Chem*, **1957**, *29*, 1824
- ³² A. Ikeda-Ohno, S. Tsushima, C. Hennig, T. Yaitab, G. Bernhard *Dalton Trans*, **2012**, *41*, 7190
- ³³ A. Robert, B. Meunier *New J Chem*, **1988**, *12*, 885
- ³⁴ J. Limburg, R. H. Crabtree, G. W. Brudvig *Inorg Chim Acta*, **2000**, *297*, 301
- ³⁵ L. K. Weavers, I. Hua, M. R. Hoffmann *Water Environ Res*, **1997**, *69*, 1112

-
- ³⁶ P. K. Ghosh, B. S. Brunshwig, M. Chou, C. Creutz, N. Sutin *J Am Chem Soc*, **1984**, *106*, 4772
- ³⁷ F. Bolletta, A. Juris, M. Maestri, D. Sandrini *Inorg Chim Acta*, **1980**, *44*, L175
- ³⁸ B. C. Gau, H. Chen, Y. Zhang, M. L. Gross *Anal Chem*, **2010**, *82*, 7821
- ³⁹ G. Navon, N. Sutin *Inorg Chem*, **1974**, *13*, 2159
- ⁴⁰ E. S. Rountree, B. D. McCarthy, T. T. Eisenhart, J. L. Dempsey *Inorg Chem*, **2014**, *53*, 9983
- ⁴¹ A. J. Bard, L. R. Faulkner *Electrochemical Methods: Fundamentals and Applications*, 2nd ed., John Wiley & Sons, Inc.: Hoboken, NJ, **2001**
- ⁴² C. Constentin, J.-M. Savéant *ChemElectroChem*, **2014**, *1*, 1226
- ⁴³ C. Constentin, S. Drouet, M. Robert, J.-M. Savéant *J Am Chem Soc*, **2012**, *134*, 11235
- ⁴⁴ H. Inoue, T. Shimada, Y. Kou, Y. Nabetani, D. Masui, S. Takagi, H. Tachibana *ChemSusChem* **2011**, *4*, 173
- ⁴⁵ T. Nakagawa, C. A. Beasley, R. W. Murray *J Phys Chem C*, **2009**, *113*, 12958
- ⁴⁶ A. Mills, P. A. Duckmanton, J. Reglinski *Chem Commun*, **2010**, *46*, 2397
- ⁴⁷ M. Hara, C.C. Waraksa, J. T. Lean, B. A. Lewis, T. E. Mallouk *J Phys Chem A*, **2000**, *104*, 5275
- ⁴⁸ M. Hara, J. T. Lean, T. E. Mallouk *Chem Mater*, **2001**, *13*, 4668
- ⁴⁹ N. D. Morris, M. Suzuki, T. E. Mallouk *J Phys Chem A*, **2004**, *108*, 9115
- ⁵⁰ P. G. Hoertz, Y. I. Kim, W. J. Youngblood, T. E. Mallouk *J Phys Chem B*, **2007**, *111*, 6845
- ⁵¹ W. J. Youngblood, S.-H. A. Lee, Y. Kobayashi, E. A. Hernandez-Pegan, P. G. Hoertz, T. A. Moore, A. L. Moore, D. Gust, T. E. Mallouk *J Am Chem Soc*, **2009**, *131*, 926
- ⁵² G. La Ganga, F. Nastasi, S. Campagna, F. Puntoriero *Dalton Trans*, **2009**, 9997
- ⁵³ F. Puntoriero, A. Sartorel, M. Orlandi, G. La Ganga, S. Serroni, M. Bonchio, F. Scandola, S. Campagna *Coord Chem Rev*, **2011**, *255*, 2594
- ⁵⁴ S. D. Tilley, M. Cornuz, K. Sivula, M. Grätzel *Angew Chem Int Ed*, **2010**, *49*, 6405
- ⁵⁵ J. Kiwi, M. Grätzel *Angew Chem*, **1979**, *18*, 624
- ⁵⁶ K. Kalyanasundaram, M. Grätzel *Angew Chem Int Ed*, **1979**, *18*, 701
- ⁵⁷ K. Okeyoshi, R. Yoshida *Adv Funct Mater*, **2010**, *20*, 708
- ⁵⁸ K. C. Pillai, A. S. Kumar, J.-M. Zen *J Mol Catal A: Chem*, **2000**, *160*, 277
- ⁵⁹ V. Y. Shafirovich, N. K. Khannanov, V. V. Strelets *Nouv J Chim*, **1980**, *4*, 81
- ⁶⁰ B. S. Brunshwig, M. H. Chou, C. Creutz, P. Ghosh, N. Sutin *J Am Chem Soc*, **1983**, *105*, 4832
- ⁶¹ V. Artero, M. Fontecave *Chem Soc Rev*, **2013**, *42*, 2338
- ⁶² a) M. Morita, C. Iwakura, H. Tamura *Electrochim Acta*, **1979**, *24*, 357; b) M. Morita, C. Iwakura, H. Tamura *Electrochim Acta*, **1977**, *22*, 325
- ⁶³ T. Takashima, K. Hashimoto, R. Nakamura *J Am Chem Soc*, **2012**, *134*, 1519
- ⁶⁴ I. Zaharieva, P. Chernev, M. Risch, K. Klingan, M. Kohlhoff, A. Fischerb, H. Dau *Energy Environ Sci*, **2012**, *5*, 7081
- ⁶⁵ M. M. Najafpour, S. Nayeri, B. Pashaei *Dalton Trans*, **2011**, *40*, 9374
- ⁶⁶ M. M. Najafpour, M. A. Tabrizi, B. Haghighi, Govindjee *Dalton Trans*, **2012**, *41*, 3906
- ⁶⁷ D. M. Robinson, Y. B. Go, M. Greenblatt, G. C. Dismukes *J Am Chem Soc*, **2010**, *132*, 11467
- ⁶⁸ F. Jiao, H. Frei *Chem Commun*, **2010**, *46*, 2920

-
- ⁶⁹ M. M. Najafpour, T. Ehrenberg, M. Wiechen, P. Kurz *Angew Chem Int Ed*, **2010**, *49*, 2233
- ⁷⁰ M. W. Kanan, J. Yano, Y. Surendranath, M. Dincă, V. K. Yachandra, D. G. Nocera *J Am Chem Soc*, **2010**, *132*, 13692
- ⁷¹ M. W. Kanan, D. G. Nocera *Science*, **2008**, *321*, 1072
- ⁷² M. W. Kanan, Y. Surendranath, D. G. Nocera *Chem Soc Rev*, **2009**, *38*, 109
- ⁷³ D. G. Nocera *Acc Chem Res*, **2012**, *45*, 767
- ⁷⁴ J. G. Mc Alpin, Y. Surendranath, M. Dincă, T. A. Stich, S. A. Stoian, W. H. Casey, D. G. Nocera, R. D. Britt *J Am Chem Soc*, **2010**, *132*, 6882
- ⁷⁵ Y. Surendranath, M. W. Kanan, D. G. Nocera *J Am Chem Soc*, **2010**, *132*, 16501
- ⁷⁶ S. Y. Reece, J. A. Hamel, K. Sung, T. D. Jarvi, A. J. Esswein, J. J. H. Pijpers, D. G. Nocera *Science*, **2011**, *334*, 645
- ⁷⁷ M. Dincă, Y. Surendranath, D. G. Nocera *Proc Natl Acad Sci USA*, **2010**, *107* (23), 10337
- ⁷⁸ Y. Cong, M. Chen, T. Xu, Y. Zhang, Q. Wang *Appl Catal B Environ*, **2014**, *147*, 733
- ⁷⁹ Z. Chen, T. J. Meyer *Angew Chem Int Ed*, **2013**, *52*, 700
- ⁸⁰ R. Brimblecombe, G. C. Dismukes, G. F. Swiegers, L. Spiccia *Dalton Trans*, **2009**, 9347
- ⁸¹ X. Sala, I. Romero, M. Rodriguez, L. Escriche, A. Llobet *Angew Chem Int Ed*, **2009**, *48*, 2842
- ⁸² L. Li, L. L. Duan, Y. H. Xu, M. Gorlov, A. Hagfeldt, L. C. Sun *Chem Commun*, **2010**, *46*, 7307
- ⁸³ B. Limburg, E. Bouwman, S. Bonnet *Coord Chem Rev*, **2012**, *256*, 1451
- ⁸⁴ S. W. Gersten, G. J. Samuels, T. J. Meyer *J Am Chem Soc*, **1982**, *104*, 4029
- ⁸⁵ F. Liu, J. J. Concepcion, J. W. Jurss, T. Cardolaccia, J. L. Templeton, T. J. Meyer *Inorg Chem*, **2008**, *47*, 1727
- ⁸⁶ J. P. Collin, J. P. Sauvage *Inorg Chem*, **1986**, *25*, 135
- ⁸⁷ K. Nagoshi, S. Yamashita, M. Yagi, M. Kaneko *J Mol Catal A: Chem*, **1999**, *144*, 71
- ⁸⁸ C. Sens, I. Romero, M. Rodríguez, A. Llobet, T. Parella, J. Benet-Buchholz *J Am Chem Soc*, **2004**, *126*, 7798
- ⁸⁹ L. Duan, F. Bozoglian, S. Mandal, B. Stewart, T. Privalov, A. Llobet, L. Sun *Nat Chem*, **2012**, *4*, 418
- ⁹⁰ H. Lv, Y. V. Geletii, C. Zhao, J. W. Vickers, G. Zhu, Z. Luo, J. Song, T. Lian, D. G. Musaev, C. L. Hill *Chem Soc Rev*, **2012**, *41*, 7572
- ⁹¹ D. L. Long, E. Burkholder, L. Cronin *Chem Soc Rev*, **2007**, *36*, 105
- ⁹² B. S. Bassil, M. Ibrahim, R. Al-Oweini, M. Asano, Z. Wang, J. van Tol, N. S. Dalal, K.-Y. Choi, R. N. Biboum, B. Keita, L. Nadjjo, U. Kortz *Angew Chem Int Ed*, **2011**, *50*, 5961
- ⁹³ S. S. Mal, U. Kortz *Angew Chem Int Ed*, **2005**, *44*, 3777
- ⁹⁴ A. Sartorel, M. Carraro, G. Scorrano, R. D. Zorzi, S. Geremia, N. D. McDaniel, S. Bernhard, M. Bonchio *J Am Chem Soc*, **2008**, *130*, 5006
- ⁹⁵ Y. V. Geletii, B. Botar, P. Kögerler, D. A. Hillesheim, D. G. Musaev, C. L. Hill *Angew Chem Int Ed*, **2008**, *47*, 3896
- ⁹⁶ Y. V. Geletii, Z. Huang, Y. Hou, D. G. Musaev, T. Lian, C. L. Hill *J Am Chem Soc*, **2009**, *131*, 7522

-
- ⁹⁷ M. Orlandi, R. Argazzi, A. Sartorel, M. Carraro, G. Scorrano, M. Bonchio, F. Scandola *Chem Commun*, **2010**, 46, 3152
- ⁹⁸ F. Puntoriero, G. L. Ganga, A. Sartorel, M. Carraro, G. Scorrano, M. Bonchio, S. Campagna *Chem Commun*, **2010**, 46, 4725
- ⁹⁹ A. Sartorel, P. Miro', E. Salvadori, S. Romain, M. Carraro, G. Scorrano, M. Di Valentin, A. Llobet, C. Bo, M. Bonchio *J Am Chem Soc*, **2009**, 131, 16051
- ¹⁰⁰ Y. V. Geletii, C. Besson, Y. Hou, Q. Yin, D. G. Musaev, D. Quiñonero, R. Cao, K. I. Hardcastle, A. Proust, P. Kögerler, C. L. Hill *J Am Chem Soc*, **2009**, 131, 17360
- ¹⁰¹ Z. Chen, J. J. Concepcion, X. Hu, W. Yang, P. G. Hoertz, T. J. Meyer *Proc Nat Acad Sci U. S. A.*, **2010**, 107, 7225
- ¹⁰² F. M. Toma, A. Sartorel, M. Iurlo, M. Carraro, P. Parisse, C. Maccato, S. Rapino, B. Rodriguez Gonzalez, H. Amenitsch, T. Da Ros, L. Casalis, A. Goldoni, M. Marcaccio, G. Scorrano, G. Scoles, F. Paolucci, M. Prato, M. Bonchio *Nat Chem*, **2010**, 2, 826
- ¹⁰³ F. M. Toma, A. Sartorel, M. Iurlo, M. Carraro, S. Rapino, L. Hooper-Burkhardt, T. Da Ros, M. Marcaccio, G. Scorrano, F. Paolucci, M. Bonchio, M. Prato *ChemSusChem*, **2011**, 4, 1447
- ¹⁰⁴ A. Sartorel, M. Truccolo, S. Berardi, M. Gardan, M. Carraro, F. M. Toma, G. Scorrano, M. Prato, M. Bonchio *Chem Commun*, **2011**, 47, 1716
- ¹⁰⁵ N. D. McDaniel, F. J. Coughlin, L. L. Tinker, S. Bernhard *J Am Chem Soc*, **2008**, 130, 210
- ¹⁰⁶ a) J. F. Hull, D. Balcells, J. D. Blakemore, C. D. Incarvito, O. Eisenstein, G. W. Brudvig, R. H. Crabtree *J Am Chem Soc*, **2009**, 131, 8730; b) J. D. Blakemore, N. D. Schley, D. Balcells, J. F. Hull, G. W. Olack, C. D. Incarvito, O. Eisenstein, G. W. Brudvig, R. H. Crabtree *J Am Chem Soc*, **2010**, 132, 16017; c) A. Savini, P. Belanzoni, G. Bellachioma, C. Zuccaccia, D. Zuccaccia, A. Macchioni *Green Chem*, **2011**, 13, 3360
- ¹⁰⁷ N. D. Schley, J. D. Blakemore, N. K. Subbaiyan, C. D. Incarvito, F. D'Souza, R. H. Crabtree, G. W. Brudvig *J Am Chem Soc*, **2011**, 133, 10473
- ¹⁰⁸ C. Wang, J.-L. Wang, W. Lin *J Am Chem Soc*, **2012**, 134, 19895
- ¹⁰⁹ A. Savini, G. Bellachioma, G. Ciancaleoni, C. Zuccaccia, D. Zuccaccia, A. Macchioni *Chem Commun*, **2010**, 46, 9218
- ¹¹⁰ a) A. Bucci, A. Savini, L. Rocchigiani, C. Zuccaccia, S. Rizzato, A. Albinati, A. Llobet, A. Macchioni *Organometallics*, **2012**, 31, 8071; b) W. I. Dzik, S. E. Calvo, J. N. H. Reek, M. Lutz, M. A. Ciriano, C. Tejel, D. G. H. Hettterscheid, B. de Bruin *Organometallics*, **2011**, 30, 372
- ¹¹¹ A. Savini, G. Bellachioma, S. Bolano, L. Rocchigiani, C. Zuccaccia, D. Zuccaccia, A. Macchioni *ChemSusChem*, **2012**, 5, 1415
- ¹¹² R. Cao, H. Ma, Y. V. Geletii, K. I. Hardcastle, C. L. Hill *Inorg Chem*, **2009**, 48, 5596
- ¹¹³ a) D. G. H. Hettterscheid, J. N. H. Reek *Angew Chem Int Ed*, **2012**, 51, 9740; b) R. Lalrempuia, N. D. McDaniel, H. Müller-Bunz, S. Bernhard, M. Albrecht *Angew Chem*, **2010**, 122, 9959; *Angew Chem Int Ed*, **2010**, 49, 9765; c) T. P. Brewster, J. D. Blakemore, N. D. Schley, C. D. Incarvito, N. Hazari, G. W. Brudvig, R. H. Crabtree *Organometallics*, **2011**, 30, 965; d) A. R. Parent, J. D. Blakemore, G. W. Brudvig, R. H. Crabtree *Chem Commun*, **2011**, 47, 11745; e) J.

-
- D. Blakemore, N. D. Schley, G. W. Olack, C. D. Incarvito, G. W. Brudvig, R. H. Crabtree *Chem Sci*, **2011**, *2*, 94; f) A. R. Parent, T. P. Brewster, W. De Wolf, R. H. Crabtree, G. W. Brudvig *Inorg Chem*, **2012**, *51*, 6147; g) A. Volpe, A. Sartorel, C. Tubaro, L. Meneghini, M. Di Valentin, C. Graiff, M. Bonchio *Eur J Inorg Chem*, **2014**, 665.
- ¹¹⁴ (a) J. D. Blakemore, M. W. Mara, M. N. Kushner-Lenhoff, N. D. Schley, S. J. Konezny, I. Rivalta, C. F. A. Negre, R. C. Snoeberger, O. Kokhan, J. Huang, A. Stickrath, L. A. Tran, M. L. Parr, L. X. Chen, D. M. Tiede, V. S. Batista, R. H. Crabtree, G. W. Brudvig *Inorg Chem*, **2013**, *52*, 1860; (b) J. Huang, J. D. Blakemore, D. Fazi, O. Kokhan, N. D. Schley, R. H. Crabtree, G. W. Brudvig, D. M. Tiede *Phys Chem Chem Phys*, **2014**, *16*, 1814
- ¹¹⁵ J. M. Thomsen, S. W. Sheehan, S. M. Hashmi, J. Campos, U. Hintermair, R. H. Crabtree, G. W. Brudvig, *J Am Chem Soc* **2014**, *136*, 13826
- ¹¹⁶ O. Diaz Morales, T. J. P. Hersbach, D. G. Hettterscheid, J. N. H. Reek, M. T. M. Koper, *J Am Chem Soc* **2014**, *136*, 10432
- ¹¹⁷ L. Sun, L. Hammarström, B. Åkermark, S. Styring *Chem Soc Rev*, **2001**, *30*, 36
- ¹¹⁸ J. Limburg, J. S. Vrettos, L. M. Liable-Sands, A. L. Rheingold, R. H. Crabtree, G. W. Brudvig *Science*, **1999**, *283*, 1524
- ¹¹⁹ M. M. Najafpour, A. N. Moghaddam, H. Dau, I. Zaharieva *J Am Chem Soc*, **2014**, *136*, 7245
- ¹²⁰ E. Karlsson, B. L. Lee, T. Åkermark, E. Johnston, M. D. Kärkäs, J. Sun, O. Hansson, J. E. Bäckvall, B. Åkermark *Angew Chem Int Ed*, **2011**, *50*, 11715
- ¹²¹ W. Ruettinger, M. Yagi, K. Wolf, S. Bernasek, G. C. Dismukes *J Am Chem Soc*, **2000**, *122*, 10353
- ¹²² M. Yagi, K. V. Wolf, P. J. Baesjou, S. L. Bernasek, G. C. Dismukes, *Angew Chem Int Ed*, **2001**, *40*, 2925
- ¹²³ R. Brimblecome, G. F. Swiegers, G. C. Dismukes, L. Spiccia *Angew Chem Int Ed*, **2008**, *47*, 7335
- ¹²⁴ R. Brimblecome, A. Koo, G. C. Dismukes, G. Swiegers, L. Spiccia *J Am Chem Soc*, **2010**, *132*, 2892
- ¹²⁵ R. K. Hocking, R. Brimblecombe, L.-Y. Chang, A. Singh, M. H. Cheah, C. Glover, W. H. Casey, L. Spiccia *Nature Chem*, **2011**, *3*, 461
- ¹²⁶ R. Al-Oweini, A. Sartorel, B. S. Bassil, M. Natali, S. Berardi, F. Scandola, U. Kortz, M. Bonchio *Angew Chem Int Ed*, **2014**, *53*, 11182
- ¹²⁷ W. C. Ellis, N. D. McDaniel, S. Bernhard, T. J. Collins *J Am Chem Soc*, **2010**, *132*, 10990
- ¹²⁸ J. Lloret Fillol, Z. Codolà, I. Garcia-Bosch, L. Gómez, J. J. Pla, M. Costas *Nat Chem*, **2011**, *3*, 807
- ¹²⁹ G. Chen, L. Chen, S.-M. Ng, W.-L. Man, T.-C. Lau *Angew Chem Int Ed*, **2013**, *52*, 178
- ¹³⁰ D. Wasylenko, C. Ganesamoorthy, J. Borau-Garcia, C. Berlinguette *Chem Commun*, **2011**, *47*, 4249
- ¹³¹ D. J. Wasylenko, R. D. Palmer, E. Schott, C. P. Berlinguette *Chem Commun*, **2012**, *48*, 2107
- ¹³² H. Lei, A. Han, F. Li, M. Zhang, Y. Han, P. Du, W. Lai, R. Cao *Phys Chem Chem Phys*, **2014**, *16*, 1883
- ¹³³ D. Wang, J. T. Groves *Proc Natl Acad Sci USA*, **2013**, *110* (39), 15579
- ¹³⁴ T. Nakazono, A. R. Parent, K. Sakai *Chem Commun*, **2013**, *49*, 6325

-
- 135 C.-F. Leung, S.-M. Ng, C.-C. Ko, W.-L. Man, J. Wu, L. Chen, T.-C. Lau *Energy Environ Sci*, **2012**, *5*, 7903
- 136 Q. Yin, J. M. Tan, C. Besson, Y. V. Geletii, D. G. Musaev, A. E. Kuznetsov, Z. Luo, K. I. Hardcastle, C. L. Hill *Science*, **2010**, *328*, 342
- 137 Z. Huang, Z. Luo, Y. V. Geletii, J. W. Vickers, Q. Yin, D. Wu, Y. Hou, Y. Ding, J. Song, D. G. Musaev, C. L. Hill, T. Lian *J Am Chem Soc*, **2011**, *133*, 2068
- 138 J. J. Stracke, R. G. Finke *J Am Chem Soc*, **2011**, *133*, 14872
- 139 M. Natali, S. Berardi, A. Sartorel, M. Bonchio, S. Campagna, F. Scandola *Chem Commun*, **2012**, *48*, 8808
- 140 H. Lv, J. Song, Y. V. Geletii, J. W. Vickers, J. M. Sumliner, D. G. Musaev, P. Kögerler, P. F. Zhuk, J. Bacsá, G. Zhu, C. L. Hill *J Am Chem Soc*, **2014**, *136*, 9268
- 141 D. Hong, J. Jung, J. Park, Y. Yamada, T. Suenobu, Y.-M. Lee, W. Nam, S. Fukuzumi *Energy Environ Sci*, **2012**, *5*, 7606
- 142 M. Zhang, M.-T. Zhang, C. Hou, Z.-F. Ke, T.-B. Lu *Angew Chem Int Ed*, **2014**, *53*, 13042
- 143 S. M. Barnett, K. I. Goldberg, J. M. Mayer *Nat Chem*, **2012**, *4*, 498
- 144 M.-T. Zhang, Z. Chen, P. Kang, T. J. Meyer *J Am Chem Soc*, **2013**, *135*, 2048
- 145 M. K. Coggins, M.-T. Zhang, Z. Chen, N. Song, T. J. Meyer *Angew Chem Int Ed*, **2014**, *53*, 12226
- 146 T. Zhang, C. Wang, S. Liu, J.-L. Wang, W. Lin *J Am Chem Soc*, **2014**, *136*, 273
- 147 a) J. Hawecker, J. M. Lehn, R. Ziessel *J Chem Soc Chem Commun*, **1984**, 328; b) J. Hawecker, J. M. Lehn, R. Ziessel *Helv Chim Acta*, **1986**, *69*, 1990
- 148 H. Hori, F. P. A. Johnson, K. Koike, O. Ishitani, T. Ibusuki *J Photochem Photobiol A*, **1996**, *96*, 171
- 149 J. M. Smieja, C. P. Kubiak *Inorg Chem*, **2010**, *49*, 9283
- 150 S. Sato, T. Morikawa, T. Kajino, O. Ishitani *Angew Chem Int Ed*, **2013**, *52*, 988
- 151 a) K. Tanaka, D. Ooyama *Coord Chem Rev*, **2002**, *226*, 211; b) H. Nagao, T. Mizukawa, K. Tanaka *Inorg Chem*, **1994**, *33*, 3415; c) D. Oyama, T. Tomon, K. Tsuge, K. Tanaka *J Organomet Chem*, **2001**, *619*, 299
- 152 M. R. M. Bruce, E. Megehee, B. P. Sullivan, H. H. Thorp, T. R. Otooie, A. Downard, J. R. Pug, T. J. Meyer *Inorg Chem*, **1992**, *31*, 4864
- 153 M. R. DuBois, D. L. DuBois *Acc Chem Res*, **2009**, *42*, 1974
- 154 A. M. Khenkin, I. Efremenko, L. Weiner, J. M. L. Martin, R. Neumann *Chem Eur J*, **2010**, *16*, 1356
- 155 a) M. Bourrez, F. Molton, S. Chardon-Noblat, A. Deronzier *Angew Chem Int Ed*, **2011**, *50*, 9903; b) J. M. Smieja, M. D. Sampson, K. A. Grice, E. E. Benson, J. D. Froehlich, C. P. Kubiak *Inorg Chem*, **2013**, *52*, 2484
- 156 H. Takeda, H. Koizumi, K. Okamoto, O. Ishitani *Chem Commun*, **2014**, *50*, 1491
- 157 C. Costentin, S. Drouet, M. Robert, J.-M. Savéant *Science*, **2012**, *338*, 90
- 158 a) M. Beley, J. P. Collin, R. Ruppert, J. P. Sauvage *J Chem Soc Chem Commun*, **1984**, 1315; b) M. Beley, J. P. Collin, R. Ruppert, J. P. Sauvage *J Am Chem Soc*, **1986**, *108*, 7461
- 159 a) S. Sakaki *J Am Chem Soc*, **1992**, *114*, 2055; b) G. B. Balazs, F. C. Anson *J Electroanal Chem*, **1992**, *322*, 325

¹⁶⁰ F. Abba, G. Desantis, L. Fabbrizzi, M. Licchelli, A. M. M. Lanfredi, P. Pallavicini, A. Poggi, F. Ugozzoli *Inorg Chem*, **1994**, *33*, 1366

¹⁶¹ J. Qiao, Y. Liu, F. Hong, J. Zhang *Chem Soc Rev*, **2014**, *43*, 631

2. CHAPTER

Cobalt molecular species

2.1 Introduction

The work of this thesis is focused on the study of Earth-abundant species and in particular this chapter and the next one are related to Cobalt species. As already introduced in Chapter 1, artificial photosynthesis needs the presence of catalytic systems in order to perform its associated redox events. As a matter of fact, water oxidation is considered so far the real bottleneck of the entire process and it requires more studies in order to improve its efficiency.

As explained above, in this work we underline molecular species: 1) to clarify mechanistic insights tuning structure and properties, 2) to achieve information of different systems and 3) possibly give an overview to design a final device.

In particular, during the Ph.D. we analysed and characterized some Cobalt-based molecular WOC: 1) a cubane-like species (see section 2.2) and 2) a Co-based multinuclear compound with a totally inorganic polyoxometallate ligand (see Chapter 3).

2.2 A Cobalt-based cubane as WOC

During the first part of this work attention has been focused on a Cobalt-based oxo cluster, water oxidation catalyst with formula $[\text{Co}_4\text{O}_4(\text{O}_2\text{CCH}_3)(\text{py})_4]$ (**1**, py = pyridine). This species was introduced in literature some years ago and used as catalyst in oxidation processes. ^(1,2)

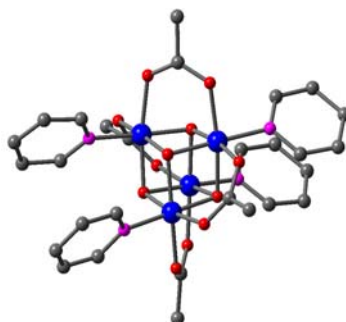


Fig. 2.1: Representation of **1**, blue: Cobalt, red: Oxygen, pink: Nitrogen, grey: Carbon, Hydrogen are no shown for clarity reasons

The X-ray analysis of **1** shows a cubane-like structure Co_4O_4 , stabilized by four acetates ligands bridging two Co atoms and four pyridines as apical ligands of Co. We decided to investigate this molecule in water oxidation catalysis for several reasons: 1) the cubane-like architecture in the coordination of Co atoms was already proposed as a model of the OEC cluster, 2) **1** can be considered as a molecular fragment of the Co-Pi oxide, the Nocera's catalyst, ⁽³⁾ so far one of the most performing WOC, 3) Cobalt is an Earth-abundant metal, with low cost, 4) its catalytic activity in oxidation of organic molecules was already known, ⁽²⁾ 5) organic ligands can be tuned in order to study possible structure-activity correlation.

The species was synthesized and characterized following procedures reported in literature, ⁽²⁾ and the identity of the species was confirmed by $^1\text{H-NMR}$, UV-Vis, FT-IR and ESI-MS techniques. (see section 6.1)

At first, we focused on electrochemical characterization of **1**, by means of cyclic voltammetry (CV) in aqueous solution at pH = 7 (phosphate buffer 0.2 M).

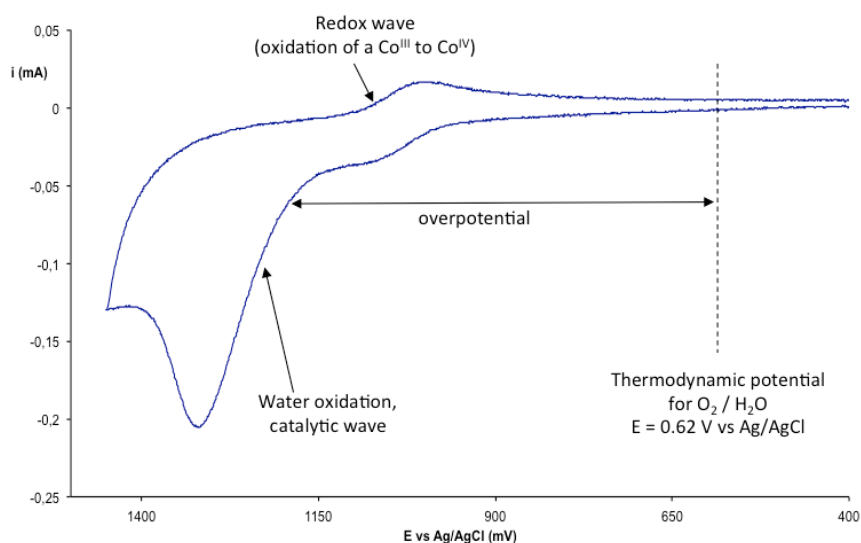


Fig. 2.2: Cyclic voltammetry of **1** in aqueous media: phosphate buffer 0.2 M, pH = 7, [cat] = 0.5 mM, WE: glassy carbon (d = 3mm), CE: Pt wire, RE: Ag/AgCl, scan rate: 100 mV/s

The anodic scan shows a first reversible wave at $E_{1/2} = 1.05$ V vs Ag/AgCl, due to the oxidation of one of the Co^{III} centres to Co^{IV} . This process is then followed by an intense wave due to water oxidation, starting at an onset of 1.17 V vs Ag/AgCl and reaching a current peak at 1.3 V. The overpotential for water oxidation

catalysed by **1** can be determined by the difference between the experimental potential measured at the onset of the catalytic wave and the thermodynamic potential for water oxidation (0.62 V vs Ag/AgCl at pH = 7). In these conditions, an overpotential of 550 mV was obtained, which is comparable to other Co-based system present in literature, but significantly higher than the one measured for the Cobalt oxide catalyst of 280 mV. ^(4,5) The overpotential is a very important parameter in order to evaluate WOC activity: the lowest the overpotential, the best is the catalyst, because it means that less energy is required to activate the electrochemical process.

Moving from the CV characterization, the activity of **1** was investigated in a photo-activated system, ⁽⁶⁾ which is mimicking the light driven activation in an ideal photoactivated device for artificial photosynthesis.

Light-driven water oxidation catalysis was investigated considering a system widely used in literature, ⁽⁷⁾ exploiting Ru(bpy)₃²⁺ (bpy = 2,2'- bipyridine) as photosensitizer and Sodium persulfate (NaS₂O₈) as sacrificial oxidant (electron acceptor).

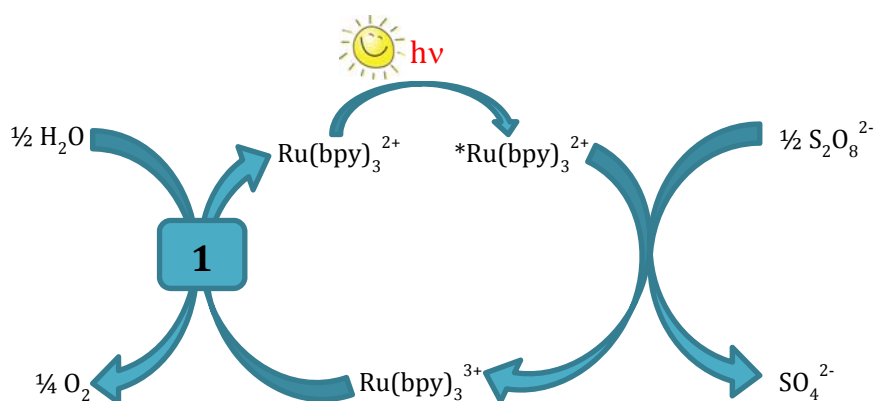
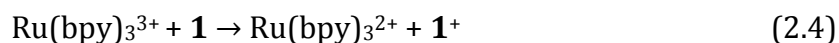
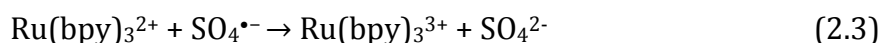
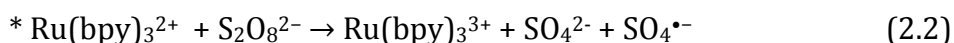
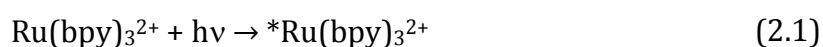


Fig. 2.3: Schematic representation of the photo-induced system

The reaction scheme of the light-driven system is represent in Fig. 2.3: after

absorption of one photon, $\text{Ru}(\text{bpy})_3^{2+}$ is promoted to its excited state $^*\text{Ru}(\text{bpy})_3^{2+}$ (Eq. 2.1), which then reacts transferring an electron to persulfate (oxidative quenching of $^*\text{Ru}(\text{bpy})_3^{2+}$). The result of this electron transfer is the formation of the oxidized form of the photosensitizer, $\text{Ru}(\text{bpy})_3^{3+}$, with contemporary formation of a sulfate ion SO_4^{2-} , and a sulfate radical $\text{SO}_4^{\bullet-}$ (Eq. 2.2). These latter derive from breaking of the O-O bond in persulfate, upon addition of one electron. The sulfate radical $\text{SO}_4^{\bullet-}$ is a strong oxidizing species ($E = 2.4 \text{ V vs NHE}$), and reacts with a second molecule of $\text{Ru}(\text{bpy})_3^{3+}$, forming SO_4^{2-} and $\text{Ru}(\text{bpy})_3^{3+}$ (Eq. 2.3). Therefore, the net result from the absorption of one photon is the conversion of two $\text{Ru}(\text{bpy})_3^{2+}$ to $\text{Ru}(\text{bpy})_3^{3+}$, and transformation of persulfate into sulfate ions.

Then, $\text{Ru}(\text{bpy})_3^{3+}$ acts as a photogenerated oxidant, oxidizing the catalyst **1** (Eq. 2.4), until it reaches the active form, capable of oxidizing water. A high rate of reaction between $\text{Ru}(\text{bpy})_3^{3+}$ and the catalyst is important to guarantee stability of the photosensitizer, since $\text{Ru}(\text{bpy})_3^{3+}$ is susceptible to self degradation, by auto-oxidation of the bpy organic ligands. As a final remark, a comment on the role of the sulfate radical should be given. As mentioned above, this is a high oxidizing species, and in principle it could react directly with the catalyst; this will be also the case for **1** (*vide infra*).

In Fig. 2.4 a typical O_2 evolution kinetic is reported, where the gas formation starts once the solution containing the three components **1** / $\text{Ru}(\text{bpy})_3^{2+}$ / $\text{S}_2\text{O}_8^{2-}$ is irradiated, and stops after about one hour, due to photosensitizer degradation. The common parameters used to evaluate a catalyst activity in this system are: 1) the turn over number (TON), 2) the turn over frequency (TOF) and 3) the quantum yield (QY).

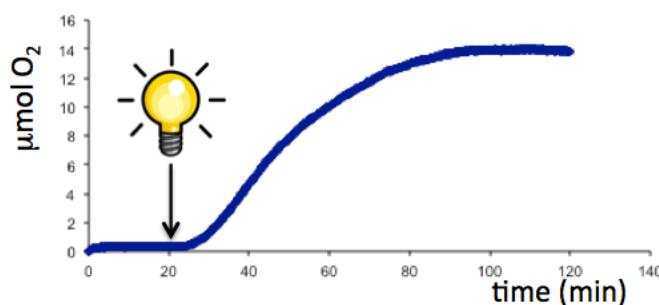


Fig. 2.4: Example of O_2 evolution kinetic, in borate buffer 80 mM, pH = 8, $[\mathbf{1}] = 1.5 \text{ mM}$, $[\text{Rubpy}] = 1 \text{ mM}$, $[\text{S}_2\text{O}_8^{2-}] = 9 \text{ mM}$

A deep screening of different conditions on this system has been done, changing the concentration of the catalyst and the nature of the aqueous buffer used as solvent. The presence of a buffer solution avoids a deep decrease of the pH, since the production of O₂ is contemporary with formation of H⁺. In particular, we focused the attention on phosphate buffer 40 mM pH = 7 and borate buffer 80 mM pH = 8; the catalyst concentrations tested were in the range of 5-100 μM, see Tab. 2.1. ⁽⁶⁾ Herein, our results are compared with those simultaneously reported by the group of Prof. C. Dismukes (Princeton University) ⁽⁸⁾ with the same catalyst.

In the system S₂O₈²⁻/ Ru(bpy)₃²⁺/1, depending on the conditions the number of TON changes, reaching a maximum value of 40 at pH = 7, the production of oxygen is limited by the photodegradation of Ru(bpy)₃²⁺, verified by UV-Vis spectroscopy where a partial abatement of its characteristic absorption at 450 nm is observed. The maximum value of TOF achieved is 0.95×10⁻² s⁻¹, which is comparable to the other photo-induced Co-based systems. ⁽⁹⁾

| | (ref. 6) | Dismukes et al. (ref. 8) |
|----------------------------|--|---|
| Reaction conditions | [1] = 5-100 μM (8 different concentrations); [Ru(bpy) ₃] ²⁺ = 1 mM; [S ₂ O ₈] ²⁻ = 5 mM; in 20 mM phosphate buffer pH = 7 or 80 mM borate buffer pH = 8 | [1] = 50 μM; [Ru(bpy) ₃] ²⁺ = 0.5 mM; [S ₂ O ₈] ²⁻ = 35 mM; [SO ₄] ²⁻ = 70 mM; in HCO ₃ ⁻ buffer pH = 7; SiF ₆ ²⁻ buffer pH = 5.8 and 4.8 |
| TON | 12-40 at pH 7; 23-37 at pH 8 (after 35 min) | 40 (after 60 min) |
| TOF | 0.02 s ⁻¹ * (per catalyst mole) (0.95×10 ⁻² s ⁻¹) | 0.02 s ⁻¹ (per catalyst mole) |
| Quantum yield | 0.10-0.23 at pH 7; 0.18-0.30 at pH 8 | --- |
| Chemical yield | 30-50% at pH 7; 28-34% at pH 8 | 11 % |

Tab. 2.1: Sum up of more interesting features in photoactivated catalytic system with [1] compared with other data presented in literature in quite similar conditions, (* = Condition of maximum Φ: [Co₄cubane] = 1.87 × 10⁻⁵ M; [Ru(bpy)₃]²⁺ = 1 mM; [S₂O₈]²⁻ = 5 mM, in borate buffer 80 mM, pH = 8)

An important parameter in light-driven water oxidation is the quantum yield (ϕ) of the process, defined as the ratio between the amount of generated O_2 and the photons absorbed by the system. ⁽¹⁰⁾ In particular, the dependence of ϕ from the concentration of **1** displays a bell-shaped profile in both tested media (Fig. 2.5). Moreover, the maximum ϕ in the two conditions is obtained at different concentration of **1** (20 μ M at pH = 8 and 70 μ M at pH = 7). It is also worth to mention that in borate buffer, the system reaches a notable quantum yield of 0.30, which is one of the highest values reported so far with $Ru(bpy)_3^{2+}$ as photosensitizer.

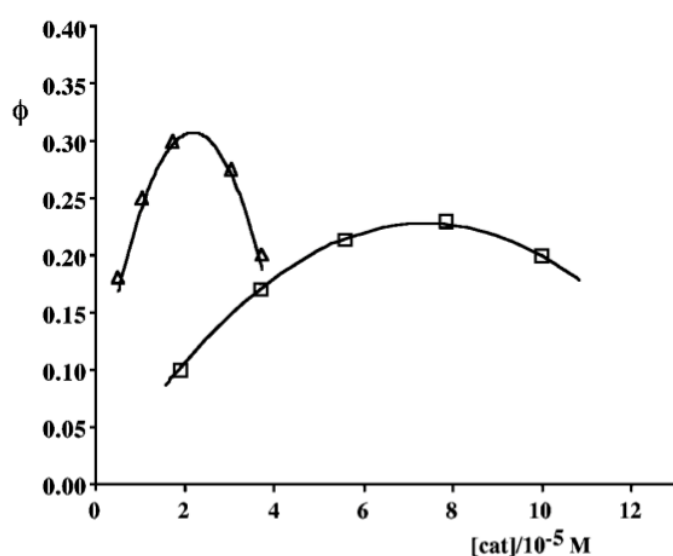


Fig. 2.5: Dependence of photochemical quantum yield for oxygen production vs catalyst concentration. $[Ru(bpy)_3^{2+}] = 1$ mM, $[S_2O_8^{2-}] = 5$ mM, excitation wavelength is 450 nm. Triangles are data in borate buffer at pH = 8, squares are data in phosphate buffer at pH = 7 ⁽⁶⁾

The bell shaped profiles in Fig. 2.5 are likely explained by side reactions involving oxidized forms of the catalyst, more competitive at high catalyst concentration. ⁽⁶⁾ In particular, direct quenching of the excited state of the photosensitizer $*Ru(bpy)_3^{2+}$ by intermediates of **1** may occur, leading to unproductive light absorption.

The high efficiency of the system $S_2O_8^{2-}/Ru(bpy)_3^{2+}/\mathbf{1}$ prompted us to investigate some features of the photoactivated cycle. In particular, the most critical step of such systems is recognized to be the kinetics of electron transfer events from the catalyst to the oxidized photosensitizer, $Ru(bpy)_3^{3+}$. These were measured by

laser flash photolysis experiments in collaboration with the group of Prof. Scandola in Ferrara. Bimolecular rate constants for this process (Eq. 2.4) turned out to be $1.2 \times 10^7 \text{ M}^{-1}\text{s}^{-1}$ and $1.6 \times 10^7 \text{ M}^{-1}\text{s}^{-1}$ at pH = 7 and 8, respectively. These values are one order of magnitude higher than those reported using Iridium oxide nanoparticles, known as one of the most efficient catalysts for water oxidation. ⁽¹¹⁾

The rate constant of the ET (Eq. 2.4) is very important in order to limit photosensitizer decomposition, due to the presence of parallel reactions such as auto-oxidation of its organic ligand. These side pathways imply lower quantum yield and partial deactivation of the photo-catalytic capacity in the whole system. As a final remark, a role of the sulfate radical $\text{SO}_4^{2\cdot-}$ needs to be considering for oxidizing **1** to the active form, capable of oxidizing water. Indeed, the reduction potential of $\text{Ru}(\text{bpy})_3^{3+/2+}$ is 1.06 vs Ag/AgCl, apparently not enough high to carry on water oxidation with **1**, beginning at ca 1.15 V vs Ag/AgCl (pH = 7) and at ca 1.10 V vs Ag/AgCl (pH = 8). Therefore, direct oxidation of **1** by $\text{SO}_4^{2\cdot-}$ is occurring.

2.3 Structure-activity correlation

Exploiting the interesting results and the molecular nature of **1**, we thought to modify the structure of the compound in order to tune its reactivity, focusing in particular on the organic ligands. ⁽¹²⁾

We considered different *para*-substituted pyridines as terminal ligands of the cubane cluster, to exert a direct conjugation to the Co_4O_4 cluster; moreover pyridines are recognized as less labile than acetates. ⁽¹³⁾ For this aim the isostructural series with formula $[\text{Co}^{\text{III}}_4(\mu\text{-O})_4(\mu\text{-CH}_3\text{COO})_4(\text{p-NC}_5\text{H}_4\text{X})_4]$, hereafter **1-X** (**X** = Me, t-Bu, OMe, Br, COOMe, CN), were synthesized and screened as WOC under dark and illumination conditions. The **1-X** species were obtained according to slight changes of the literature protocol for **1**, while their identity and stability in solution were confirmed by ¹H-NMR, ESI-MS, UV-Vis and FT-IR techniques.

The effect of **X** on the catalyst has been evaluated in electrochemical and photo-induced systems and below, in the next sections, results of the structure-activity correlation are reported and discussed. With respect to the studies in aqueous

buffer at pH = 7-8 cited in section 2.2, we decided to use mixed solvent conditions (1:1, acetonitrile:borate buffer 10 mM at pH = 8). The advantages of this medium are related to the longer stability of the photosensitizer, one of the most relevant causes of inhibition in oxygen formation. Indeed, it is known that one of the degradation pathways for $\text{Ru}(\text{bpy})_3^{3+}$ is provided by a first step of OH^- ions attack on bpy ligands, thus moving to a mixed solvent reduces the probability of such events.

2.3.1 Electrochemical potentials

Inspection of the **1-X** WOC properties was initially addressed under dark conditions, by means of cyclic voltammetry. Under anodic scan, the first observed event deals with one electron waves, due to the oxidation of the initial state of the cubane (where all the Cobalt centers have an oxidation state III, Co_4^{III} , identified as S_0 , in analogy with the natural OEC) to a mixed valent intermediate, where one of the atoms in cubane cluster is oxidized to the IV state ($\text{Co}_3^{\text{III}}\text{Co}^{\text{IV}}$, identified as S_1). This process is reversible for all the **1-X** species, and the value of the reduction potential changes with the nature of X, with lower values of $E_{1/2}$ observed for electron donating substituents, and higher values observed for electron-withdrawing groups (Fig. 2.6).

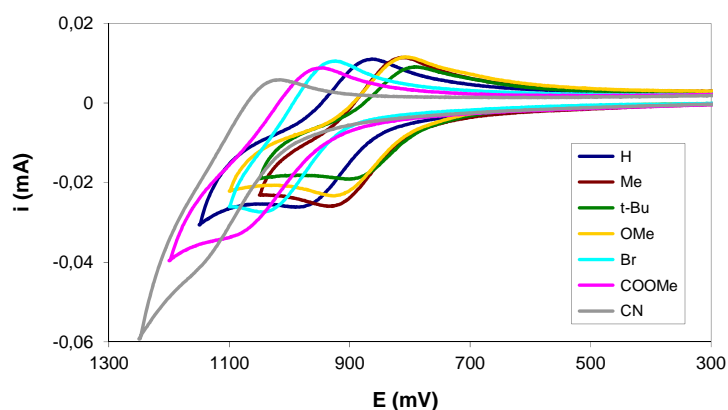


Fig. 2.6: Cyclic voltammograms of 2 mM **1-X** in 1:1= CH_3CN : 40 mM phosphate buffer, pH = 7 (in the absence of **1-X** no appreciable current is observed in this potential range). WE: glassy carbon ($d = 3 \text{ mm}$), CE: Pt wire, RE: Ag/AgCl, scan rate: 100 mV/s ⁽¹²⁾

Interestingly, a correlation between the reduction potential values in the **1-X** series with the Hammett parameter σ can be obtained: the plot of ΔE_x [$\Delta E = E_{1/2}$

(1)- $E_{1/2}$ (**1-X**)] versus σ_X turned out to exhibit a linear dependence with a negative slope, Fig. 2.7. Hence, we could conclude that the first redox event in the cubane series **1-X** is correlated with the electronic nature of the substituent in *para* position of the pyridinic ligands.

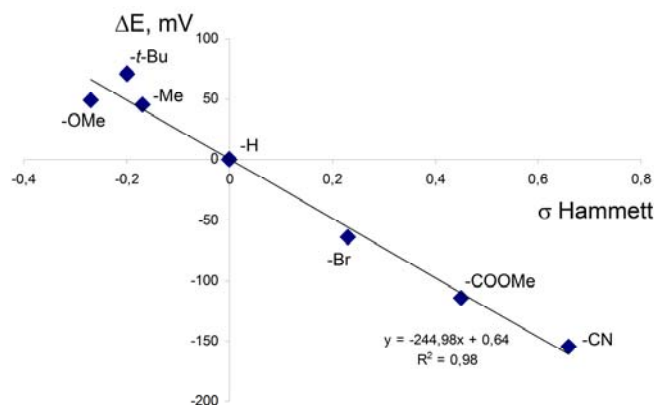


Fig. 2.7: Plot of ΔE ($\Delta E = E_{1/2}$ for **1-H**^{1+/0} - $E_{1/2}$ for **1-X**^{1+/0} in 1:1, acetonitrile:10 mM borate buffer pH = 8) vs the σ Hammett constant; for **X** = CN and COOMe the $E_{1/2}$ values refer to 50:50, acetonitrile:40 mM phosphate buffer pH = 7 ⁽¹²⁾

2.3.2 ET constant rate

The variance of the first oxidation potential in **1-X** series influences also the light-driven system and in particular the rate of the ET from the catalyst to the oxidized photosensitizer, Ru(bpy)₃³⁺ (Eq. 2.4). We considered k_H the bimolecular rate constant for the process involving **1** as catalyst and k_X the constant among the series of substituted **1-X** complexes (Tab. 2.2); the ET rate constants have been obtained by laser flash photolysis in collaboration with Prof. Scandola at the University of Ferrara.

| X ^a | $E_{1/2}$ (mV) ^b | η (mV) ^c | k ($10^8 \text{ M}^{-1}\text{s}^{-1}$) ^d | ϕ ^e |
|-----------------------|-----------------------------|--------------------------|---|---------------------|
| OMe | 877 | 570 | 2.51 | 0.40 ^f |
| t-Bu | 855 | 500 | 1.39 | 0.05 |
| Me | 880 | 520 | 1.92 | 0.15 |
| H | 926 | 550 | 1.33 | 0.13 |
| Br | 990 | 530 | 0.60 | 0.16 |
| COOMe | 1040 ^g | 510 | 0.70 | 0.23 |
| CN | 1081 ^g | 510 | 0.14 | 0.13 |

Tab. 2.2 ^a substituent in *para* position on the pyridine ligand. ^b $E_{1/2}$ (**1-X**⁺/**1-X**) in 1:1 ACN/10 mM aqueous borate buffer (pH = 8) vs Ag/AgCl. ^c overpotential of water discharge in 0.2 M aqueous phosphate buffer (pH = 7), determined at an anodic current value of 50 μ A (current density = 0.7 mA·cm⁻²) with a scan rate = 100 mV/s. ^d bimolecular rate constant for ET in Eq. 2.4 for **1-X** in 1:1, acetonitrile :10 mM aqueous borate buffer (pH = 8). ^e quantum yield (ϕ) obtained for the photochemically-driven process (λ_{exc} = 450 nm), determined over the first 30 minutes of reaction. ^f maximum value observed with freshly prepared solutions of **1-OCH₃**.
^g $E_{1/2}$ in 1:1 ACN/10 mM aqueous phosphate buffer (pH = 7) since the waves in 1:1 ACN/ 10 mM borate buffer (pH = 8) are not resolved due to overlapping with water oxidation discharge

With the available data, we obtained a linear trend plotting $\log(k_X/k_H)$ vs Hammett σ , Fig. 2.8.

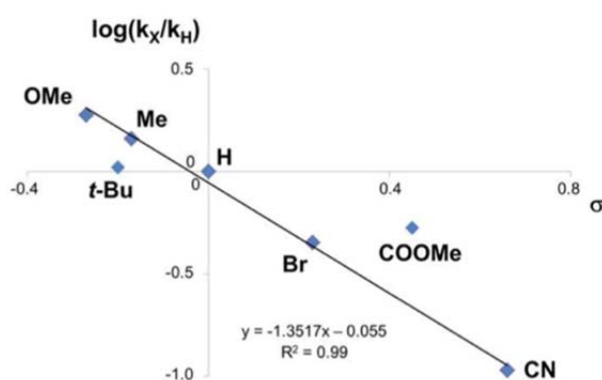


Fig. 2.8: Hammett linear free energy relationship plot of photoinduced ET rate constants between $\text{Ru}(\text{bpy})_3^{3+}$ and **1-X**⁽¹²⁾

In the plot, the negative slope is indicative of an enhancement of the photoinduced ET performed by electron-rich pyridines. Hence, we can conclude that the process is controlled by thermodynamic, since reactions are faster for easy oxidizable species but also influenced by electronic and steric effects involved in supramolecular interactions: this outcome can be responsible of the linearity deviation observed for **1-tBu** and **1-COOCH₃**, as appreciable in Fig. 2.7.

Furthermore, in the mixed solvent, it is possible to appreciate that the bimolecular constant rate k_H , for the ET between $\text{Ru}(\text{bpy})_3^{3+}$ and **1** is one order of magnitude higher than in aqueous solution ($1.3 \times 10^8 \text{ M}^{-1}\text{s}^{-1}$ in 1:1, acetonitrile: borate buffer 10 mM, pH = 8). This result owes with the increase into the difference between potentials of couples $\text{Ru}(\text{bpy})_3^{3+/2+}$ and **1**^{+/1} in mixed solvent, giving a more exergonic process for Eq. 2.4, hence defining more driving force for this reaction.

2.3.3 Photo induced kinetic experiments

Besides the electrochemical and kinetic parameters related to the first oxidation event on **1**, leading to **1⁺**, it is interesting to explore also how the substituents X influence the catalytic activity in water oxidation. From the electrochemical point of view, the overpotential for the substituted **1-X** lies in a narrow range between 500 and 570 mV without a visible correlation with Hammett σ (Tab. 2.2). This may suggest that in the overall catalytic cycle some steps could be favored by electron-donor, other by electron-withdrawing substituents.

The catalytic activity was then studied in the photo-activated system described above, in mixed solvent and in collaboration with the group of Prof. Campagna in Messina. In these conditions the efficiency of the system is higher: the persulfate is completely consumed in 3 hours, achieving a TON of 140 for **1-X** (Fig. 2.9). As already mentioned, the improvement of the performance is likely due to the stabilization of the photosensitizer in the mixed solvent. Considering the substituent effect, insertion of the quantum yield ϕ in a Hammett plot fails to reveal a specific trend of activity in the series **1-X**, as observed in the overpotential evaluation.

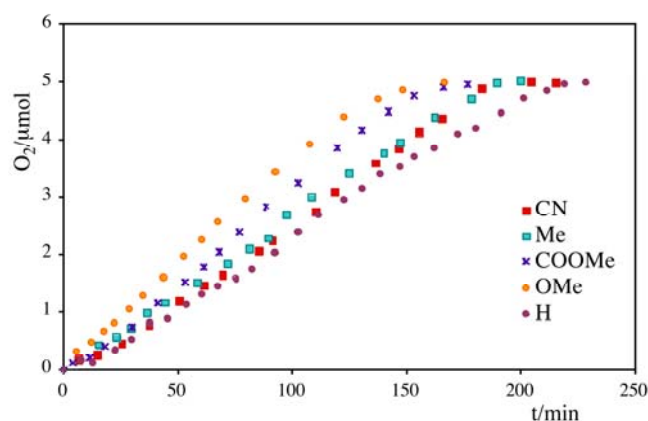


Fig. 2.9: Oxygen production kinetics by representative **1-X** catalysts used in this work (X is shown in panel). [**1-X**] = 18 μM, [Ru(bpy)₃²⁺] = 1 mM, [S₂O₈²⁻] = 5 mM in 1:1, acetonitrile:10 mM borate buffer (2 ml, pH=8), $\lambda_{\text{irr}} > 400$ nm. A total of 140 TONs is reached upon quantitative conversion of sacrificial persulfate. ⁽¹²⁾

Interestingly, in the described experimental conditions, a very high quantum yield ϕ was found with **1-OCH₃**, reaching a value of 0.40, which is so far the best value reported in literature for water oxidation light-driven system.

2.4 An open question: is cubane **1** a real molecular catalyst for water oxidation?

The development of molecular species able to catalyse water oxidation is really attractive because they provide tunable media to understand mechanism and identify the reactive intermediates. However, a recurring issue comes from the question whether the catalyst retains its homogeneous nature or a heterogeneous catalytically active species is produced *in situ*.⁽¹⁴⁾

Very recently, Nocera et al. have published new results affirming through different techniques that the catalytic activity of **1** in water oxidation is due to Co^{II} impurities.⁽¹⁵⁾ They have reported that the product obtained from the literature synthetic procedure⁽²⁾ contains impurities, which can be removed by silica chromatography. Comparing the CV of the product prepared via the literature procedure (**crude-1**) and of the product isolated after flash chromatography (**pure-1**), a very different behaviour is observed, since lack of the catalytic wave is found with **pure-1** (Fig. 2.10). The authors state that the absence of a catalytic wave for **pure-1**, is indicative of the presence of Co^{II} impurities in **crude-1**, acting as a source for the formation of the active WOC Co-P_i in sufficient oxidative conditions.⁽¹³⁾

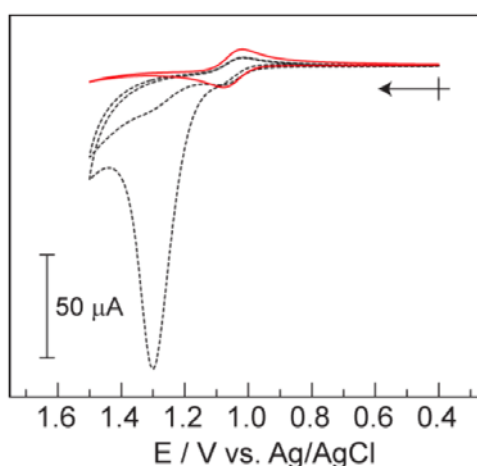


Fig. 2.10: CVs of **crude-1** (dashed black line) and **pure-1** (solid red line) 1 mM in 0.2 M KPi buffer, pH = 7. Two scans are presented for **crude-1** demonstrating the loss of activity upon the second scan⁽¹⁵⁾

However, the authors observed a residual activity of **pure-1** in the photoactivated cycle, adopting the conditions used by Dismukes et al.⁽⁸⁾

This scenario leaves an open issue, whether **1** behaves or not as a molecular WOC. This requires further investigations since **pure-1** has not been analysed in the photocatalytic system with the mixed solvent, employed above. Therefore, we repeated the purification procedure suggested by Nocera et al., obtaining **pure-1** and we characterized it by CV in 0.2 M phosphate buffer, pH = 7, confirming the absence of a catalytic wave (Fig. 2.11 a)). However, when performed in 1:1 acetonitrile: 10 mM borate buffer, pH = 8, an anodic wave is appearing at E = 1.2 V, immediately after the reversible wave due to **1** → **1**⁺ event occurring at E = 0.93 V vs Ag/AgCl (Fig. 2.11 b)).

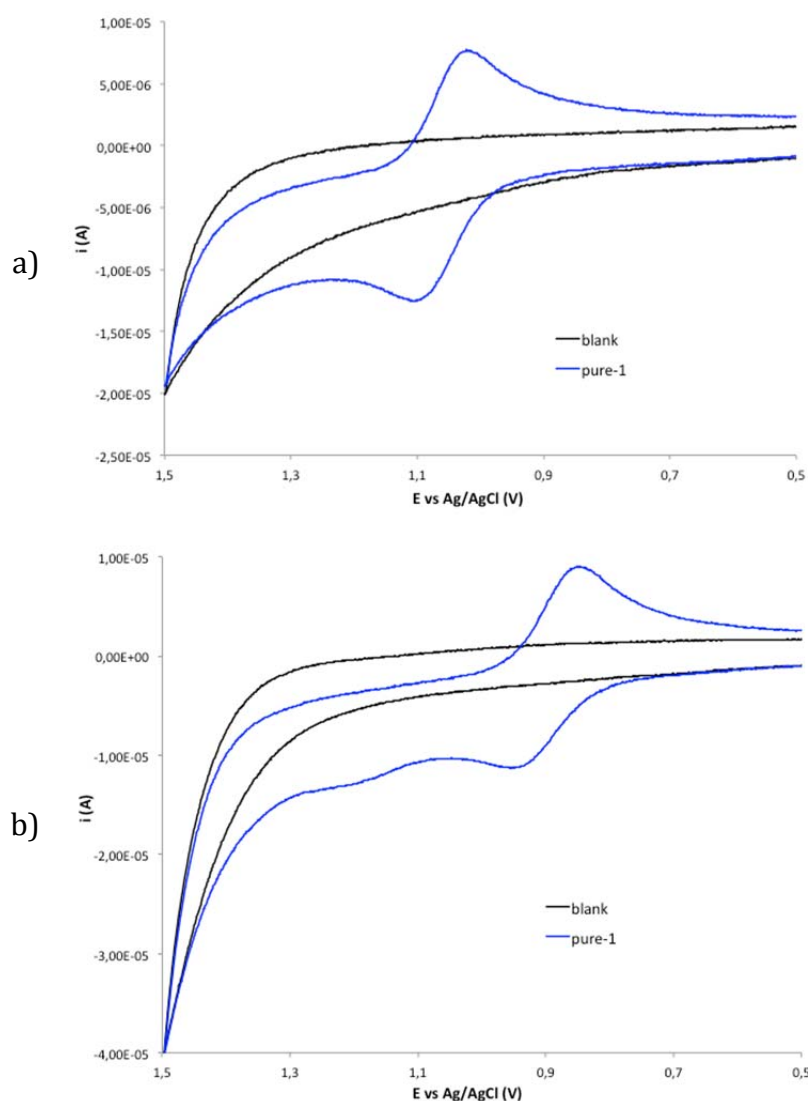
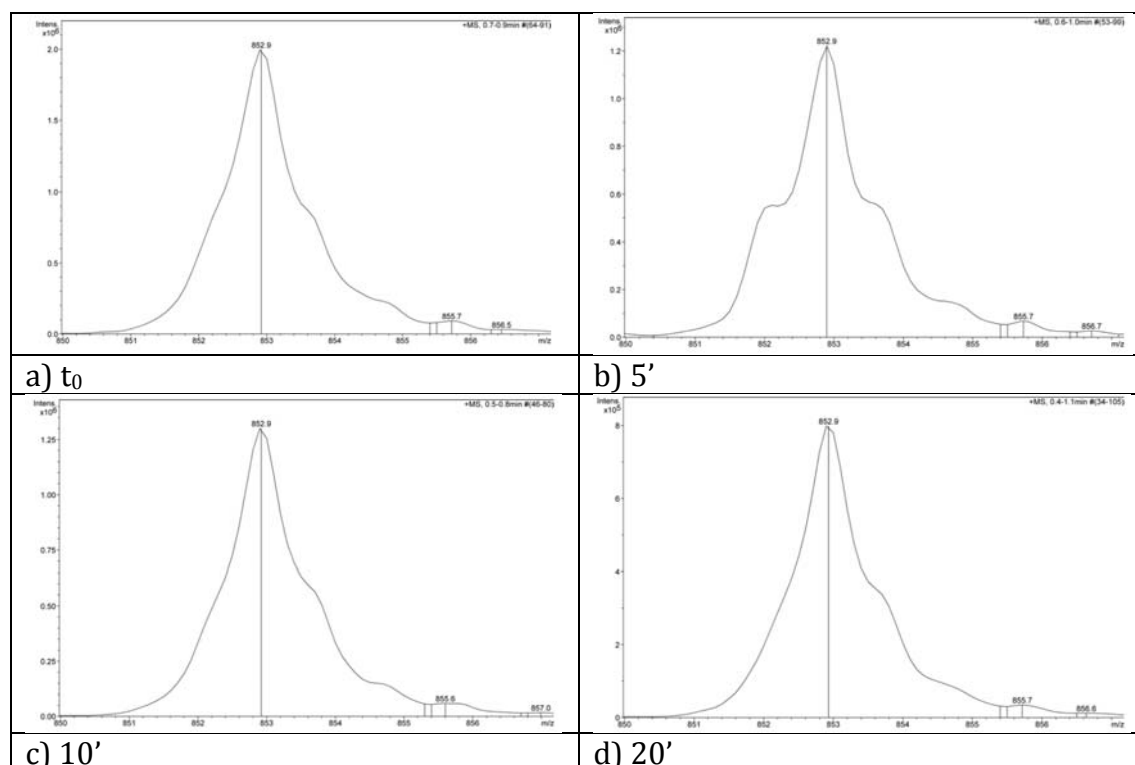


Fig. 2.11: CV of [**pure-1**] = 1 mM in **a)** 0.2 M phosphate buffer, pH = 7 and **b)** in 1:1 acetonitrile:10 mM borate buffer, pH = 8. WE: glassy carbon (d = 3 mm), CE: Pt wire, RE: Ag/AgCl, scan rate: 100 mV/s

The photoactivated system $S_2O_8^{2-}/Ru(bpy)_3^{2+}/$ **pure-1**, where Nocera et al. found oxygen activity, is currently under investigation in the mixed solvent.

One possible approach, to understand the role played by the species **1**, could be to verify its fate under operating conditions: a preliminary study on **1** has been developed through a labelling experiment, followed by ESI-MS. In particular, we have run photocatalysis in labelled water ($H_2^{18}O$ at 5%), verifying the possible incorporation of ^{18}O in the catalyst structure and recording the mass spectrum of the species at different illumination time ($t = 0, 5, 10, 20$ and 60 minutes). During the whole light-driven experiment, we observed the persisting of the peak at 853 m/z (indicative of the **1-H**⁺), with the mass distribution of this peak remaining the same showing the stability of the cluster, see Fig. 2.12. The only change appears in the spectrum after about five minutes of illumination due to the presence of a peak at $m/z = 852$, ascribable to the formation of **1**⁺, the mixed valent $Co_3^{III}Co^{IV}$ species formed after the first oxidation step from the parent **1**.



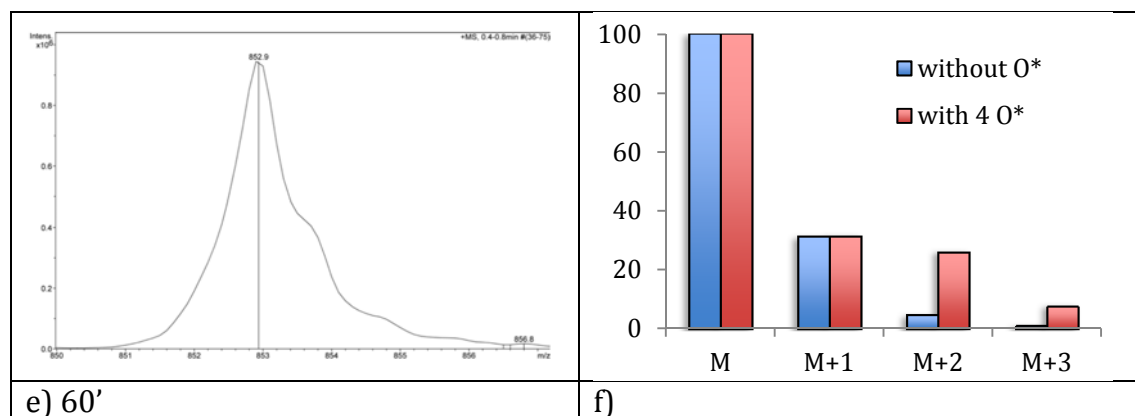


Fig. 2.12: Electrospray ionization mass spectra analysis of **pure-1** in the photocatalytic system at time = **a)** 0 (in dark), **b)** 5, **c)** 10, **d)** 20, **e)** 60 minutes, **f)** mass distribution calculated with and without ¹⁸O. [**1**] = 58 μM in Co, [Ru(bpy)₃²⁺] = 1 mM, [S₂O₈²⁻] = 5 mM in 10 mM borate buffer (pH=8), light source monochromatic LEDs (λ_{irr} = 450 nm)

Moreover, no changes in mass distribution were observed along the spectra of Fig. 2.12 a)-e), indicating no incorporation of ¹⁸O from water in the Co₄O₄ moiety in **1**. In Fig. 2.12 f) the mass distribution calculated for **1** with (red histograms) and without (blue histograms) labelled Oxygen in the Co₄O₄ core: the experimental data fit the theoretical prediction without ¹⁸O incorporation. Indeed, focusing on the peak at m/z = M+2, it shows an appreciable difference between the two possible situations: in the presence of ¹⁸O exchange the intensity of the M+2 peak is equivalent to the intensity of the M+1, which is not our case. This means that: 1) in photo catalytic conditions oxygen from the oxo-cluster is not involved and 2) water provides for O₂ formation, 3) the structure of **1** is stable in the adopted photocatalytic conditions. Therefore, a possible role of **1** as competent WOC can not be excluded.

The conclusion drawn by experimental data can be indicative of a mechanism similar to the so-called “roller coaster” proposed by Sala et al. ⁽¹⁶⁾ We hypothesize a partial removal of an acetate group from the structure with a consequent coordination of a water molecule on a Co atom then, after the oxidation and formation of an oxo complex, the water nucleophilic attack is expected. The process should conclude with releasing of oxygen after proton removal, as schematically represented in Fig. 2.13.

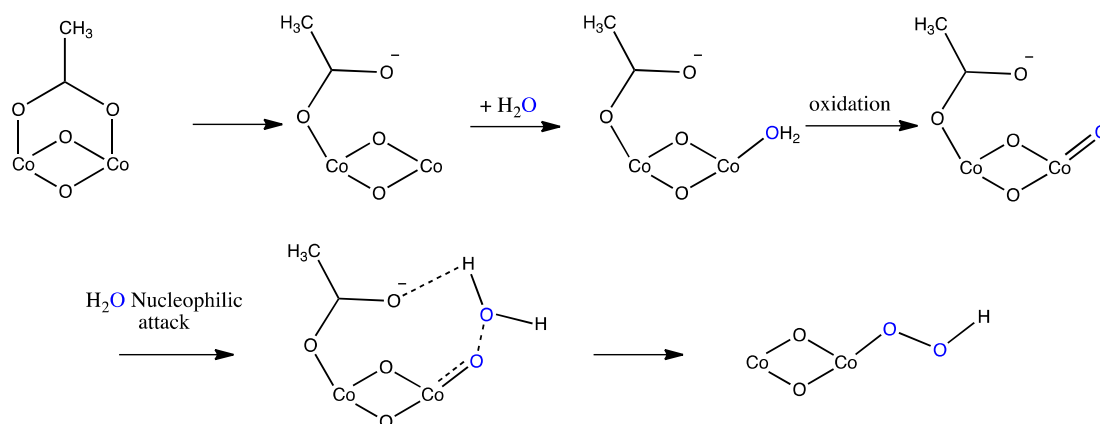


Fig. 2.13: Schematic representation of a possible mechanism of water oxidation by **1**

Further studies will be performed in the characterization of **1** along the photocatalytic cycle, in order to understand the real catalytic system and whether or not the presence of the species **1** is pivotal in the mechanism. EPR analysis and EXAFS studies on the Co K edge are already planned.

However, even though the debate on the real nature of the catalyst is open, there are some aspects of our previous work that preserve their integrity, in particular the correlations between the electronic effect of the substituent in *para*-position on the pyridines and: 1) the first oxidation potential of the Co₄O₄ **1** core, 2) the ET constant rate in the light-driven system between the photosensitizer Ru(bpy)₃²⁺ and **1** species.

2.5 Dyads photosensitizer-catalyst

Considering the catalytic activity of the species **1**, we found attractive to design possible photosensitizer-catalyst dyads in order to: 1) rise the ET rate, fundamental parameter for the efficiency of the light-driven system, 2) assemble the entire process onto a semiconductor, to create a photoelectrode able to oxidize water. This device coupled with a similar artifice for the production of hydrogen could be employed to perform the photo-assisted water splitting, which is the final goal of artificial photosynthesis.

2.5.1 Dyads: no covalent interactions

At the beginning of this study, we considered to verify interactions between **1** and $\text{Ru}(\text{bpy})_3^{2+}$ in solution; indeed the possibility of a specific interaction between the two species emerged from the high ET constant rate evaluated by flash photolysis experiments, see Section 2.2.

The approach of fluorescence/phosphorescence titrations was selected and the experiments were performed, exploiting the photosensitizer emission.

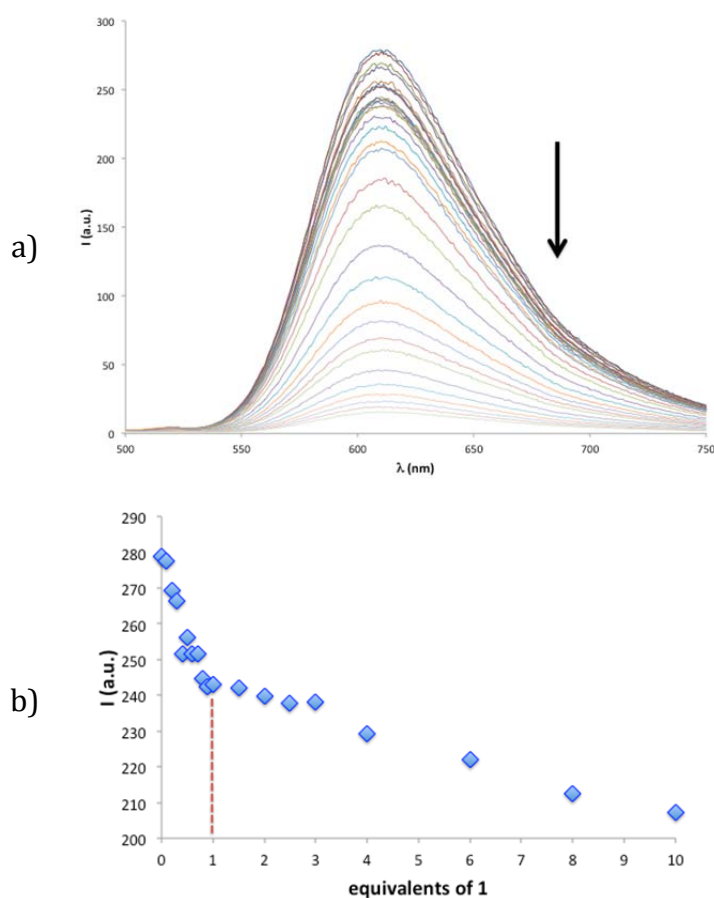


Fig. 2.14: Quenching titration experiment of the $\text{Ru}(\text{bpy})_3^{2+}$ emission, adding aliquots of **1**; 2 mL $[\text{Ru}(\text{bpy})_3^{2+}] = 10^{-5}$ M in acetonitrile; $\lambda_{\text{exc}} = 450$ nm: **a)** intensity vs λ **b)** plot intensity ($\lambda = 610$ nm) vs equivalents of **1**

In Fig. 2.14 a) a typical titration is reported: it is possible to appreciate the quenching of the phosphorescence of $^*\text{Ru}(\text{bpy})_3^{2+}$ adding increasing aliquots of **1**. From the plot of the phosphorescence intensity versus number of equivalents of **1**, Fig. 2.14 b), a slight change in the slope resulting after one equivalent of **1** can be indicative of an average 1:1 interaction between the two species.

Considering a Stern-Volmer procedure, the data processing brings to a binding constant (K_{SV}) of about $3.2 \times 10^4 \text{ M}^{-1}$. The value of the K_{SV} is comparable with other examples reported in literature for interactions between $\text{Ru}(\text{bpy})_3^{2+}$ species and other benzylic systems. ⁽¹⁷⁾

For data processing, we consider the dynamic quenching, hence intermolecular deactivation of the sensitizer emission. In order to obtain the K_{SV} with the Stern-Volmer equation, we plot the ratio between initial value of the emission and its intensity during the titration versus the quencher concentration, in our case **1**. The slope of the linear trend is K_{SV} considered a good approximation of the real binding constant, K_b , which also counts the lifetime of the excited state.

$$\text{Stern-Volmer equation:} \quad I_0/I = 1 + K_{SV} \times [Q] \quad (2.6)$$

$$\text{Binding constant equation:} \quad I_0/I = 1 + K_b \times \tau_0 \times [Q] \quad (2.7)$$

In Eq. 2.6-7, I is the intensity of the recorded emission of $\text{Ru}(\text{bpy})_3^{2+}$, Q is the quencher (**1** in this case) and τ_0 is the life time of $\text{Ru}(\text{bpy})_3^{2+}$.

The study was then extended to the series **1-X** in two different solvents: phosphate buffer and acetonitrile in order to evaluate the different substituent effect in the association with the sensitizer. Once more, data had been processed with Stern-Volmer, binding constants were obtained by the slope of the plot normalized emission intensity versus quencher concentration: the values are reported in Tab. 2.3 and show a very slight trend of K_{SV} increase moving to more electron-withdrawing groups.

| X^a | $K_{SV} (\text{M}^{-1}, \text{ACN})$ | $K_{SV} (\text{M}^{-1}, \text{phosphate buffer})$ |
|--------------|--------------------------------------|---|
| OMe | 2.20×10^4 | 1.10×10^4 |
| t-Bu | 1.12×10^4 | 1.50×10^4 |
| Me | 9.57×10^3 | 1.46×10^3 |
| H | 3.21×10^4 | 3.14×10^3 |
| Br | 1.66×10^4 | - ^b |
| COOMe | 1.76×10^4 | 2.48×10^4 |
| CN | 2.43×10^4 | 1.93×10^4 |

Tab. 2.3: Values of K_{SV} for the sensitizer $\text{Ru}(\text{bpy})_3^{2+}$ obtained by titration with the **1-X** series. ^a substituent in *para* position on the pyridine ligand, ^b no Stern-Volmer correlation was found for **1-Br** data emission in phosphate buffer

We also tried to correlate binding constants values for the series **1-X** with the Hammett parameter σ . From Fig. 2.15, it is possible to see that 1) the substituent effect is very slight and 2) less electronic density on the pyridines seems favor interactions in both conditions. The Hammett plots show positive slopes of 0.20 and 0.67, found in acetonitrile and in phosphate buffer, respectively.

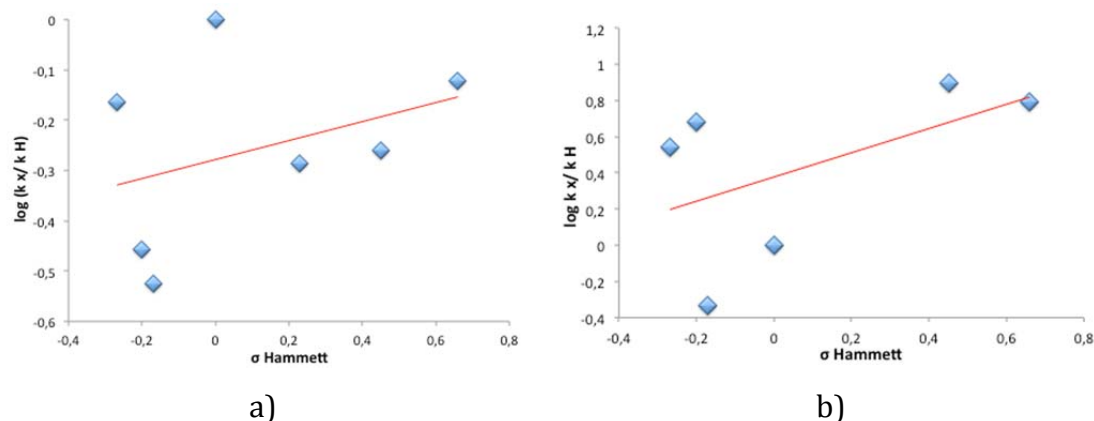


Fig. 2.15: Hammett correlation for K_{sv} between (**1-X**) and $\text{Ru}(\text{bpy})_3^{2+}$ in **a)** ACN e **b)** phosphate buffer, pH = 8

Concerning the nature of the interaction between $\text{Ru}(\text{bpy})_3^{2+}$, and **1-X**, these latter are neutral compounds, thus electrostatic interactions with the sensitizer can be excluded; similarly, hydrogen bonds are unlikely to occur, since no hydrogen bond donors are present in the two molecules. A reasonable hypothesis was the π - π stacking, involving the aromatic systems of the pyridines in **1-X** and the bipyridines in $\text{Ru}(\text{bpy})_3^{2+}$. However, since we found low performance and weak effects we move to more incisive covalent modifications in order to increase specific π - π interactions to boost supramolecular association.

2.5.2 Photosensitizer – Catalyst Dyads: the synthetic approach

A covalent approach ensures the possibility to introduce a target structural property into molecules. For this reason we explored synthetic routes to amplify the aromatic surface of our system in order to maximize productive associations between catalyst **1** and the sensitizer.

In particular, we aimed at extending the aromatic character of the ligands in **1**, by introducing a pyrene moiety in the pyridine or carboxylate functions of the

cubane.

Therefore, we planned to synthesize the ligands **2_p** and **2_m** in Fig. 2.16, to use them in the synthesis of modified cubanes.

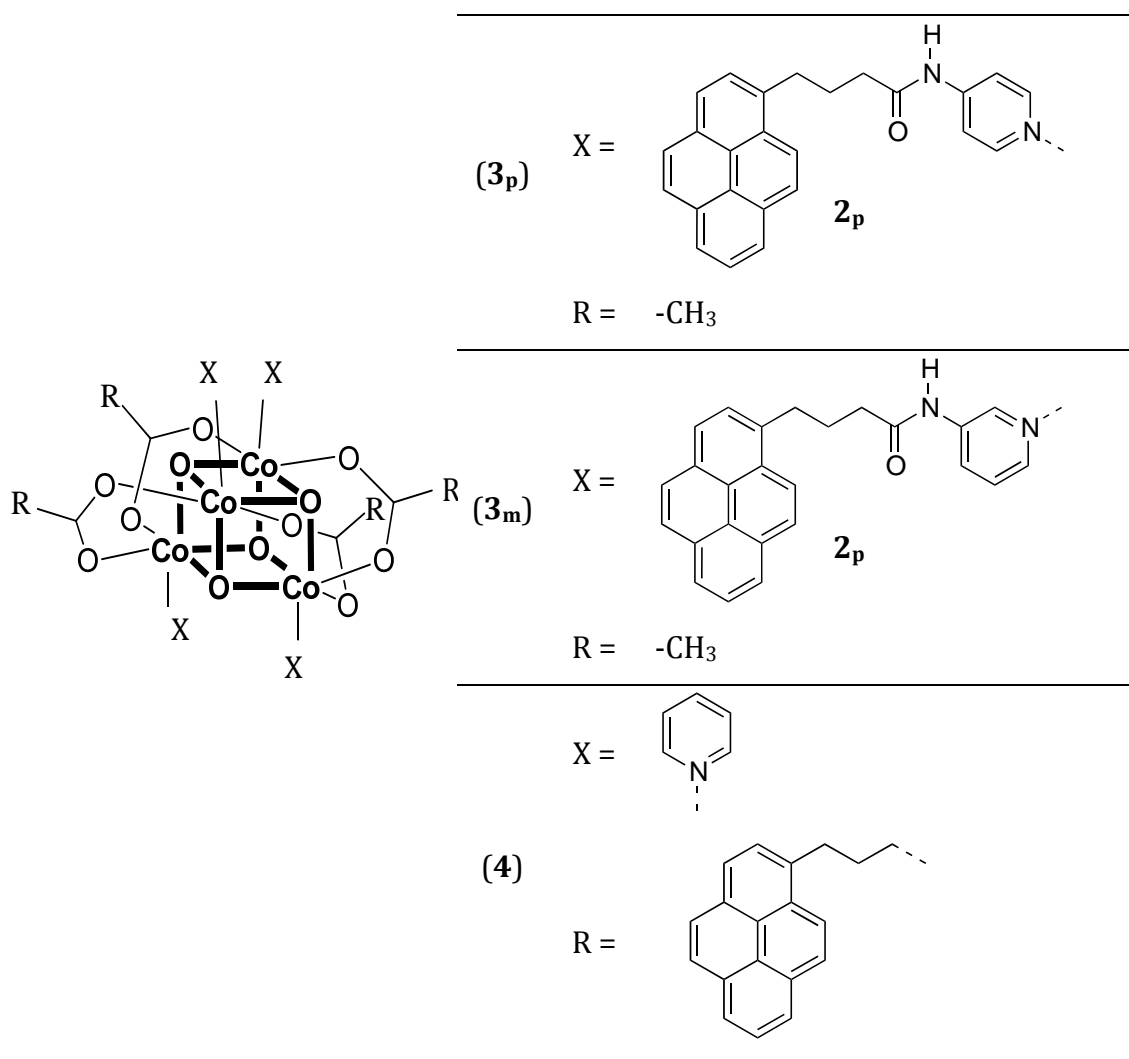


Fig. 2.16: Structures of the three obtained novel compounds

The novel pyridinic ligands (**2_p**, **2_m**) for the synthesis of compounds **3_p** and **3_m** were synthesized from the acyl chloride of 4-pyrene-butirric acid and 4-amino pyridine or 3-aminopyridine in anhydrous THF; while the derivative of 4-pyrene-butirric acid for the synthesis of **4** is commercially available.

The ligands **2_p** and **2_m** have been characterized with ¹H-NMR and ESI-MS, confirming their identity. Then catalysts **3_p** and **3_m** have been obtained in methanol under reflux, in presence of Co(NO₃)₂·6H₂O, CH₃COONa·3H₂O, ligands **2_p** or **2_m** and adding H₂O₂ after half an hour from the beginning of heating. Stirring and reflux are maintained for 4 hours, the mixture is then cooled at room

temperature. The aqueous phase is removed adding CH_2Cl_2 and after evaporation of the solvent the compound is washed with diethyl ether and water. The synthetic procedure is similar to the one of the cubane **1** except for the several final washings. **3_p** and **3_m** were characterized by $^1\text{H-NMR}$: the spectrum of **3_p** is reported in Fig. 2.17 as a representative case. ESI-MS analysis for both the species show the molecular ion peak at 1994 m/z.

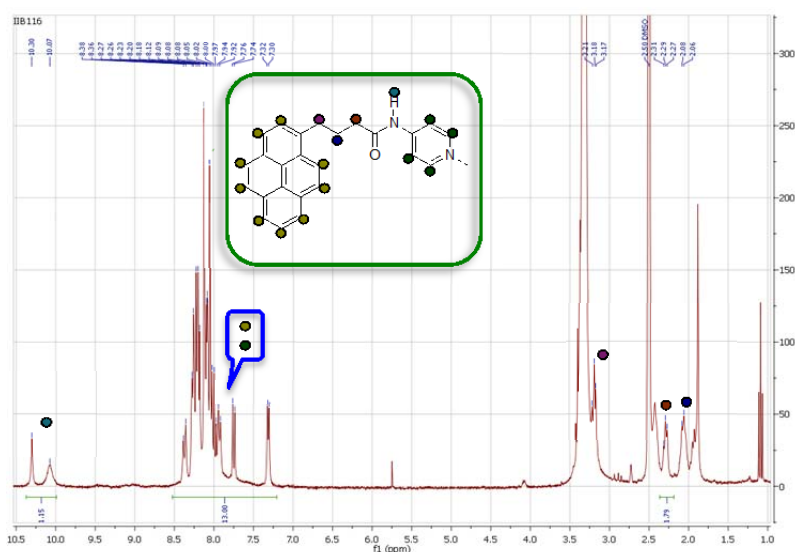


Fig. 2.17: $^1\text{H-NMR}$ spectrum of (**3_p**), 300 MHz, DMSO-d_6

Concerning synthesis of product **4**: to the salt of the pyren-butirric acid formed in situ $\text{Co}(\text{NO}_3)_2 \cdot 6\text{H}_2\text{O}$ and N-pyridine in methanol are added. After 4 hours under stirring and reflux, CH_2Cl_2 is added, the separated organic phase is anhydriified and filtrated. Adding n-hexane a dark precipitate appears, purified after several washing with diethyl ether and methanol. The product has been characterized with $^1\text{H-NMR}$, Fig. 2.18, and ESI-MS, which shows a peak at 1765 m/z, the identity is confirmed also with other technique such as FT-IR showing peculiar stretching due to the cubane-like core structure between 770 and 580 cm^{-1} in the spectrum. ⁽²⁾

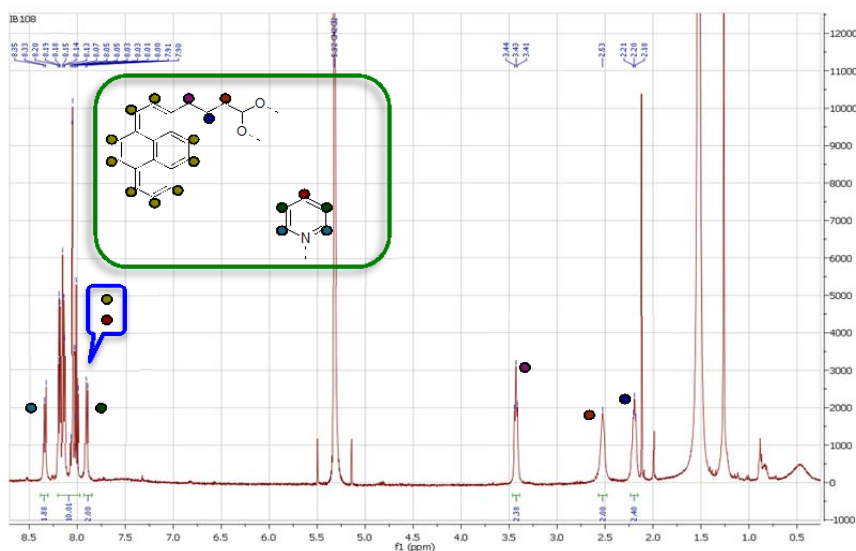


Fig. 2.18: $^1\text{H-NMR}$ spectrum of (4), 500 MHz, CD_2Cl_2

In conclusion, we obtained three novel species with a more extended aromatic area interesting for higher π - π interactions with the photosensitizer.

Two limits of these products are the low synthetic yield (about 13%) and low solubility, in particular in aqueous solutions where the catalytic activity is more appealing. Some studies are on going in collaboration with Universities of Ferrara and Messina in order to evaluate 1) ET constants rate with the photosensitizer and 2) the behavior in the light-driven catalytic system.

2.6 A brief conclusion

A preliminary conclusion can be reported on the basis of studies performed and described so far in sections 2.2 and 2.3:

- 1) cubane species **1** has been evaluated as a possible molecular WOC both in electrochemical and light-driven systems;
- 2) correlations structure-activity have been noticed for different substituted pyridines in the **1-X** series with effect on thermodynamics and kinetics features;
- 3) interactions between the photosensitizer and species **1** in solution have been analysed in order to understand their mutual relationship in the light-driven system,
- 4) from the previous studies, a covalent approach was adopted in order to introduce a more extended aromatic area on the catalyst structure and maximize

interactions, with the consequent synthesis of three novel compounds.

The further progress will be focused on 1) deeper investigations of the system considering the results of the group of Nocera, 2) understanding the mechanism and 3) the actual role played by **1**.

2.7 References

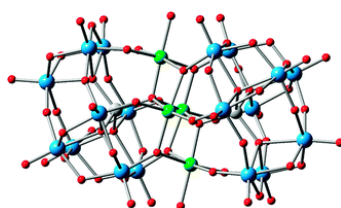
-
- ¹ J. K. Beattie, T. W. Hamblie, J. A. Klepetko, A. F. Masters, P. Turner *Polyhedron*, **1998**, *17*, 1343
 - ² R. Chakrabarty, S. J. Bora, B. K. Das *Inorg Chem*, **2007**, *46*, 9450
 - ³ M. D. Symes, Y. Surendranath, D. A. Lutterman, D. G. Nocera *J Am Chem Soc*, **2011**, *133*, 5174
 - ⁴ A. Sartorel, M. Carraro, F. M. Toma, M. Prato, M. Bonchio *Energy Env Sci*, **2012**, *5*, 5592
 - ⁵ D. J. Wasylenko, C. Ganesamoorthy, J. Borau- Garcia, C. P. Berlinguette *Chem Commun*, **2011**, *47*, 4249
 - ⁶ G. La Ganga, F. Puntoriero, S. Campagna, I. Bazzan, S. Berardi, M. Bonchio, A. Sartorel, M. Natali, F. Scandola *Faraday Discuss*, **2012**, *155*, 177
 - ⁷ (a) A. R. Parent, R. H. Crabtree, G. W. Brudvig *Chem Soc Rev*, **2013**, *42*, 2247; (b) F. P. Rotzinger, S. Munavalli, P. Comte, J. K. Hurst, M. Graetzel, F. J. Pern, A. J. Frank *J Am Chem Soc*, **1987**, *109*, 6619; (c) H. S. White, W. G. Becker, A. J. Bard *J Phys Chem* **1984**, *88*, 1840
 - ⁸ N. S. McCool, D. M. Robinson, J. E. Sheats, G. C. Dismukes *J Am Chem Soc*, **2011**, *133*, 11446
 - ⁹ F. Jiao, H. Frei *Angew Chem Int Ed*, **2009**, *48*, 1841
 - ¹⁰ A. Sartorel, M. Bonchio, S. Campagna, F. Scandola *Chem Soc Rev*, **2013**, *42*, 2262
 - ¹¹ W. J. Youngblood, S.-H. A. Lee, Y. Kobayashi, E.A. Hernandez-Pagan, P.G. Hoertz, T. A. Moore, A. L. Moore, D. Gust, T. E. Mallouk *J Am Chem Soc*, **2009**, *131* (3), 926
 - ¹² S. Berardi, G. La Ganga, M. Natali, I. Bazzan, F. Puntoriero, A. Sartorel, F. Scandola, S. Campagna, M. Bonchio *J Am Chem Soc*, **2012**, *134*, 11104
 - ¹³ P. F. Smith, C. Kaplan, J. E. Sheats, D. M. Robinson, N. S. McCool, N. Mezle, G. C. Dismukes *Inorg Chem*, **2014**, *53*, 2113
 - ¹⁴ M. D. Kärkäs, O. Verho, E. V. Johnston, B. Åkermark *Chem Rev*, **2014**, DOI: 10.1021/cr400572f
 - ¹⁵ A. M. Ullman, Y. Liu, M. Huynh, D. K. Bediako, H. Wang, B. L. Anderson, D. C. Powers, J. J. Breen, H. D. Abruña, D. G. Nocera *J Am Chem Soc*, **2014**, *136* (50), 17681
 - ¹⁶ X. Sala, S. Maji, R. Bofill, J. García-Antón, L. Escriche, A. Llobet *Acc Chem Res*, **2014**, *47*, 504
 - ¹⁷ E. M. Tuite, D. B. Rose, P. M. Ennis, J. M. Kelly *Phys Chem Chem Phys*, **2012**, *14*, 3681

3. CHAPTER

Cobalt Polyoxometalates as molecular WOC

3.1 The first example of a Cobalt-based POM as molecular WOC

Polyoxometalates have been previously introduced (see section 1.6.2) as a versatile family of ligands with good stability, in particular through oxidative stress due to their pure inorganic nature. ⁽¹⁾ In the Introduction, it was also discussed how these polyanionic ligands can stabilize multimetallic cores, that can be reminiscent of a fragment of a metal oxide phase. Therefore, Cobalt-based POMs (Co-POMs) have been considered among the most promising candidates as molecular WOCs, since their structural features can be compared with fragments of Cobalt oxide, that are among the most active WOCs to date. ^(2, 3, 4) Ideally, the POM framework should stabilize these Cobalt-oxo clusters avoiding their coalescence, prolonging the stability and activity of the catalyst. The forefather of Cobalt base POMs as molecular WOC is the $[\text{Co}_4(\text{H}_2\text{O})_2(\text{PW}_9\text{O}_{34})_2]^{10-}$ species reported by Hill et al. ⁽⁵⁾ that was claimed to be active in oxygen evolution in neutral pH, in the presence of $\text{Ru}(\text{bpy})_3^{3+}$ as chemical or photogenerated oxidant. Despite several experiments seemed to support stability of this Cobalt based POM under operating conditions, a following study evidenced a significant transformation of the catalyst, as shown by a drastic change in the rate of reaction of the Cobalt based POM with the oxidant $\text{Ru}(\text{bpy})_3^{3+}$, upon aging (Fig. 3.1). ⁽⁶⁾ This result was therefore speaking in favour of a partial transformation of the catalyst into a more active species.



a)

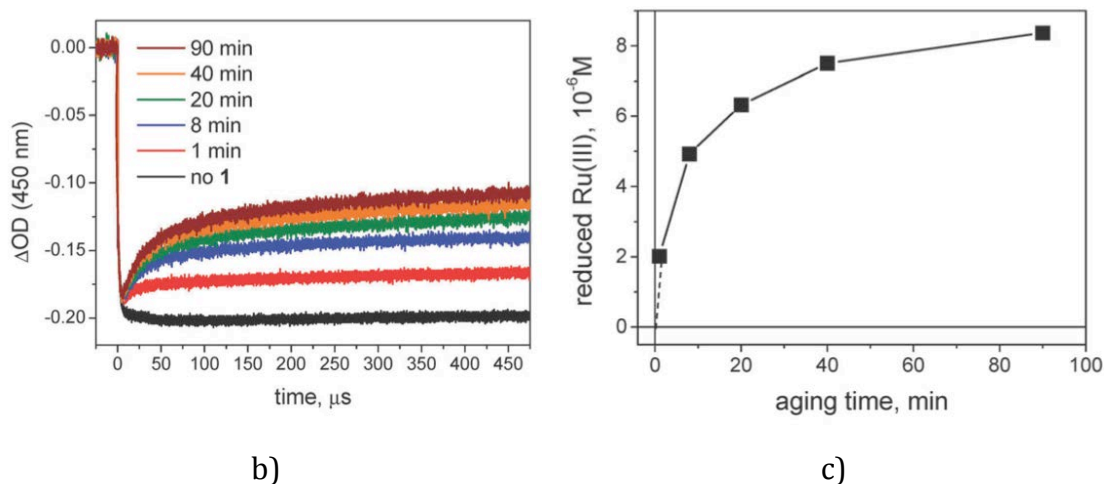


Fig. 3.1: a) Structure of $[\text{Co}_4(\text{H}_2\text{O})_2(\text{PW}_9\text{O}_{34})_2]^{10-}$; **b)** ET kinetics measured using 5.0×10^{-5} M solution of $[\text{Co}_4(\text{H}_2\text{O})_2(\text{PW}_9\text{O}_{34})_2]^{10-}$ at various aging times. 1 min: solid catalyst dissolved in 80 mM phosphate buffer, pH = 8 and measured immediately. 8-90 min: prepared from a 10^{-3} M stock solution of $[\text{Co}_4(\text{H}_2\text{O})_2(\text{PW}_9\text{O}_{34})_2]^{10-}$ in 80 mM phosphate buffer, pH = 8, at various time intervals; **c)** amount of $\text{Ru}(\text{bpy})_3^{3+}$ being reduced by 5.0×10^{-5} M $[\text{Co}_4(\text{H}_2\text{O})_2(\text{PW}_9\text{O}_{34})_2]^{10-}$ in laser flash photolysis (450 ms time window), as a function of the aging time of the solution used ⁽⁶⁾

Despite the nature of the active species has not been clarified, the report by Hill et al. stimulated great efforts in developing Cobalt based POMs as WOC. In literature several examples have been reported and recently reviewed ⁽¹⁾ such as: $[\text{CoMo}_6\text{O}_{24}\text{H}_6]^{3-}$ and $[\text{Co}_2\text{Mo}_{10}\text{O}_{38}\text{H}_4]^{6-}$, ⁽⁷⁾ $[\text{Co}_9(\text{H}_2\text{O})_6(\text{OH})_3(\text{PW}_9\text{O}_{34})_3]^{16-}$ ⁽⁸⁾ and $[\text{Co}_4(\text{H}_2\text{O})_2(\text{VW}_9\text{O}_{34})_2]^{10-}$. ⁽⁹⁾ In particular, Cobalt based POMs with high nuclearity seem quite promising candidates, due to their improved stability at neutral pH, even supported onto different solid phases. ⁽¹⁰⁾

Therefore, we focused our studies on some high nuclearity POMs and on their behaviour in the $\text{Ru}(\text{bpy})_3^{2+}/\text{S}_2\text{O}_8^{2-}$ photoactivated cycle.

3.2 High nuclearity Cobalt based polyoxometalates

The high nuclearity Cobalt based polyoxometalates considered in this study are represented in Fig. 3.2 and consist of three types: $[\text{Co}_9(\text{H}_2\text{O})_6(\text{OH})_3(\text{PW}_9\text{O}_{34})_3]^{16-}$ (hereafter **Co₉**), $[\text{Co}_6(\text{H}_2\text{O})_{30}\{\text{Co}_9\text{Cl}_2(\text{OH})_3(\text{H}_2\text{O})_9(\text{SiW}_8\text{O}_{31})_3\}]^{5-}$ (hereafter **Co₁₅**) and $[\{\text{Co}_4(\text{OH})_3\text{PO}_4\}_4(\text{PW}_9\text{O}_{34})_4]^{16-}$ (hereafter **Co₁₆**). **Co₉** was provided by the group

of Prof. J. R. Galán Mascarós (ICIQ Tarragona, Spain), while **Co**₁₆ was provided by the group of Prof. U. Kortz (Jacobs University Bremen, Germany).

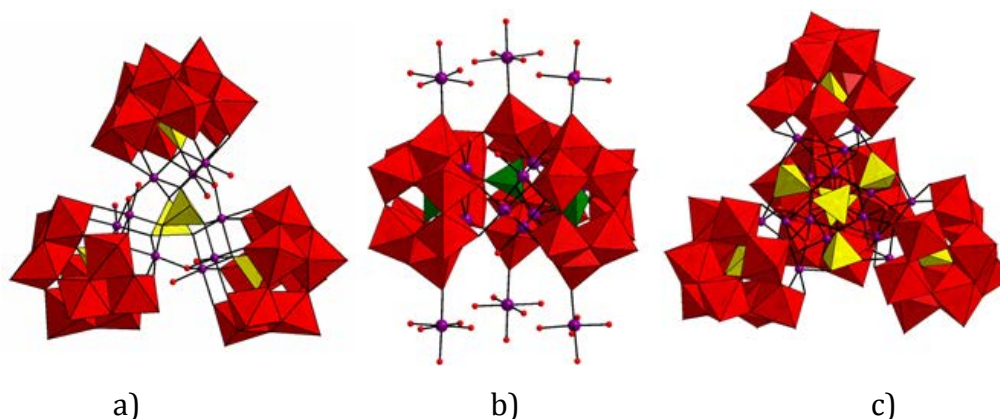


Fig. 3.2: Representation of: **a)** $[\text{Co}_9(\text{H}_2\text{O})_6(\text{OH})_3(\text{PW}_9\text{O}_{34})_3]^{16-}$ (**Co**₉), **b)**

$[\text{Co}_6(\text{H}_2\text{O})_{30}\{\text{Co}_9\text{Cl}_2(\text{OH})_3(\text{H}_2\text{O})_9(\text{SiW}_8\text{O}_{31})_3\}]^{5-}$ (**Co**₁₅), **c)** $[\{\text{Co}_4(\text{OH})_3\text{PO}_4\}_4(\text{PW}_9\text{O}_{34})_4]^{16-}$ (**Co**₁₆)

At first, the study of these species was focused on laser flash photolysis experiments, in collaboration with Prof. Scandola at the University of Ferrara, to reveal the possibility for these Co-POMs to promote electron transfer to photogenerated $\text{Ru}(\text{bpy})_3^{3+}$. The investigation of the POMs was performed in aqueous phosphate buffer at pH 8, containing $\text{Ru}(\text{bpy})_3^{2+}$ and $\text{Na}_2\text{S}_2\text{O}_8$, and the results are summarized in Tab. 3.1.

| Co-POM | Stability | k (M ⁻¹ s ⁻¹) | number of ET |
|-------------------------|-----------|--------------------------------------|--------------|
| Co ₉ | Yes | 2.1×10 ⁹ | 7.5 |
| Co ₁₅ | Yes | 5.0×10 ⁹ | 32 |
| Co ₁₆ | Yes | 4.5×10 ⁹ | 20 |

Tab. 3.1: Kinetic parameters of reactions of Co-POMs with $\text{Ru}(\text{bpy})_3^{3+}$ photogenerated, obtained by laser flash photolysis

The key observations of the data in Tab. 3.1 are reported as follows:

- 1) All the high nuclearity Cobalt based POMs investigated show a behavior in flash photolysis independent of solution aging, differently from the $[\text{Co}_4(\text{H}_2\text{O})_2(\text{PW}_9\text{O}_{34})_2]^{10-}$ described above. Considering also that Co^{II} aquoions, a well-recognized WOC precursor, do not give any appreciable hole-scavenging activity in this timeframe, this behaviour rules out any major decomposition phenomena of the Co-POMs under examination.

- 2) The bimolecular rate constants, dealing with the first electron transfer from Co-POMs to $\text{Ru}(\text{bpy})_3^{3+}$, are high and close to a diffusion control. This is likely due to ionic interactions between the polyanionic WOCs and the cationic sensitizer. ^(6, 11)
- 3) All the Co-POMs can undergo multiple electron transfer event to $\text{Ru}(\text{bpy})_3^{3+}$ within a short time scale of 100 ms: in such timescale 7.5, 32 and 20 electron transfers are observed for **Co₉**, **Co₁₅** and **Co₁₆**, respectively. Considering the Cobalt nuclearity of the three WOCs, these values correspond to an average oxidation equivalents of 0.8, 2.1 and 1.2 average per Cobalt center, resulting respectively for **Co₉**, **Co₁₅** and **Co₁₆** species. In particular, the highest value of 2.1, observed for **Co₁₅**, indicates an overall change of the oxidation state of each Cobalt center from Co^{II} to Co^{IV} . This unique behavior in the high nuclearity Co-POM series may be related to the large number of water molecules coordinated to the Cobalt center in this polyanion; these may favor sequential oxidations to the metal center by contemporary releasing one proton to the solvent through a series of proton-coupled electron transfer (PCET). PCET are indeed recognized as a prominent feature for an ideal WOC operating at low overpotentials. In a Cobalt oxide based WOC, two sequential PCET on a Co^{II} -aquo moiety lead to the formation of Co^{IV} -oxo groups, that are recognized as the active forms leading to oxygen evolution. Since polyoxometalates are often described as molecular analogs of extended phases, this mechanism could likely apply also for the Co based POMs discussed here.

Further investigations were run with conductometric titrations of the Co-POMs with increasing aliquots of $\text{Ru}(\text{bpy})_3^{2+}$. As shown in Fig. 3.3, we verify a change of the slope in the plot of the conductivity versus the ratio between the titrant and Co-POMs concentrations, confirming an association phenomena in aqueous solution. The ratio at the equivalent point reflects the charge balance between the two species as underlined by the red dashed line in the plots below.

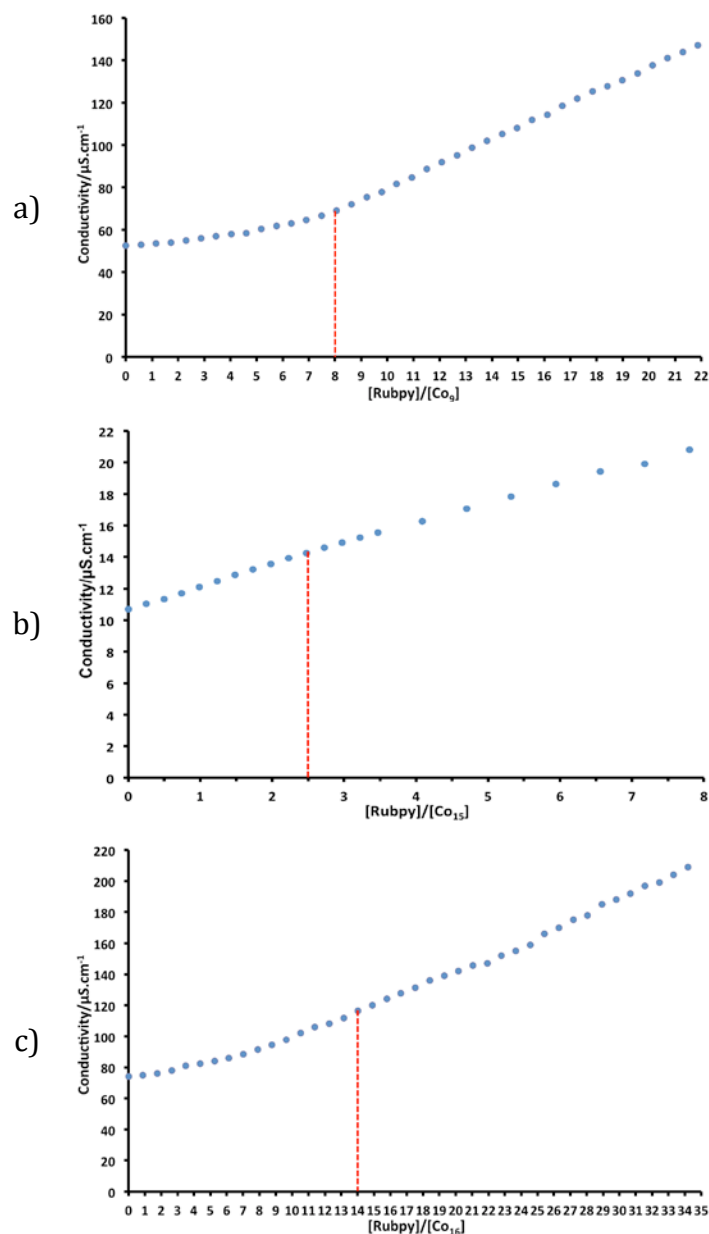


Fig. 3.3: Conductometric titrations of **Co₉**, **Co₁₅** and **Co₁₆** with Ru(bpy)₃²⁺ (in water)

From the promising results of high ET constant rate, we moved to verify their ability to evolve oxygen in the light-driven Ru(bpy)₃²⁺/ Na₂S₂O₈ system. We screened different conditions changing the concentration of the catalyst (19-147 μM in total Co amount) and the buffer media (phosphate buffer, pH = 7 or 8). The results are reported in Tab. 3.2, where they are compared with values obtained with the Co²⁺ aquoion, known to undergo Cobalt oxide CoO_x formation with high performance as WOC.

| WOC | Buffer | [WOC], μM ([Co], μM) ^a | $\mu\text{mol O}_2$ (TON) ^b | max rate $\times 10^3$, $\mu\text{mol}\cdot\text{s}^{-1}$ (TOF $\times 10^3$, s^{-1}) ^c |
|--------------------|--------|---|---|---|
| Co ₉ | P7 | 6.60 (58) | 1.16 (12) | 0.32 (3.33) |
| | P8 | 6.60 (58) | 1.02 (10.5) | 0.51 (5.35) |
| Co ₁₅ | P7 | 3.86 (58) | 2.34 (40.5) | 1.50 (25.8) |
| | P7 | 9.80 (147) | 5.73 (39) | 4.17 (28.3) |
| | P8 | 1.27 (19) | 1.97 (101) | 0.80 (41.9) |
| | P8 | 3.86 (58) | 3.06 (52) | 1.22 (21.0) |
| Co ₁₆ | P8 | 9.80 (147) | 4.11 (27) | 2.85 (19.4) |
| | P7 | 3.62 (58) | 7.06 (125) | 2.09 (36.0) |
| | P7 | 9.19 (147) | 7.53 (54) | 2.33 (15.9) |
| | P8 | 3.62 (58) | 2.01 (37) | 1.28 (23.5) |
| Co ²⁺ d | P8 | 9.19 (147) | 3.86 (28) | 2.96 (21.5) |
| | P7 | 58 | 9.05 (10.4) | 6.06 (6.97) |
| | P7 | 147 | 7.72 (3.5) | 6.55 (2.97) |
| | P8 | 19 | 3.73 (13.1) | 2.33 (8.19) |
| | P8 | 58 | 9.92 (11.4) | 6.32 (7.27) |
| | P8 | 147 | 8.60 (3.9) | 5.38 (2.44) |

Tab. 3.2: Catalytic oxygen production by irradiation of 15 ml of a 20 mM phosphate buffered solution (P7 = pH 7, P8 = pH 8), containing Ru(bpy)₃²⁺ (1 mM), S₂O₈²⁻ (5 mM) and Co-POMs or Co^{II} ions as WOC. Irradiation with a tungsten lamp with a cut-off filter a 375 nm (power density 150 W·cm⁻²). ^a total cobalt concentration. ^b TON defined as $\mu\text{mol O}_2/\mu\text{mol WOC}$. ^c TOF defined as the maximum rate of O₂ production over the $\mu\text{mol WOC}$. ^d introduced as nitrate salt

In Fig. 3.4, TON and TOF for the catalysts under selected conditions are represented in histograms.

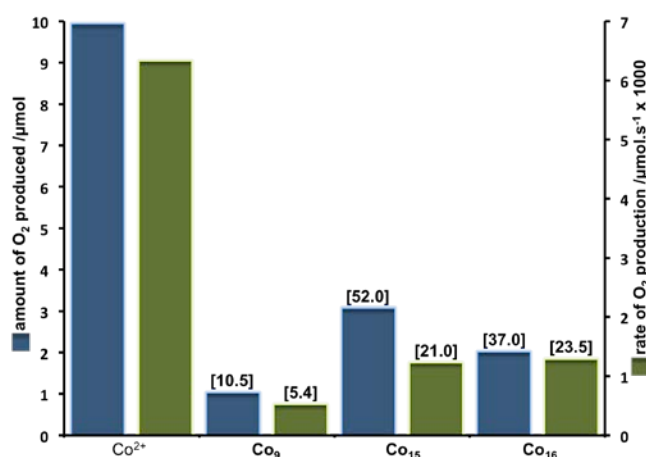


Fig. 3.4: Total O₂ production (blue bars) and maximum rate of O₂ production (green bars) in light driven water oxidation experiments. Irradiation of 15 ml of a 20 mM phosphate buffered solution (pH = 8) containing Ru(bpy)₃²⁺ (1 mM), S₂O₈²⁻ (5 mM) and Co²⁺, Co₉, Co₁₅ and Co₁₆ as the catalyst (58 μM total Co concentration). Irradiation with a tungsten lamp with a cut-off filter a 375 nm (power density 150 W·cm⁻², spot size 1 cm²). In square brackets above the histograms of the three Co-POMs TON and TOF $\times 1000$ (s⁻¹) are also reported.

As a first evidence, all the three Co-POMs show immediate oxygen evolving activity upon illumination of the solution, leading to a total O₂ production that is however markedly inferior with respect to Co^{II} ions (Fig. 3.4), as it was reported also for [Co₄(H₂O)₂(PW₉O₃₄)₂]¹⁰⁻.^(12, 13) In the high nuclearity Co-based POM series, the best performance is still provided by **Co₁₅**. In optimized conditions (total Cobalt concentration 19 μM in 20 mM phosphate buffer pH = 8, see Tab. 3.2) the turnover number reaches up to 101 with a turnover frequency of 41.9×10⁻³ s⁻¹, in line with other Cobalt based POMs reported in the literature operating in such photo-activated cycle.^(7, 14) By running the oxygen evolving reaction with monochromatic emitting LEDs as a light source (λ = 450 nm, photon flux = 2.63×10⁻⁸ einstein/s), a quantum yield of 0.08 was measured (total Co concentration 147 μM, 20 mM phosphate buffer, pH = 7).⁽¹⁵⁾

However, the evidences above do not guarantee the actual role of **Co₉**, **Co₁₅** and **Co₁₆** as water oxidation catalysts, since other Cobalt-based species, derived from the pristine structures, could be the competent oxygen evolving catalysts.

In this sense, the dependence of water oxidation activity on pH of the three WOCs is markedly different with respect to that of free Co^{II} ions, introduced as Co(NO₃)₂·6H₂O; indeed, while the reactivity of Co^{II} ions slightly increases from pH = 7 to pH = 8, the activity of **Co₉**, **Co₁₅** and **Co₁₆** follows an opposite trend. These observations suggest the involvement of different catalytic species rather than Cobalt oxide particles derived from free Co^{II} ions. Indeed, infrared spectra of the recovered catalyst after the catalytic cycle seem to confirm the residual presence of polyoxometalate based species, even if small wavenumber shifts, with respect to the pristine catalyst, could not exclude a partial rearrangement of the original structures (Fig. 3.5). Preliminary studies have been conducted in collaboration with Prof. Holger Dau (Berlin) employing XAS spectroscopy, recognized as one of the state-of-the-art techniques to characterize WOCs. Analysis of the spent reaction mixture reveal an edge shift of the XANES, consistent with an average increase of oxidation state of Cobalt to +2.5. Importantly, this spectra are markedly different with respect to Co^{III}-oxide species acting as WOC.⁽¹⁶⁾ Therefore, the most likely scenario is the residual presence of Cobalt based polyoxometalate molecular species in solution, where the Cobalt centres have been partially oxidized during the photocatalytic cycle.

Moreover, the average change in oxidation state could be an indication of the number of Cobalt centres involved in the catalytic cycle. Registration of the EXAFS part of the spectra for the three Co-POMs under photocatalytic conditions, to probe the structural changes responsible for oxygenic activity, is planned.

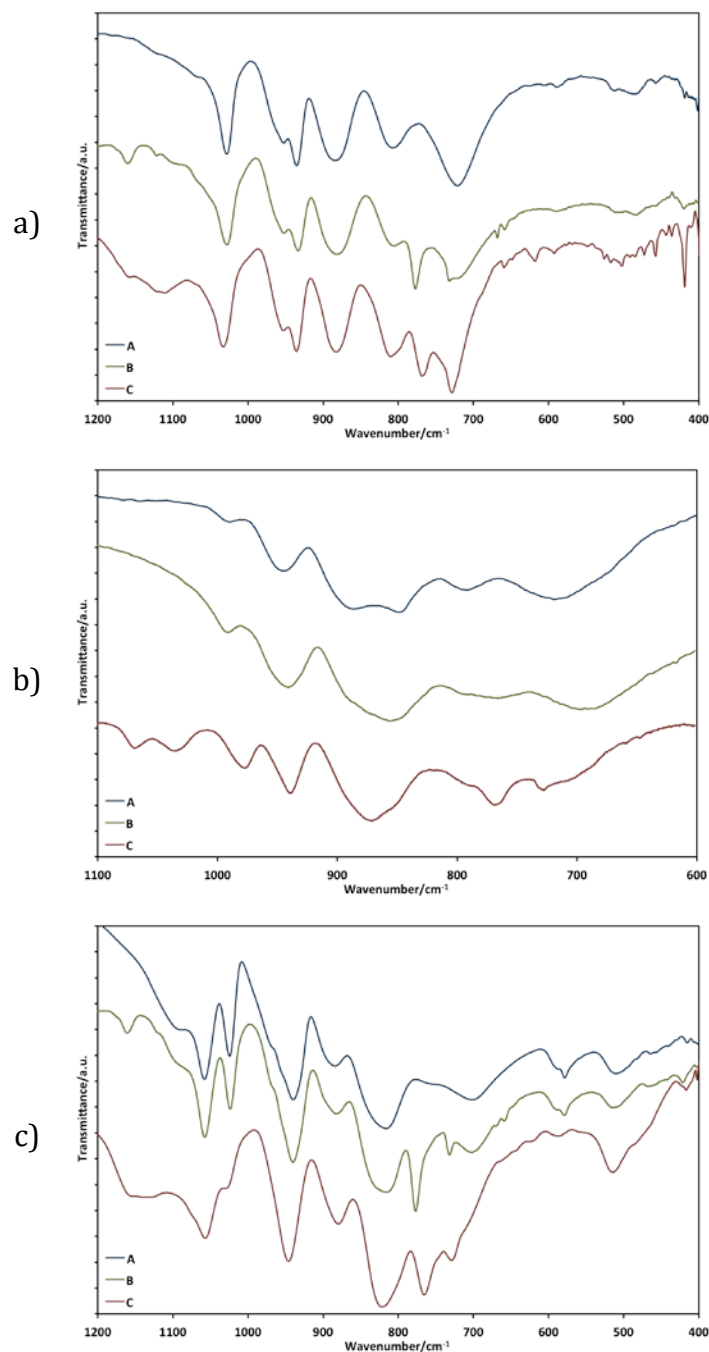


Fig. 3.5: **a)** FT-IR spectra of pristine **Co₉**(A; blue), adduct of **Co₉·Ru(bpy)₃²⁺** after conductimetric titration (B; green) and precipitate retrieved after water-oxidation reaction(C; red). **b)** FT-IR spectra of pristine **Co₁₅**(A; blue), adduct of **Co₁₅·Ru(bpy)₃²⁺** after conductimetric titration(B; green), and precipitate retrieved after water-oxidation reaction(C; red). **c)** FT-IR spectra of pristine **Co₁₆** (A; blue), adduct of **Co₁₆·Ru(bpy)₃²⁺** after conductimetric titration(B; green) and precipitate retrieved after water-oxidation reaction(C; red).

3.3 Conclusions and Perspectives

In conclusion, we have investigated three high nuclearity Co-POMs as WOC.

Some interesting information are:

- 1) the very promising activity of such species in the kinetics of electron transfer to a photogenerated $\text{Ru}(\text{bpy})_3^{3+}$, since all the Co-POMs examined give a stable behaviour over time, high second order kinetic constants, multiple ET in a very short timescale of 100 ms.
- 2) All the Co-POMs display oxygenic activity in the photoactivated cycle. The most promising species, **Co₁₅**, reaches up to 100 TON and a quantum yield of 0.08.
- 3) The integrity and the nature of the actual catalyst have been investigated, speaking in favour of a Cobalt based POM as the actual WOC, although some structural rearrangements can not be excluded.

These results speak in favour of Co-POMs as very promising candidates for the development of photoactivated devices for artificial photosynthesis, since they can combine the high activity of Cobalt as a WOC with the peculiar properties of POMs, in particular their very high kinetic constants with $\text{Ru}(\text{bpy})_3^{3+}$, while their polyanionic charge can be exploited to design electrostatic interactions in order to assemble them onto materials.

3.4 References

-
- ¹ H. Lv, Y. V. Geletii, C. Zhao, J. W. Vickers, G. Zhu, Z. Luo, J. Song, T. Lian, D. G. Musaev, C. L. Hill *Chem Soc Rev* **2012**, *41*, 7572
 - ² F. Jao, H. Frei *Angew Chem Int Ed*, **2009**, *48*, 1841
 - ³ M. W. Kanan, Y. Surendranath, D. G. Nocera *Chem Soc Rev*, **2008**, *321*, 109
 - ⁴ J. B. Gerken, J. G. McAlpin, J. Y. C. Chen, M. L. Rigsby, W. H. Casey, R. D. Britt, S. S. Stahl *J Am Chem Soc*, **2012**, *133*, 14431
 - ⁵ Q. Yin, J. M. Tan, C. Besson, Y. V. Geletii, D. G. Musaev, A. E. Kuznetsov, Z. Luo, K. I. Hardcastle, C. L. Hill *Science*, **2010**, *328*, 342
 - ⁶ M. Natali, M. Orlandi, S. Berardi, S. Campagna, M. Bonchio, A. Sartorel, F. Scandola *Inorg Chem*, **2012**, *51*, 7324

-
- ⁷ S. Tanaka, M., K. Sakai *Chem Commun*, **2012**, *48*, 1653
- ⁸ S. Goberna-Ferron, L. Vigarà, J. Soriano-López, J. R. Galán-Mascarós *Inorg Chem*, **2012**, *51*, 11707
- ⁹ H. Lv, J. Song, Y. V. Geletii, J. W. Vickers, J. M. Sumliner, D. G. Musaev, P. Kögerler, P. F. Zhuk, J. Bacsà, G. Zhu, C. L. Hill *J Am Chem Soc*, **2014**, *136*, 9268
- ¹⁰ a) J. Soriano-López, S. Goberna-Ferron, L. Vigarà, J. J. Carbó, J. M. Poblet, J. R. Galán-Mascarós *Inorg Chem*, **2013**, *52*, 4753–4755; b) X.-B. Han, Z.-M. Zhang, T. Zhang, Y.-G. Li, W. Lin, W. You, Z.-M. Su, E.-B. Wang *J Am Chem Soc*, **2014**, *136* (14), 5359
- ¹¹ M. Ibrahim, Y. Lan, B. S. Bassil, Y. Xiang, A. Suchopar, A. K. Powell, U. Kortz *Angew Chem Int Ed*, **2011**, *50*, 4708
- ¹² J. W. Vickers, H. Lv, J. M. Sumliner, G. Zhu, Z. Luo, D. G. Musaev, Y. V. Geletii, C. L. Hill *J Am Chem Soc*, **2013**, *135*, 14110
- ¹³ It is worth to mention that in such light activated cycle, oxygen production is inhibited by degradation of the photosensitizer, as confirmed by UV-Vis of the spent reaction mixture. This is a well-recognized limit of this system (see reference 15 details), mainly due to the type of sacrificial acceptor employed.
- ¹⁴ P.-E. Car, M. Guttentag, K. K. Baldrige, R. Alberto, G. R. Patzke *Green Chem*, **2012**, *14*, 1680
- ¹⁵ A. Sartorel, M. Bonchio, S. Campagna, F. Scandola *Chem Soc Rev*, **2013**, *42*, 2262
- ¹⁶ R. Schiwon, K. Klingan, H. Dau, C. Limberg *Chem Commun*, **2014**, *50*, 100

4. CHAPTER

A novel Copper catalyst for Water Oxidation

4.1 Introduction

In recent years, as already discuss above (section 1.6), research in water oxidation catalysis has been focused on the development of first row transition metals catalysts, due to their Earth-abundance and limited cost. In particular, Copper-based catalysts such as a Cu-bpy (bpy=2,2'-bipyridine), ^(1a, b) a Cu-carbonate system ⁽²⁾ and a Cu-peptide ⁽³⁾ have attracted great interest due to the simplicity of their systems. Such catalysts have been tested in electrochemical water oxidation in alkaline conditions (pH = 8-13) achieving good results in terms of overpotentials and in TON and TOF values.

Up to the present, the combination of these Copper catalysts with light activated systems, aimed at the development of a sunlight activated device for water splitting, has not been explored.

4.2 Results and discussion

4.2.1 Synthesis and characterization

We decided to focus our attention on a particular compound: a Copper(II) complex of 1,4,8,11-Tetraazacyclotetradecane, (hereafter **Cu-Cyclam**, Fig. 4.1). The choice of this macrocyclic ligand was based on its several interesting features: 1) the cyclam ligand is commercial and cheap, 2) it complexes transition metal via tetradentate mode, with high complexation constant; ^(2, 4) 3) the cyclam ligand lends to structure modifications and possibly to different system skills, 4) it is known to stabilize high valent states of Copper, ⁽⁵⁾ 5) this ligand was recently exploited to design an efficient Ni^{II} based WOC. ⁽⁶⁾

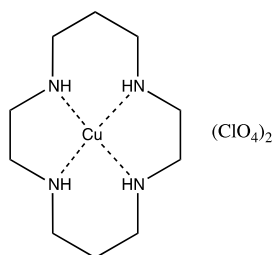


Fig. 4.1: Representation of **Cu-Cyclam**

(Cu-Cyclam) \cdot (ClO₄)₂ was easily synthesized and isolated in 70% yield after crystallization, by stoichiometric reaction of 1,4,8,11-tetraazacyclotetradecane and Cu(ClO₄)₂ in tetrahydrofuran. ⁽⁷⁾ In the solid state, the Copper atom displays a distorted octahedral geometry, where the tetradentate Cyclam ligand is coordinating the four equatorial positions, while the two perchlorate ions occupy the apical sites of the metal. ⁽⁸⁾ Thanks to this particular arrangement the apical positions are expected to be labile and susceptible to exchange in solution, in the presence of coordinating species.

The identity and stability of the **Cu-Cyclam** complex was verified also in aqueous solution, by means of Electrospray Ionization Mass Spectrometry (ESI-MS) registered under positive ion mode, that shows a base peak at $m/z = 362$, and a second peak at $m/z = 364$ with 80% relative intensity. These are ascribable to the [Cu-Cyclam \cdot ClO₄]⁺ ion (see Fig. 4.2), with a contribution to the M+2 peak of the ³⁷Cl and ⁶⁵Cu isotopes.

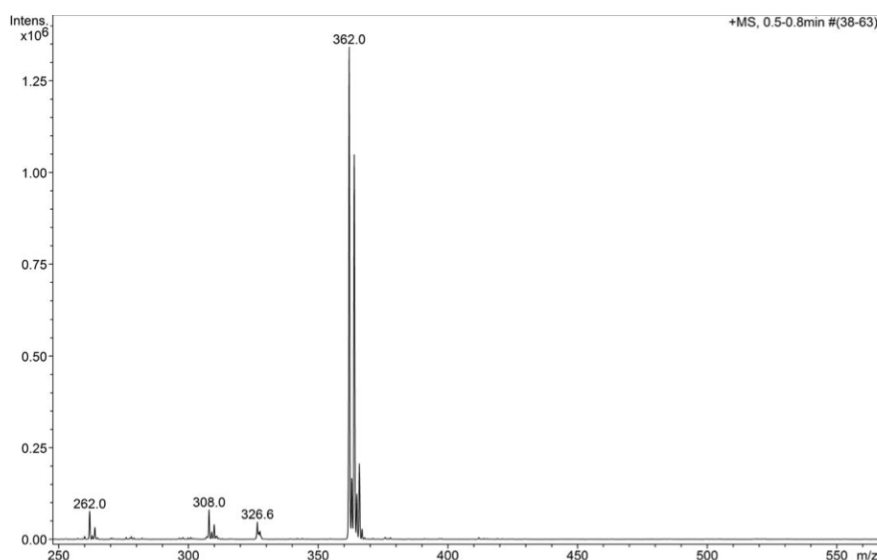


Fig. 4.2: ESI-MS spectra of a 10⁻⁵ M solution in CH₃CN + 0.1% HCOOH of **Cu-Cyclam**.

UV-Vis analysis was performed to characterize and verify the stability of **Cu-Cyclam** in the experimental conditions screened in our studies (*vide infra*). In particular, UV-Vis spectroscopy in alkaline aqueous solution (pH = 12, NaOH / sodium acetate) shows a broad absorption at 506 nm, ascribable to Cu^{II} d-d transitions. The unchanged spectra over fifteen hours (Fig. 4.3) is indicative of

stability of **Cu-Cyclam** under this alkaline environment, where the catalytic activity was investigated.

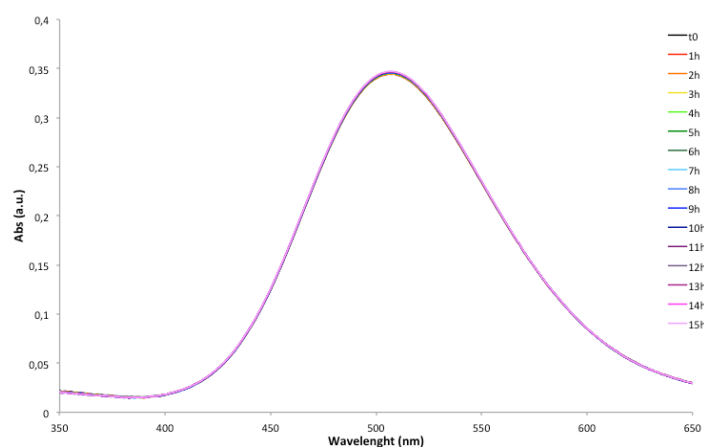


Fig. 4.3: UV-Vis kinetic spectra of 5 mM solution of **Cu-Cyclam** in NaOH with NaOAc 0.1 M, pH = 12, among 15 hours.

4.2.2 Cyclic Voltammetry

At first, the study was focused on the electrochemical characterization of the compound by cyclic voltammetry; a screening analysis in different solvents, buffer, pH and concentration were performed in order to find the optimal conditions for electrocatalysis.

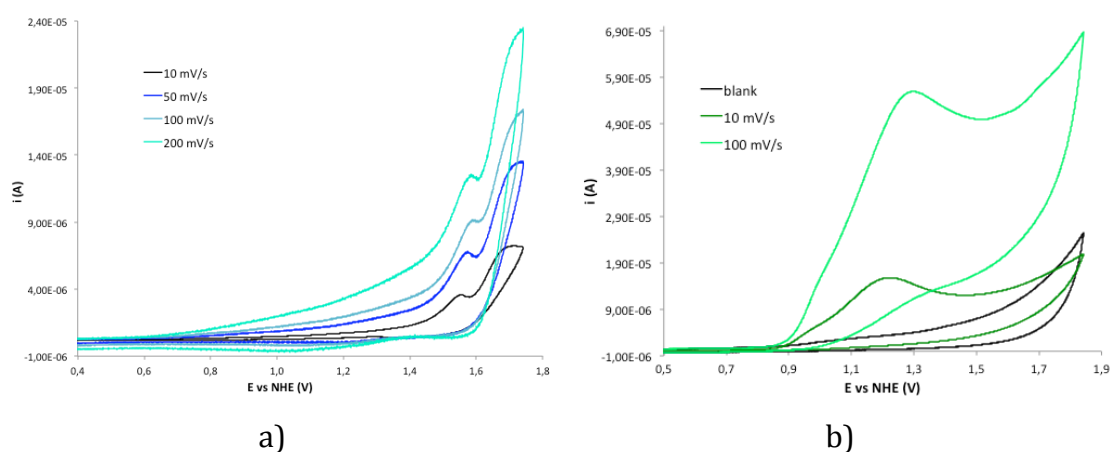


Fig. 4.4: Cyclic voltammetry of a) 0.5 mM **Cu-Cyclam** in acetonitrile, TBAPF₆ 0.1 M, WE: glassy carbon, CE: Pt wire, RE: SCE (KCl sat), potentials are then referred to (NHE), scan rate: see legend. b) 0.5 mM **Cu-Cyclam** in 0.2 M phosphate buffer, pH = 8, WE: glassy carbon, CE: Pt wire, RE: SCE (KCl sat), potentials are then referred to (NHE), scan rate: see legend

In Fig. 4.4 two different conditions where **Cu-Cyclam** species has been characterized are reported as example: a) the organic solvent acetonitrile, with tetrabutylammonium hexafluorophosphate as support electrolyte and b) phosphate buffer 0.2 M at pH = 8.

Among aqueous solutions, we also investigated some of the most common media used to investigate water oxidation catalysis by Copper: phosphate buffer pH = 10, bicarbonate buffer pH = 10 and sodium hydroxide with sodium acetate (NaOAc) as electrolyte (pH range = 8-12). The latter was selected as the optimal working conditions, since it gave the best electrocatalytic activity, enabling also a direct comparison with state of the art Copper catalysts.⁽⁹⁾

In NaOH/NaOAc 0.1 M and pH = 12, under anodic scan, an intense wave appears at $E > 0.80$ V vs Normal Hydrogen Electrode (NHE), reaching a peak current at $E = 1.14$ V vs NHE (Fig. 4.5). This wave was attributed to the oxidation of water to dioxygen, as confirmed by the presence of a cathodic wave at -0.26 V vs NHE observed in the reverse scan, due to reduction of oxygen formed at the glassy carbon working electrode. In Fig. 4.5 it is possible to appreciate the difference between the CV of the blank conditions (–) and the solution with the **catalyst** (–).

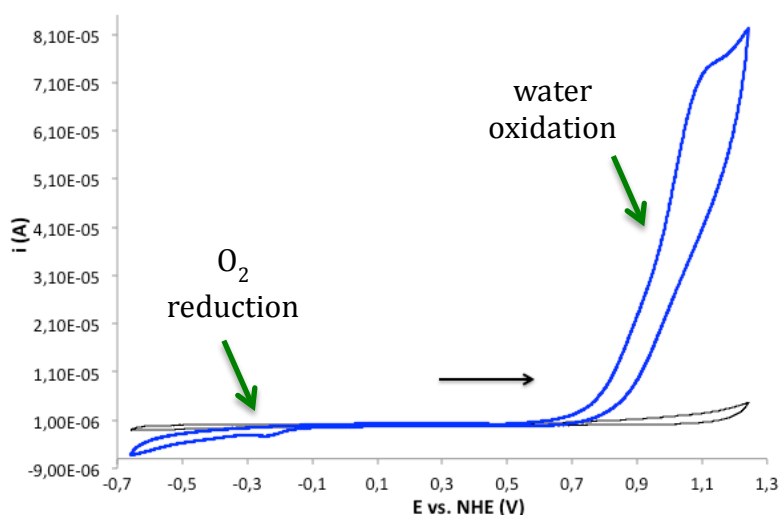


Fig. 4.5: Cyclic voltammetry of 0.5 mM **Cu-Cyclam** in NaOH, NaOAc 0.1 M, pH = 12, WE: glassy carbon, CE: Pt wire, RE: SCE (KCl sat), potentials are then referred to (NHE), scan rate: 100 mV/s

In order to exclude possible heterogeneous evolution in situ of the system during CV experiments the voltammogram of $\text{Cu}(\text{ClO}_4)_2 \cdot 6\text{H}_2\text{O}$ (the copper precursor used in the synthesis of **Cu-Cyclam**) was performed, since Cu^{II} aquoions are a

well-known precursors of electrodeposited Copper oxides. ⁽²⁾ Anyway, the anodic scan in the presence of Cu^{II} did not show the presence of a catalytic wave (Fig. 4.6), thus suggesting that in these conditions the formation of copper oxides is not favoured.

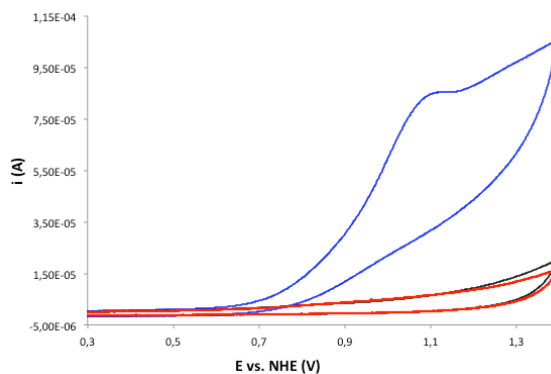


Fig. 4.6: CV comparison of NaOH pH = 12 and NaOAc 0.1 M solutions with (in black) no catalyst added, (in blue) 0.5 mM **Cu-Cyclam** and (in red) 0.5 mM Cu(ClO₄)₂·6 H₂O. Scan rate: 100 mV/s, WE: GC (d = 3 mm), CE: Pt wire, RE: Ag/AgCl, potentials are then referred to (NHE)

Another evidence of homogeneity in this system comes from “not polished working electrode” test. After the CV scan in the presence of the **Cu-Cyclam** catalyst, showing the behaviour reported above (blue trace in Fig. 4.7), the same glassy carbon working electrode was used without polishing in a fresh buffer solution, in the absence of the catalyst. In this case, a deep abatement of the intensity of the wave was observed (green trace in Fig. 4.7), ruling out a major electrodeposition of active layers on the electrode.

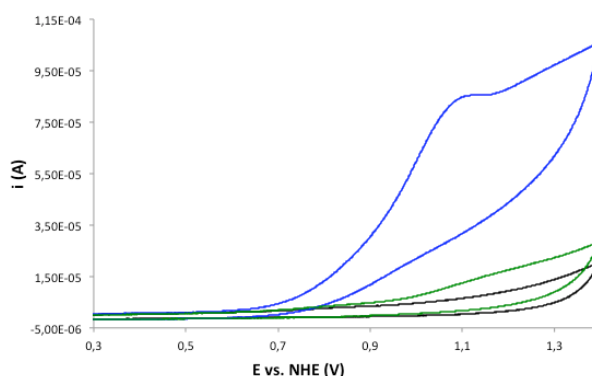


Fig. 4.7: CV comparison of NaOH pH = 12 and NaOAc 0.1 M solutions with (black) no catalyst, (blue) 0.5 mM **Cu-Cyclam** and (green) new fresh buffer with unpolished working electrode. Scan rate: 100 mV/s, WE: GC (d = 3 mm), CE: Pt wire, RE: Ag/AgCl, potentials are then referred to (NHE)

The electrochemical studies were further investigated during a Short Term Scientific Mission (STSM) within the European COST CM1205 CARISMA Action, in the research group of Profs. M. Robert and J.-M. Savéant at the University Paris 7 – Diderot. With the outfit available in the hosting Paris laboratories, CV analysis was performed with a rotating ring disk electrode (Fig. 4.8 a)). The advantage of this kind of equipment is the possibility to match the response of a glassy carbon working electrode, with a ring Platinum electrode set on the reduction potential of oxygen (-0.51 V vs NHE, with a Pt electrode). In such set-up, it is possible to measure simultaneously the anodic current at the glassy carbon upon application of an increasing bias, and the cathodic current at the Platinum ring (diagnostic for the presence of O₂); therefore, it is possible to determine the minimum potential required at the glassy carbon working electrode to evolve O₂.

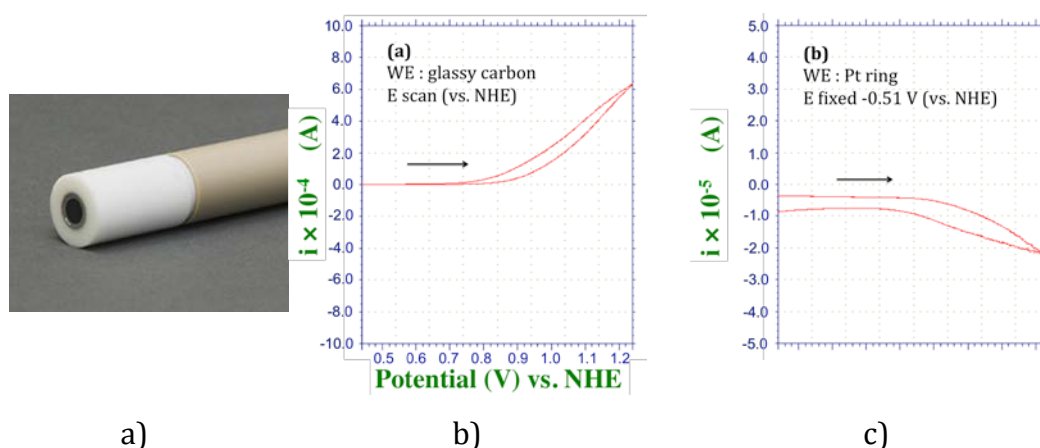


Fig. 4.8: **a)** Image of the rotating Pt disk electrode, **b)** cyclic voltammetry of **Cu-Cyclam** in 0.1 M NaOAc/NaOH, pH = 12. Internal WE: glassy carbon (d = 5 mm), CE: Platinum wire, RE: SCE (KCl sat.), potentials are then referred to NHE; scan rate: 100 mV/s. while the Platinum ring is kept at E = -0.51 V vs NHE, **c)** current registered at the external WE: Pt ring kept constant at E = - 0.51 vs NHE

The graph in Fig. 4.8 b) shows the voltammogram recorded at the glassy carbon working electrode, while the one in Fig. 4.8 c) represents the current produced at the Platinum ring electrode set at the constant potential of reduction of Oxygen (-0.51 V vs NHE, with a Platinum electrode). In these conditions, the cathodic current at the Platinum ring, diagnostic for the presence of O₂, was observed to raise upon application of E = 0.94 V vs NHE at the glassy carbon working

electrode. Since the thermodynamic potential of water oxidation at pH = 12 is 0.52 V vs NHE, an overpotential of 0.42 V for water oxidation with **Cu-Cyclam** can be estimated. This value is among the lowest reported in the literature for Cu catalysts, reported in the range 0.30 – 0.75 V. ⁽¹⁻⁵⁾

Other information about the electrochemical mechanism events can be obtained studying the current dependence on catalyst concentration and scan rate in CV experiments. As reported in Fig. 4.9 a), an increase of the peak current at 1.14 V vs NHE was observed by increasing **Cu-Cyclam** concentration. Moreover the dependence came out to be linear, which can be imputable to a single-site Copper catalysis. ⁽³⁾

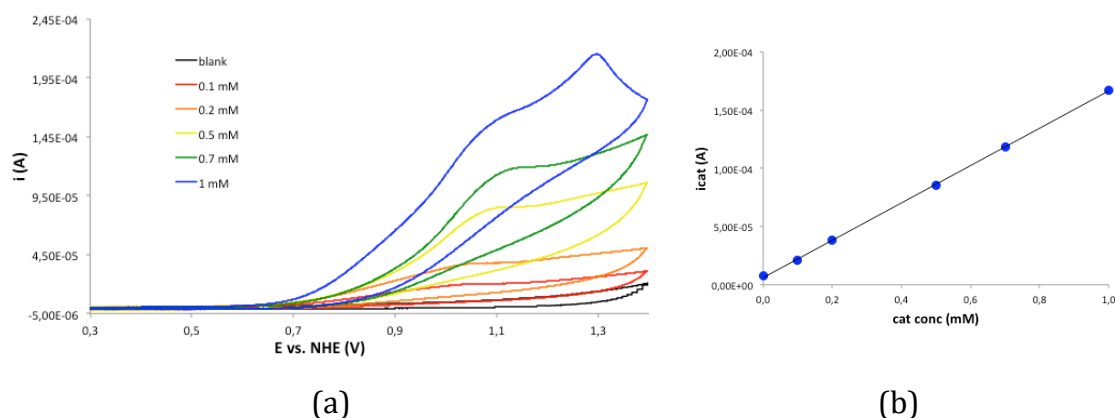


Fig. 4.9: CV of solutions in NaOH pH = 12 and NaOAc 0.1 M **a)** at different concentrations of **Cu-Cyclam** and **b)** dependence of i_{cat} (1.14 V vs NHE) on concentration of (**Cu-Cyclam**). Scan rate: 100 mV/s, WE: GC (d = 3 mm), CE: Pt wire, RE: Ag/AgCl, potentials are then referred to (NHE).

The current dependence on the square root of scan rate was then examined. The value of the catalytic peak current for the wave at 1.14 V vs NHE, normalized by the square root of the scan rate, increased with decreasing scan rate (Fig. 4.10), consistent with a rate-determining chemical step, likely ascribable to O-O bond formation. ⁽³⁾

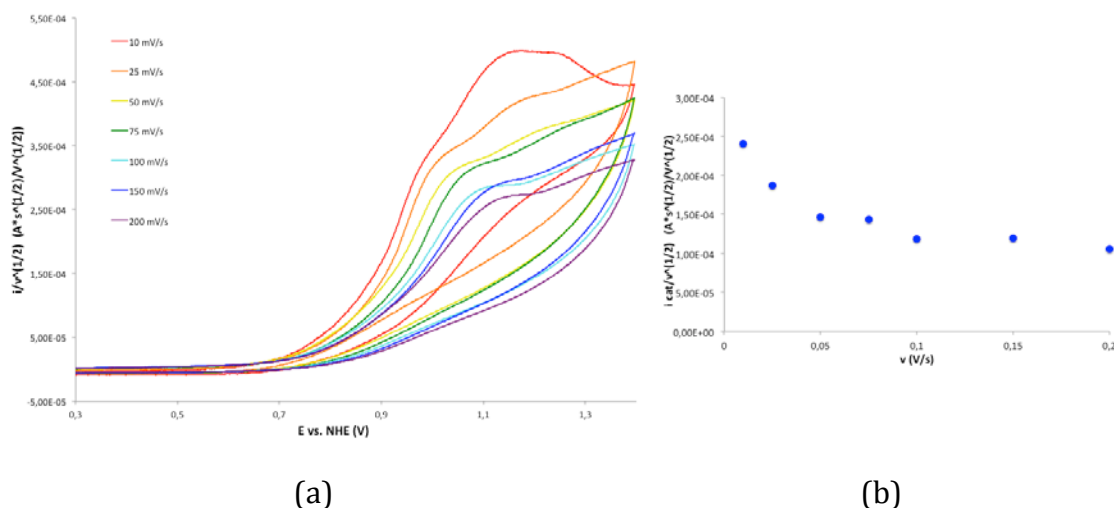


Fig. 4.10: CV of 0.5 mM **Cu-Cyclam**, solution in NaOH pH = 12 and NaOAc 0.1 M **a)** at different scan rates with normalized current ($i/v^{1/2}$) and **b)** dependence of i_{cat} (1.14 V vs NHE) on $v^{1/2}$. WE: GC (d = 3 mm), CE: Pt wire, RE: Ag/AgCl, potentials are then referred to (NHE).

4.2.3 Photoelectrochemical experiments

The interesting electrocatalytic activity of **Cu-Cyclam** in water oxidation, prompted us to investigate it in combination with a photoelectrode. Such study is particularly attractive since so far there are no examples in literature of systems combining Copper catalysts for water oxidation and light activated processes.

In particular, we focused on hematite semiconductor (α -Fe₂O₃), for its peculiar features: 1) abundance and low cost of Iron; 2) band gap of 2.0-2.2 eV, enabling absorption in the visible region of the solar emission; 3) suitable energy level of the valence band, with respect to the thermodynamic requirement for water oxidation; ⁽¹⁰⁾ 4) good stability and photoelectrochemical performance in strong alkaline media, ⁽¹¹⁾ thus matching the conditions required by **Cu-Cyclam** to perform water oxidation catalysis.

The experiments were run with FTO electrodes where a layer of hematite was deposited via a hydrothermal route, ⁽¹²⁾ provided by the group of Prof. Caramori from University of Ferrara. These photoanodes were used as working electrode in presence and absence of **Cu-Cyclam** 0.5 mM in NaOH/NaOAc solution at pH = 12 (Fig. 4.11).

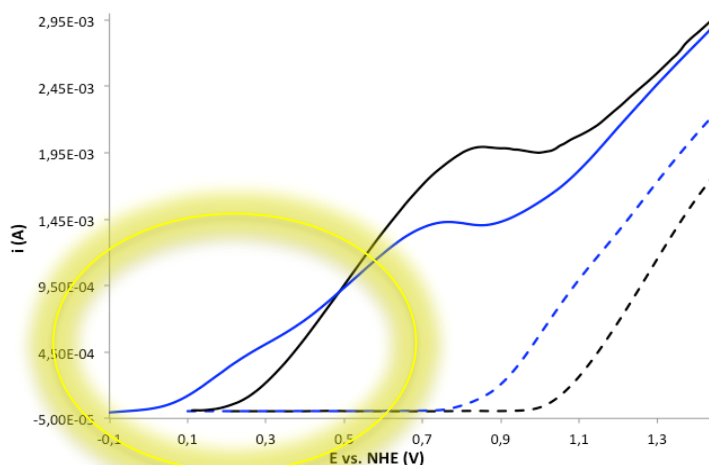


Fig. 4.11: Cyclic voltammetry of 0.5 mM **Cu-Cyclam** in NaOAc/NaOH, pH 12 in the presence (blue, solid line) and in the absence (blue, dashed line) of light; blank scans in the absence of catalyst are shown in black, solid line (in the presence of light) and in black, dashed line (in the absence of light). WE: hematite (1 cm² geometric surface area); CE: Pt wire; RE: Ag/AgCl, potentials are then referred to (NHE); scan rate: 10 mV/s; light source: Mercury-Tungsten lamp, 150 W, cut-off filter at 375 nm (power density 90 mW·cm⁻²)

The experiments performed in the absence of illumination (dashed lines in Fig. 4.11), show the presence of an anodic current, ascribable to water oxidation,⁽¹³⁾ that occurs at lower potentials when **Cu-Cyclam** is added in solution (dashed blue curve) compared with blank setting (dashed black curve). When the hematite based electrode is illuminated with an Hg-W lamp (power density = 90 mW·cm², with a cut off filter at 375 nm) a photocurrent is observed to raise at $E = 0.25$ V vs NHE in absence of catalyst (solid, black curve in Fig. 4.11), as expected for hematite semiconductors. Interestingly, when **Cu-Cyclam** was added in solution, the potential of the onset of the photocurrent is anticipated at $E = 0.05$ V vs NHE (solid blue curve in Fig 4.11).

This is consistent with an oxidation process occurring in the presence of the Copper species.

At higher bias the photocurrent of hematite alone is higher than the one registered in the presence of the catalyst. This can be explained on the basis of the good efficiency of hematite in water oxidation catalysis at high applied potentials, where charge recombination is less favoured. In the same conditions, in the presence of **Cu-Cyclam**, the performance of α -Fe₂O₃ is partially inhibited,

since the value of the photocurrent is lower than with hematite alone. This effect can be due to charge recombination promoted by copper. However, the optimal operating conditions for a photoanode should account the lowest possible applied potential (ideally zero) and therefore, we investigated the nature of the photocurrent in the presence of **Cu-Cyclam** at low applied bias, to check if this can be ascribed to water oxidation.

In order to verify our hypothesis and quantify the Faradaic yield, we run photo chronoamperometry experiments, measuring the amount of Oxygen. Therefore, an Oxygen probe was plunged in the solution in the presence of the catalyst and the hematite semiconductor at the applied potentials of 0.24 and 0.39 V vs NHE , under 1 sun irradiation (100 mWcm^{-2}). In both experiments, in the presence of **Cu-Cyclam** 1mM, no Oxygen was detected, while in the blank solution the gas evolution is found, as normally expected in the presence of hematite catalytic behaviour, see Fig. 4.12.

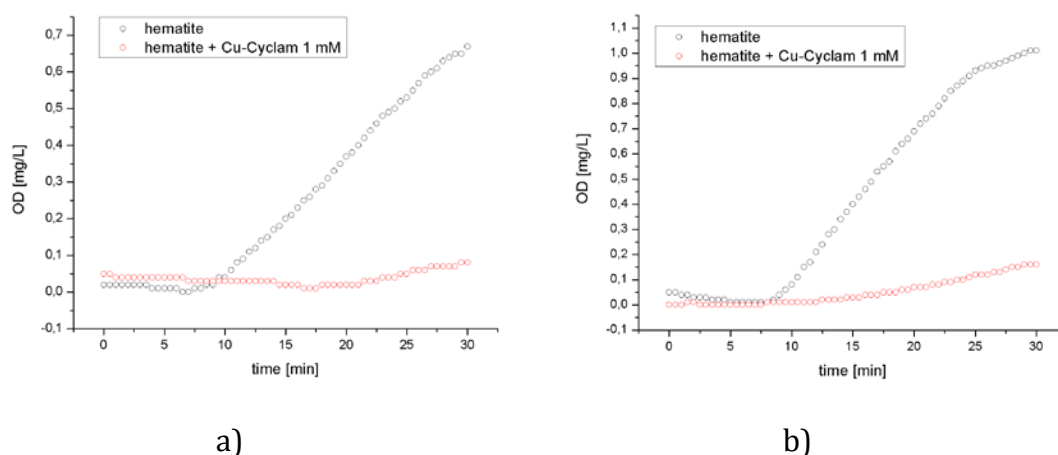


Fig. 4.12: Oxygen detection in NaOH/ NaOAc 0.1 M, pH = 12, under 1 sun illumination (100 mWcm^{-2}), without (black points) and with (red points) **Cu-Cyclam**, 1mM. Potential applied at 8 min: **a)** 0.24, **b)** 0.39 V vs NHE. WE: hematite (1 cm^2 geometric surface area), CE: Pt electrode, RE: SCE, potentials are then referred to (NHE)

We can conclude from these results that the **Cu-Cyclam** is acting as a direct sacrificial agent, capturing the hematite semiconductor holes and enhancing the photocurrent at low applied bias, but without producing oxygen. The increase of photocurrent observed, could likely be associated to **Cu-Cyclam** degradation.

Nevertheless, the achieved insight is interesting because it underlines the particular care needed when a molecular species is studied in combination with

a large band gap semiconductor. The interface between the molecular level and the photoelectrode material requires a deep investigation in order to optimize experimental conditions.

4.2.4 A limit of this system: stability

The CV analysis results brought us to consider bulk electrolysis experiments in order to exploit the whole amount of catalyst present in solution, and obtain information on the current and charge produced. The instrumental outfit, Fig. 4.13 a), permitted to use a 10 mL solution in a carbon beaker used as the working electrode, with Platinum wire and Ag/AgCl as counter electrode and reference electrode, respectively.

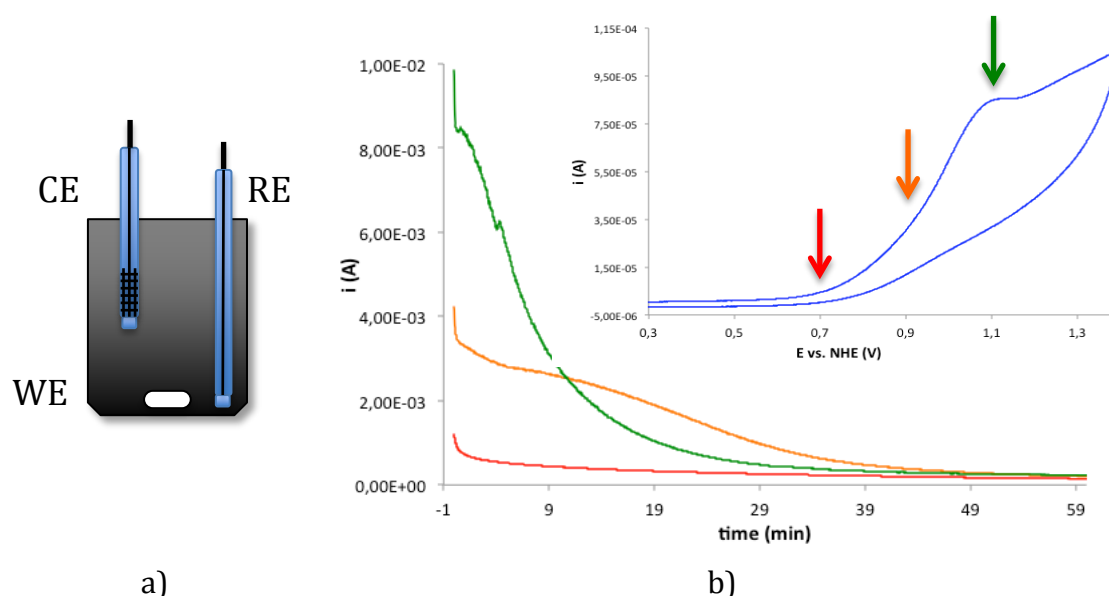


Fig. 4.13: **a)** Schematic representation of the outfit for electrolysis experiment, **b)** Examples of electrolysis results for **Cu-Cyclam** [0.5 mM in NaOH and NaOAc 0.1 M, pH 12, potential applied (-) 0.7 V vs NHE, (-) 0.94 V vs NHE and (-) 1.14 V vs NHE, WE: solid carbon, CE: Pt wire, RE: Ag/AgCl, potentials are then referred to (NHE), sacrificial reagent at CE: $\text{Na}_2\text{S}_2\text{O}_8$ 3M

In Fig. 4.13 b), the current produced during electrolysis at different applied potentials is reported. Different electrolysis experiments were performed, changing the potential applied at the working electrode, set at 0.70 V vs NHE (foot-of-the-wave of water oxidation), 0.94 V vs NHE (potential at which the minimum overpotential is calculated) and 1.14 V vs NHE (peak of the wave). In all cases, it is possible to observe that the electrolysis currents decrease over

time, and become negligible after about 50 minutes of electrolysis. This speaks in favour of a major abatement of the catalytic activity, likely ascribable to a transformation of the catalyst into an inactive species, upon application of the anodic bias. Indeed, CV and UV-Vis characterization run on the solutions after electrolysis confirm such hypothesis: the CV after electrolysis show an abatement of the intensity of the catalytic wave of water oxidation (Fig. 4.14 a)), while in the UV-Vis spectra the typical absorption at 506 nm of **Cu-Cyclam** is not anymore present, and a new band at 490 nm is observed (Fig. 4.14 b)). The identity of this species is still under investigation, but partial degradation of the organic ligand and/or a dimerization of the copper species through μ -oxo bridge could be envisaged. (4)

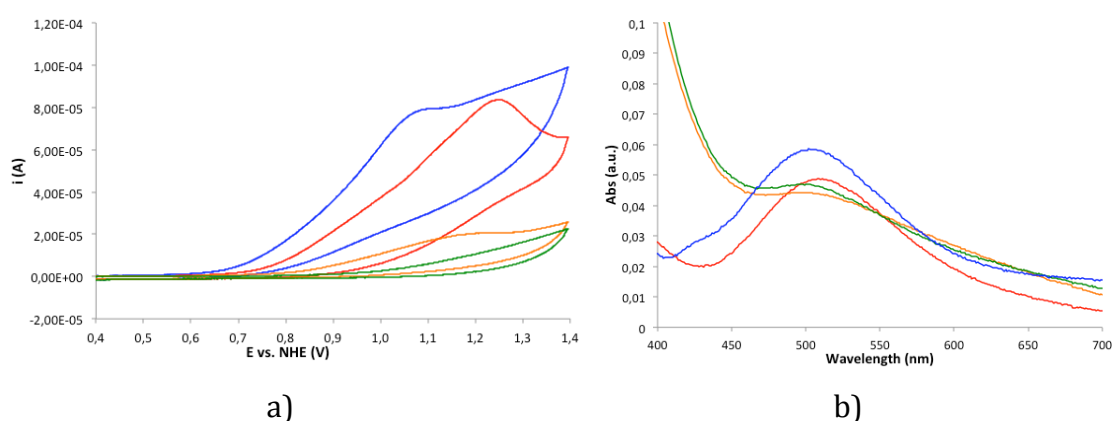


Fig. 4.14: **a)** CV voltammograms for **Cu-Cyclam** in NaOH/0.1 M NaOAc, pH12 (-) before and after (-) 0.7 V, (-) 0.94 V and (-) 1.14 V vs NHE electrolysis, WE: GC (d = 3 mm), CE: Pt wire, RE: Ag/AgCl, potentials are then referred to (NHE); **b)** UV-Vis spectra for **Cu-Cyclam** in NaOH/0.1 M NaOAc, pH12 (-) before and after (-) 0.7 V, (-) 0.94 V and (-) 1.14 V vs NHE electrolysis

4.3 Conclusions and Perspectives

A Copper(II) complex with a nitrogen based macrocyclic ligand was proposed as a novel water oxidation catalyst, working in electrochemical and photoelectrochemical systems.

Electrochemical studies allowed to evidence: 1) the activity of the compound in water oxidation catalysis, 2) a low operating overpotential of 0.42 V, significantly lower than literature benchmarks and 3) some aspects of the mechanistic pathway of catalysis. Moreover, 4) interesting information can be obtained interfacing the Cu species with hematite semiconductors and light: the presence

of the catalyst enhances the current intensity at low potentials. However, this current is not due to Oxygen evolution but to the degradation of **Cu-Cyclam**, acting as a holes-capture for hematite photoanode. 5) From our results, we could also underline the importance of the care we have to take studying systems where molecular species and semiconductor materials are interfaced.

The limit of this system consists in the evolution of the species into inactive products, which was observed with electrolysis experiments where the catalyst was consumed after about 1 hour of applied anodic bias. In order to overcome this issue, some experiments can be design in order to avoid or limit the catalyst consumption. For example a target tuning of the organic ligand can drive the stability of the species improving its activity. Future perspectives will focus on 1) a deeper investigation of the evolution of the system and 2) the study of the catalyst performance and stability, through functionalization of the cyclam ligand.

4.4 References

- ¹ (a) S.M. Barnett, K. I. Goldberg, J. M. Mayer *Nat Chem* **2012**, *4*, 498; (b) T. Zhang, C. Wang, S. Liu, J.-L. Wang, W. Lin *J Am Chem Soc* **2014**, *136*, 273
- ² Z. Chen, T. J. Meyer *Angew Chem Int Ed*, **2013**, *52*, 700
- ³ M. Zhang, Z. Chen, P. Kang, T. J. Meyer *J Am Chem Soc* **2013**, *135*, 2048
- ⁴ P. Haack, C. Limberg *Angew Chem Int Ed*, **2014**, *53*, 4282
- ⁵ D. H. Bush *Acc Chem Res*, **1978**, *11*, 392
- ⁶ M. Zhang, M.-T. Zhang, C. Hou, Z.-F. Ke, T.-B. Lu *Angew Chem Int Ed*, **2014**, *53*, DOI: 10.1002/anie.201406983
- ⁷ B. Bosnich, C. K. Poon, M. L. Tobe *Inorg Chem*, **1965**, *4(8)*, 1102
- ⁸ P. A. Tasker, L. Sklar *J Cryst Mol Struct*, **1975**, *5*, 329
- ⁹ M. D. Kärkä, O. Verho, E. V. Johnston, B. Åkermark *Chem Rev*, **2014**, DOI: dx.doi.org/10.1021/cr400572f
- ¹⁰ P. Liao, M. C. Toroker, E. A. Carter *Nano Lett*, **2011**, *11*, 1775
- ¹¹ M. Barroso, S. R. Pendlebury, A. J. Cowanc, J. R. Durrant *Chem Sci*, **2013**, *4*, 2724
- ¹² N. Dalle Carbonare, V. Cristino, S. Berardi, S. Carli, R. Argazzi, S. Caramori, L. Meda, A. Tacca, C. A. Bignozzi *ChemPhysChem*, **2014**, *15*, 1164
- ¹³ S. D. Tilley, M. Cornuz, K. Sivula, M. Grätzel *Angew Chem*, **2010**, *122*, 6549

5. CHAPTER

Polyoxometalates in CO₂ reduction catalysis

5.1 Introduction

During the Ph.D., we were interested in investigating the redox catalysis processes involved in artificial photosynthesis, also in the field of CO₂ reduction. As already introduced in Chapter 1, artificial photosynthesis presents an architecture of processes turning molecules as water and CO₂ into higher energy products, exploitable as fuels. The oxidative process previously illustrated (water oxidation) is coupled with a reductive one, which could involve carbon anhydride. Reduction reactions of CO₂ are multi electronic, and generally the more common resulting species are formic acid and carbon monoxide. (Eq. 1.10-11)

These processes are characterized by high kinetic and thermodynamic barriers, and the competitive proton reduction into molecular hydrogen needs also to be considered. ⁽¹⁾ The presence of a catalyst helps to handle these requisites of the system in order to assist necessary electron transfers and bond rearrangements.

5.2 Results and Discussion

In this thesis, we have explored the potential of polyoxometalate ligands in CO₂ reduction. This choice was based on the high reactivity of such type of species in redox reactions, including water oxidation. In these studies, one of the main information that can be extracted is that transition metal substituted polyoxometalates can be considered as molecular fragments of metal oxides, ^(2, 3) with similar behaviour also in the reactivity. Therefore, for the design of transition metal substituted polyoxometalates aimed at catalytically reducing CO₂, we were inspired by the recent work by M. Kanan et al. ⁽⁴⁾ on the catalytic reduction of CO₂ by a Copper(I) oxide. This system is particularly promising since it works at low overpotential, in aqueous bicarbonate buffer at neutral pH. We explored then the reactivity of Copper based polyoxometalates, focusing in particular on the three families represented in species in Fig. 5.1.

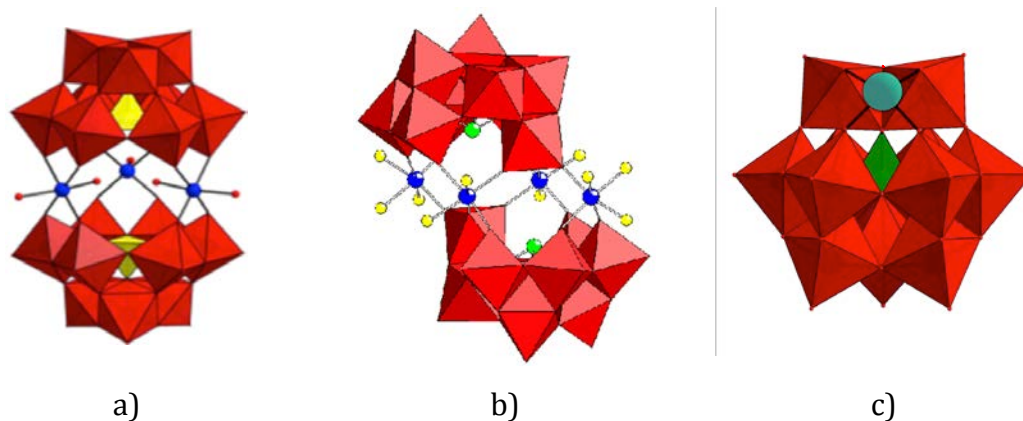


Fig. 5.1: Combined polyhedral/ball-and-stick representations of: **a)** $[\text{Cu}_3(\text{PW}_9\text{O}_{34})_2]^{12-}$, blue: Copper, yellow: Phosphorus; **b)** $[\text{Cu}_4(\text{H}_2\text{O})_{10}(\text{XW}_9\text{O}_{33})_2]^{n-}$, X = As, Sb, Se, Te, blue: Copper, green: X; **c)** $[\text{Cu}(\text{SiW}_{11}\text{O}_{39})]^{6-}$, light blue: Copper, green: Silicon

These compounds were synthesized according to literature procedures,⁽⁵⁾ while their preliminary behaviour in electrochemical reduction was investigated in our laboratory in a Master Thesis work. This study highlighted the third complex shown in Fig. 5.1 c), $[\text{CuSiW}_{11}\text{O}_{39}]^{6-}$ (hereafter **CuPOM**) as the most promising candidate for reduction of CO_2 , since it showed a huge cathodic current in bicarbonate buffer (*vide infra*). Therefore, in this work, the nature of this wave was investigated in more details, in collaboration with the group of Prof. Marc Robert (Université Paris 7 - Denis Diderot) exploiting a Short Term Scientific Mission within the European COST Action CM1205, Catalytic Routines for Small Molecule Activation (CARISMA).

The starting approach consisted in a general electrochemical characterization of the selected complex **CuPOM**, exploiting cyclic voltammetry (CV) technique in order to define the optimal conditions: solvent, buffer and any needed additives. After this screening, we planned to move to the catalytic system, studying the activity of this compound in presence of CO_2 .

Among electrochemical characterization, CV experiments of **CuPOM** (isolated as the tetrabutylammonium salt) were initially run in dimethylformamide (DMF), with ammonium hexafluorophosphate as electrolyte. In Fig. 5.2 the CVs of **CuPOM** at different scan rates are reported, and show three characteristic reversible peaks. The first monoelectronic wave is due to reduction of Cu^{II} to Cu^{I} but it is appreciable only at high scan rates because it is partially superimposed

with the second one. The second and the third wave, showing $E_{1/2}$ of -0.87 and -0.63, respectively, are indicative of multi electron reductions connected with the POM structure, concerning reduction of W^{VI} to W^V , as described in literature. ⁽⁶⁾

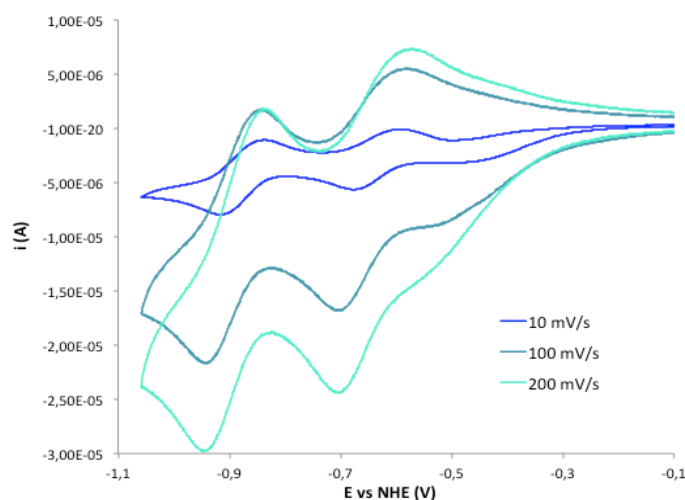


Fig. 5.2: Cyclic voltammetry of 0.5 mM **CuPOM** in DMF, NH_4PF_6 0.1 M, WE: glassy carbon, CE: Pt wire, RE: SCE (KCl sat), potentials are then referred to (NHE), scan rate: see legend

We completed the characterization of the species moving to aqueous buffers: the water soluble potassium salt of **CuPOM** was characterized in 0.2 M phosphate buffer pH = 7 and 0.5 M bicarbonate buffer pH = 7.

In bicarbonate buffer CV experiments were performed at different scan rates in order to observe the current intensity normalized with respect to the square root of the scan rate, Fig. 5.3 a). Moreover, in Fig. 5.3 b), we plotted the peak current normalized against the square root of the scan rate to study the reversibility of the process or to verify a potential evolution of the compound.

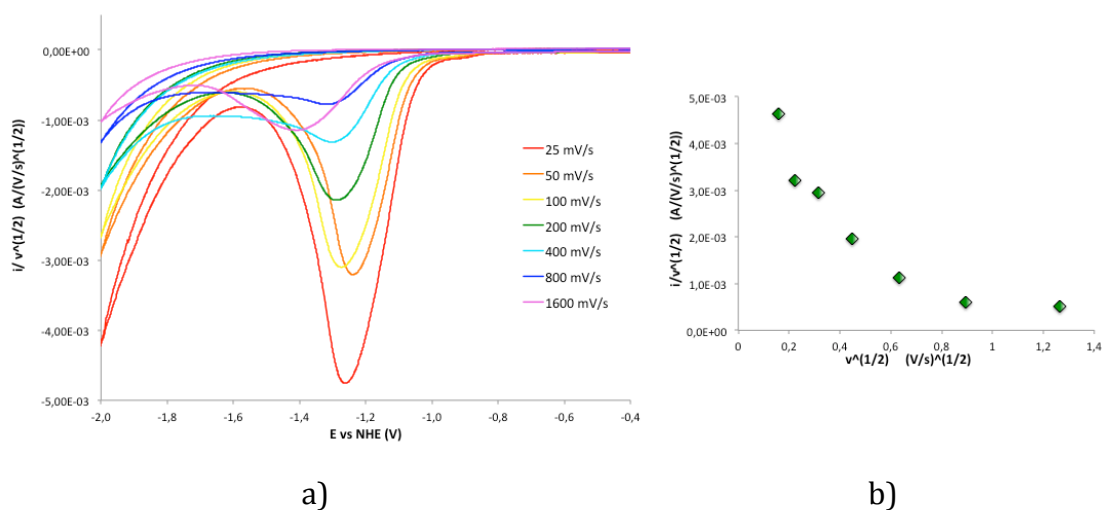


Fig. 5.3: CV of 0.5 mM **CuPOM**, solution in buffer KHCO_3 0.5 M, pH = 7 **a)** at different scan rates with normalized current ($i/v^{(1/2)}$) and **b)** dependence of i on $v^{(1/2)}$. WE : GC (d = 3 mm), CE : Pt wire, RE: Ag/AgCl, potentials are then referred to (NHE).

The value of the cathodic peak current for the wave at -1.3 V vs NHE, normalized by the square root of the scan rate, increased with decreasing scan rate, and a shift of the potential of the peak current was also observed. This behavior and the narrow shape of the waves reaching high current intensity were indicative of some irreversible evolution and consumption of the species **CuPOM**.

The characterization in 0.2 M phosphate buffer, pH = 7, confirmed the previous results: voltammograms (Fig. 5.4) showed some current intensities and shapes indicative of some particular evolution of the catalyst on the surface of the working electrode. In fact, the narrow wave at $E = 0.12$ V vs NHE visible in Fig. 5.4 a) under the anodic back scan, is attributed to oxidation of metallic copper deposited at the glassy carbon working electrode from mono substituted Cu POM, under cathodic scan. ⁽⁷⁾ Moreover, as in the case of the previous buffer, a high cathodic current was observed at more negative potentials, upto -1.3 V vs NHE (Fig. 5.4 b)) with narrow shapely irreversible wave, hence we conclude that the catalyst was decomposing.

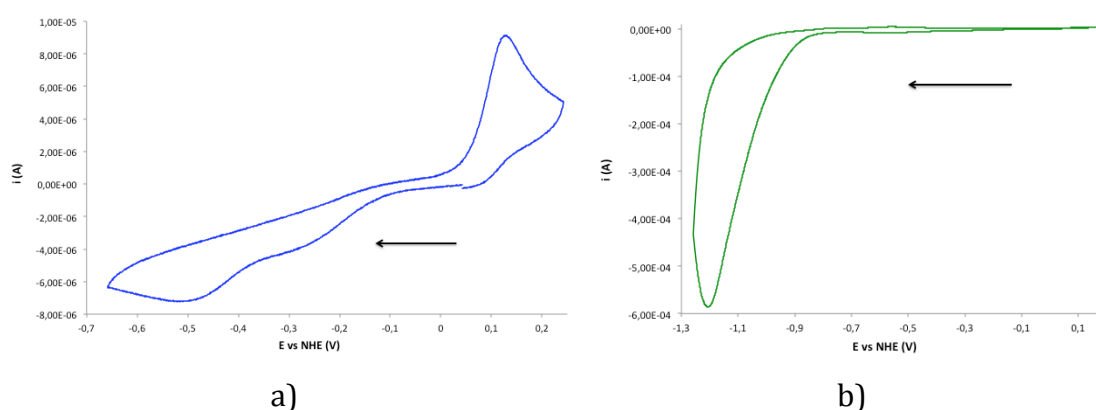


Fig. 5.4: CV of **CuPOM** 0.5 mM in phosphate buffer 0.1 M, pH = 7, WE: glassy carbon (d = 3 mm), CE: Pt wire, RE: SCE (KCl sat.), potentials are then referred to NHE, scan rate = 100 mV/s

Despite this result, we tried to perform the CV studies in the presence of CO_2 , in order to investigate the eventual presence of a catalytic process, by the variation of the reduction wave shape and intensity. We tested the behavior of the species

in presence of CO₂ but data processing showed slight changes on the shape of the cathodic waves, Fig. 5.5.

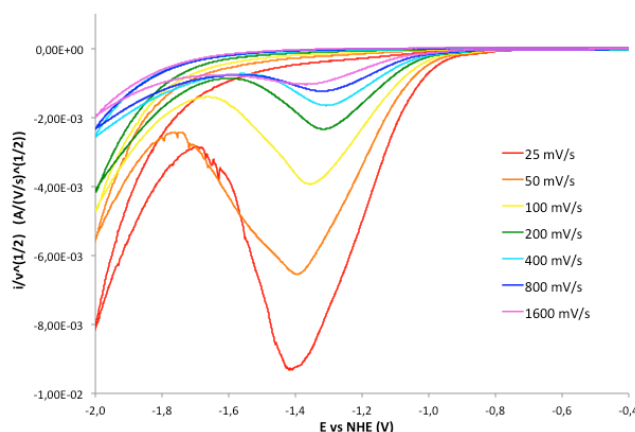


Fig. 5.5: CV of 0.5 mM CuPOM, solution in buffer KHCO₃ 0.5 M, pH = 7 at different scan rates with normalized current ($i/v^{(1/2)}$) and in presence of CO₂

However, this change can not be attributed to a catalytic process; on the contrary it confirmed that the catalyst was not stable in highly reducing electrochemical conditions. Changing some experimental conditions such as solvent and concentration of catalyst did not change the performance of the catalyst and for that reason we concluded it was not suitable for investigate in CO₂ reduction.

5.3 Conclusions and Perspectives

In this part of the Thesis, a polyoxometalate based Copper species has been investigated in the catalysis of CO₂ reduction through electrochemical system. However, the CV experiments were indicative of decomposition of the compound under cathodic scan, by releasing the Copper ion, which was deposited at the working electrode as metallic Copper. This probably defines a limit for the redox chemistry of transition metal substituted polyoxometalates, since this family of ligands is not able to stabilize enough transition metals with low oxidation state. This is probably related to the 'hard' nature of the nucleophilic oxygens, in the coordination sphere of the POM ligand. Studies need then to be focused on the design of an appropriate coordination sphere able to stabilize the Copper metal in its low oxidation states, to be stable in the highly reductive conditions needed to activate CO₂ reduction.

However, the preliminary results presented in this Chapter were useful to achieve ability and competence in the electrochemical field.

5.4 References

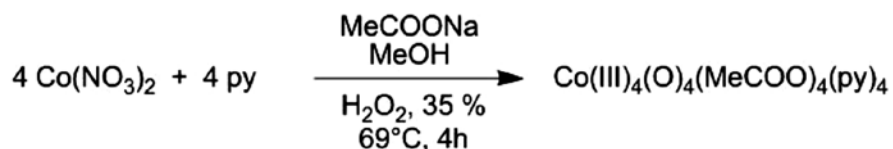
-
- ¹ J. Schneider, H. Jia, J. T. Muckerman, E. *Chem Soc Rev*, **2012**, *41*, 2036
- ² M. Carraro, N. Nsouli, H. Oelrich, A. Sartorel, A. Sorarù, S. S. Mal, G. Scorrano, L. Walder, U. Kortz, M. Bonchio *Chem Eur J* **2011**, *17*, 8371
- ³ S. Piccinin, A. Sartorel, G. Aquilanti, A. Goldoni, M. Bonchio, S. Fabris *Proc Nat Acad Sci U.S.A.* **2013**, *110*, 4917
- ⁴ C. W. Li, M. W. Kanan *J Am Chem Soc* **2012**, *134*, 7231
- ⁵ a) W. H. Knoth, P. J. Damaile, R. D. Farlee, *Organometallics* **1985**, *4*, 62; b) U. Kortz, M. G. Savelieff, B. S. Bassil, B. Keita, L. Nadjo, *Inorg. Chem.* **2002**, *41*, 783; c) F. Zonnevillage, C. M. Tourné, G. F. Tourné, *Inorg. Chem.* **1982**, *21*, 2751
- ⁶ J. E. Toth, F. C. Anson *J Electroanal Chem*, **1988**, *256*, 361
- ⁷ B. Keita, E. Abdeljalil, L. Nadjo, B. Avisse, R. Contant, J. Canny, M. Richet *Electrochem Comm*, **2000**, *2*, 145

6. CHAPTER

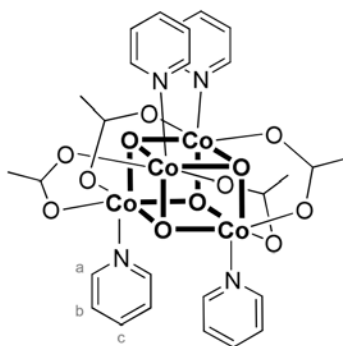
Experimental section

6.1 Synthesis

6.1.1 Synthesis of $\text{Co}_4(\mu_3\text{-O})_4(\mu\text{-O}_2\text{CMe})_4(\text{py})_4$, (1)



Synthesis of this species was performed following literature procedures (R. Chakrabarty, S. J. Bora, B. K. Das *Inorg Chem*, **2007**, 46, 9450).



2.90 g (10 mmols) of $\text{Co}(\text{NO}_3)_2 \cdot 6\text{H}_2\text{O}$ and 2.70 g (20 mmols) of $\text{CH}_3\text{CO}_2\text{Na} \cdot 3\text{H}_2\text{O}$ are dissolved in 30 mL of CH_3OH . To the stirred solution under reflux (about 65°C), 80 μL (10 mmols) of pyridine are added, and after 10-15 minutes 5 mL of 30% H_2O_2 (50 mmols) are inserted slowly into the reaction solution.

Reflux conditions under stirring are maintained for 4 hours and then the mixture is cooled to room temperature. Then, the solution is concentrated removing part of the solvent, observing the separation of a pink aqueous phase after addition of CH_2Cl_2 . The organic phase is dried over dry Na_2SO_4 . After filtration n-hexane is added to the solution obtaining an olive-green precipitate, which is separated and dried. A yield of about 90% is obtained.

$^1\text{H-NMR}$ (CD_3CN ; 300 MHz; δ , ppm): 8.38 (dd, 8H, $^2J_{a-b} = 6.6 \text{ Hz}$, $^3J_{a-c} = 1.5 \text{ Hz}$, H_a), 7.58 (tt, 4H, $^2J_{c-b} = 7.5 \text{ Hz}$, $^3J_{c-a} = 1.5 \text{ Hz}$, H_c), 7.09 (dd, 8H, $^2J_{b-a} = 6.6 \text{ Hz}$, $^2J_{b-c} = 7.5 \text{ Hz}$, H_b), 1.99 (s, 12H, $\mu\text{-O}_2\text{CCH}_3$).

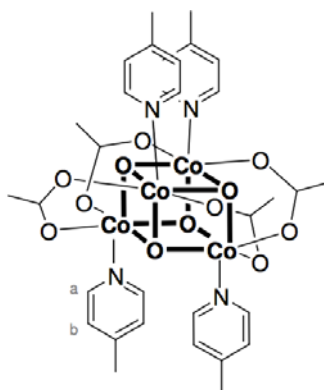
ESI-MS (FIA, flow: $\text{H}_2\text{O}:\text{CH}_3\text{CN} = 1:1 + \text{HCOOH} 0.1\%$, m/z): 852.95 [**1-H**] $^+\text{H}^+$; calculated for $[\text{C}_{28}\text{H}_{32}\text{Co}_4\text{N}_4\text{O}_{12}] \cdot \text{H}^+ = 852.94$.

FT-IR (KBr, cm^{-1}): 3114 (w), 3079 (w), 2927 (w), 1606 (w), 1534 (s), 1486 (m), 1450 (m), 1411 (s), 1341 (w), 1213 (w), 1071 (w), 1047 (w), 761* (w), 694* (m), 634* (w). (* = diagnostic of cubane structure). (w = weak, m = medium, s = strong).

6.1.2 Synthesis of $\text{Co}_4(\mu_3\text{-O})_4(\mu\text{-O}_2\text{CMe})_4(\text{p-NC}_5\text{H}_4\text{X})_4$, (**1-X**) (X = Me, t-Bu, OMe, Br, COOMe, CN)

The synthetic procedure is the same used for the previous **1** species, the difference consists in using different 4-substituted pyridines as reagent.

1-Me



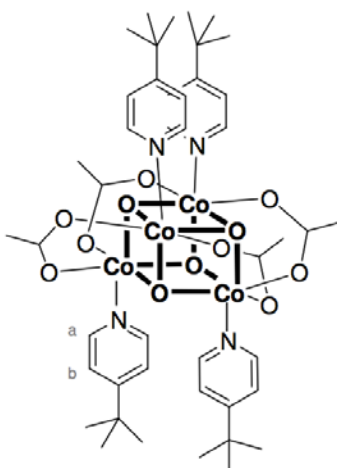
Yield: 2.01 g (88% based on cobalt).

$^1\text{H-NMR}$ (CD_3CN ; 300 MHz; δ , ppm): 8.09 (d, 8H, $J = 6.0$ Hz, Ha), 7.18 (d, 8H, $J = 6.0$ Hz, Hb), 2.33 (s, 12H, CH₃), 1.96 (s, 12H, $\mu\text{-O}_2\text{CCH}_3$).

ESI-MS (FIA, flow: $\text{H}_2\text{O}:\text{CH}_3\text{CN} = 1:1 + 0.1\%$ HCOOH; m/z): 908.9563 [**1-Me**] $\cdot\text{H}^+$; calculated for $[\text{C}_{32}\text{H}_{40}\text{Co}_4\text{N}_4\text{O}_{12}]\cdot\text{H}^+ = 909.00481$.

FT-IR (KBr, cm^{-1}): 3080 (w), 2958 (w), 2923 (w), 1717 (w), 1622 (m), 1536 (s, br), 1501 (s), 1411 (s, br), 1384 (s), 1337 (m), 1246 (w), 1226 (w), 1207 (m), 1068 (w), 1037 (w), 811 (m), 721* (w), 698* (m), 634* (m). (* = diagnostic of cubane structure). (w = weak, m = medium, s = strong, br = broad).

1-*t*Bu



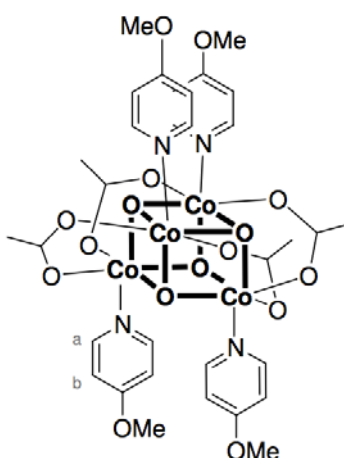
Yield: 58% based on cobalt.

¹H-NMR (CD₃CN; 300 MHz; δ, ppm): 8.34 (d, 8H, *J* = 6.2 Hz, H_a), 7.16 (d, 8H, *J* = 6.2 Hz, H_b), 1.96 (s, 12H, μ-O₂CCH₃) 1.25 (s, 36H, C(CH₃)₃).

ESI-MS (FIA, flow: H₂O:CH₃CN = 1:1 + 0.1% HCOOH; *m/z*): 1077.1490 [**1-*t*Bu**] \cdot H⁺; calculated for [C₄₄H₆₄Co₄N₄O₁₂] \cdot H⁺ = 1077.19262.

FT-IR (KBr, cm⁻¹): 3087 (w), 2966 (m), 2907 (w), 2872 (w), 2966 (m), 2872 (w), 1717 (w), 1617 (m), 1539 (m, br), 1500 (m), 1419 (s, br), 1384 (s), 1343 (w), 1274 (w), 1225 (w), 1072 (w), 1035 (w, br), 845 (w), 832 (w), 731* (w), 701* (w), 635* (m). (* = diagnostic of cubane structure). (w = weak, m = medium, s = strong, br = broad).

1-OMe



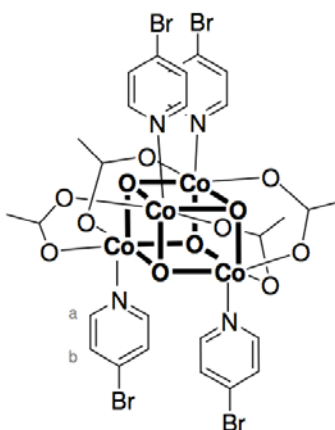
Yield: 82% based on cobalt.

¹H-NMR (CD₃CN; 300 MHz; δ, ppm): 8.12 (d, 8H, *J* = 6.9 Hz, H_a), 6.68 (d, 8H, *J* = 6.9 Hz, H_b), 3.84 (s, 12H, OCH₃), 1.97 (s, 12H, μ-O₂CCH₃).

ESI-MS (FIA, flow: H₂O:CH₃CN = 1:1 + 0.1% HCOOH; *m/z*): 972.9484 [**1-OMe**]⁺·H⁺; calculated for [C₃₂H₄₀Co₄N₄O₁₆]⁺·H⁺ = 972.98446.

FT-IR (KBr, cm⁻¹): 3017 (w), 2846 (w), 1618 (s), 1568 (m), 1541 (m, br), 1505 (s), 1414 (s, br), 1384 (s), 1346 (m), 1297 (s), 1207 (s), 1060 (m), 1037 (s), 1013 (m), 823 (m), 700* (m), 668* (m), 635* (m). (* = diagnostic of cubane structure). (w = weak, m = medium, s = strong, br = broad).

1-Br



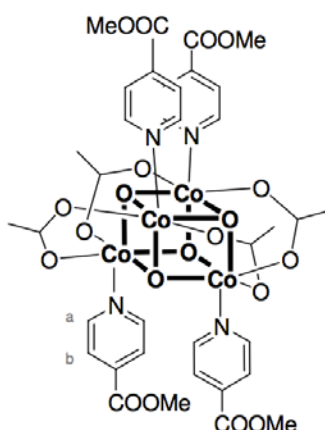
Complex **1-Br** was synthesized adapting the literature procedure. Co(NO₃)₂·6H₂O (0.48 g, 1.7 mmol) and CH₃CO₂Na·3H₂O (0.68 g, 5 mmol) are stirred in methanol (5 mL) and heated to refluxing temperature. 4-bromopyridine hydrochloride (0.32 g, 1.7 mmol) is then added to the stirred reaction mixture, followed by a portion of 11.6 M hydrogen peroxide (720 μL, 8.3 mmol), added dropwise. The reaction mixture was treated as described above for the analogous compounds. 0.42 g of a dark green solid were obtained (Yield: 85% based on cobalt).

¹H-NMR (CD₃CN; 300 MHz; δ, ppm): 8.20 (d, 8H, *J* = 6.6 Hz, H_a), 7.39 (d, 8H, *J* = 6.6 Hz, H_b), 1.99 (s, 12H, μ-O₂CCH₃).

ESI-MS (FIA, flow: H₂O:CH₃CN = 1:1 + 0.1% HCOOH; *m/z*): 1168.5 [**1-Br**]⁺·H⁺; calculated for [C₂₈H₂₈Br₄Co₄N₄O₁₂]⁺·H⁺ = 1164.58 (17%), 1166.58 (68%), 1168.58 (100%), 1169.58 (32%), 1170.58 (67%), 1172.58 (20%).

FT-IR (KBr, cm^{-1}): 3098 (w), 3030 (w), 2926 (w), 1717 (w), 1635 (m), 1590 (s), 1534 (s, br), 1479 (s), 1356 (s, br), 1342 (m), 1206 (m), 1098 (w), 1059 (w), 817 (m), 702* (m), 634* (m). (* = diagnostic of cubane structure). (w = weak, m = medium, s = strong, br = broad).

1-COOMe



Methyl 4-pyridinecarboxylate was synthesized reacting 4-pyridinecarboxylic acid (1.7 g, 13.8 mmol) and concentrated H_2SO_4 (750 μL) in methanol (50 mL) under microwave irradiation using a MW Ethos-1600 labstation (Milestone) with the following parameters: Power = 300 W until $T_{\text{bulk}} = 130^\circ\text{C}$ is reached, then Power = 240 W to maintain $T_{\text{bulk}} = 130^\circ\text{C}$ for 20 min. 1.56 g of the desired product were obtained after extraction in dichloromethane (Yield: 83%).

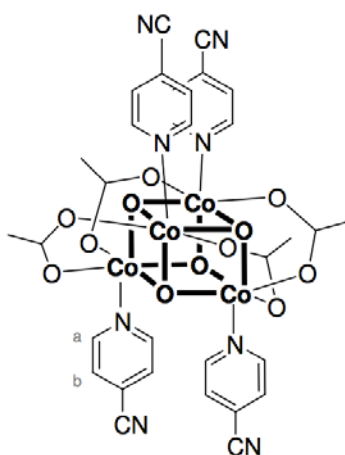
1-COOMe was synthesized adapting the general procedure described above, starting from methyl 4-pyridinecarboxylate (1.37 g, 10 mmol). 1.07 g of a dark green solid were obtained (Yield: 39% based on cobalt).

$^1\text{H-NMR}$ (CD_3CN ; 300 MHz; δ , ppm): 8.54 (d, 8H, $J = 6.5 \text{ Hz}$, H_a), 7.53 (d, 8H, $J = 6.5 \text{ Hz}$, H_b), 3.94 (s, 12H, COOCH_3), 2.01 (s, 12H, $\mu\text{-O}_2\text{CCH}_3$).

ESI-MS (FIA, flow: $\text{H}_2\text{O}:\text{CH}_3\text{CN} = 1:1 + 0.1\% \text{ HCOOH}$; m/z): 1084.9486 [**1-COOMe**] $\cdot\text{H}^+$; calculated for $[\text{C}_{36}\text{H}_{40}\text{Co}_4\text{N}_4\text{O}_{20}]\cdot\text{H}^+ = 1084.96409$.

FT-IR (KBr, cm^{-1}): 3128 (w), 3064 (w), 3014 (w), 2956 (w), 1734 (s), 1617 (w, br), 1539 (m, br), 1418 (s), 1345 (w), 1323 (w), 1292 (s), 1236 (w), 1195 (w), 1126 (m), 1062 (m), 960 (w), 868 (w), 835 (w), 768 (m), 701* (m), 634* (m), 589* (m), 575 (m). (* = diagnostic of cubane structure). (w = weak, m = medium, s = strong, br = broad).

1-CN



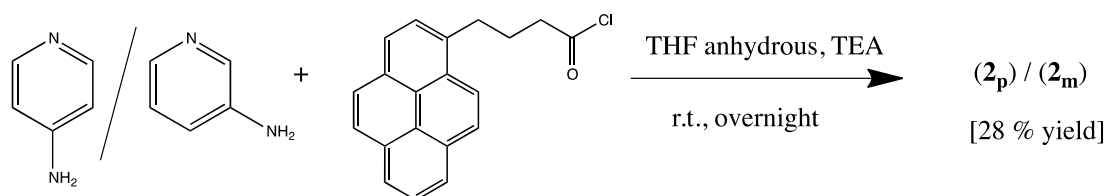
4-cyanopyridine (1.04 mL, 10 mmol) is used, and 2.16 g of a dark brown solid were obtained (Yield: 91% based on cobalt).

¹H-NMR (CD₃CN; 300 MHz; δ, ppm): 8.60 (d, 8H, *J* = 5.4 Hz, H_a), 7.50 (d, 8H, *J* = 5.4 Hz, H_b), 2.01 (s, 12H, μ-O₂CCH₃).

ESI-MS (FIA, flow: H₂O:CH₃CN = 1:1 + 0.1% HCOOH; *m/z*): 952.9053 [1-CN]·H⁺; calculated for [C₃₂H₂₈Co₄N₈O₁₂]·H⁺ = 952.92319.

FT-IR (KBr, cm⁻¹): 3113 (w), 3055 (w), 2927 (w), 2237(w), 1610 (w), 1534 (s), 1490 (m), 1413 (s), 1385 (s), 1343 (w), 1214 (w), 1065 (w), 1031 (w), 833 (m), 791 (w), 699* (m), 634* (m), 589* (m), 575 (m), 563 (m). (* = diagnostic of cubane structure). (w = weak, m = medium, s = strong).

6.1.3 Synthesis of 4-(pyren-1-yl)-N-(pyridin-4-yl)butanamide and 4-(pyren-1-yl)-N-(pyridin-3-yl)butanamide compounds (**2_m** and **2_p**)

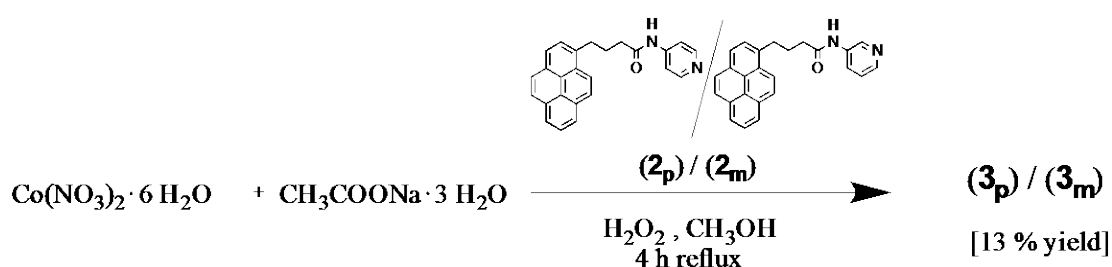


Synthetic procedure for the two ligands is the same, only one of the reagents change: on one hand (**2_m**) is used 3-amino pyridine, on the other (**2_p**) the 4-amino pyridine.

In a 50 mL balloon 213 mg (2.27 mmoles) of amino pyridine are dissolved in 20 mL of tetrahydrofuran (THF) anhydrous and 2 mL of triethylamine. To the

solution 700 mg (2.27 mmoles) of 4-pyren-1-yl-butanoyl chloride are added. The mixture is stirred at room temperature overnight. THF is removed and the product is dissolved again in CH₂Cl₂ and H₂O, the organic phase is separated and removed with rotavapor. The obtained white solid is dissolved in THF and then adding n-hexan the final reaction product precipitates. The yield achieves about 28 %.

6.1.4 Synthesis of Co₄(μ₃-O)₄(μ-O₂CCH₃)₄(4-(pyren-1-yl)-N-(pyridin-4-yl)butanamide)₄ and Co₄(μ₃-O)₄(μ-O₂CCH₃)₄(4-(pyren-1-yl)-N-(pyridin-3-yl)butanamide)₄ compounds (**3_p** and **3_m**)



Synthetic procedure of these two compounds is the same, the only variation is due to the use of the different reagent **2_m** or **2_p** to obtain the desired product.

In a 50 mL balloon 108.85 mg (0.374 mmoles) of Co(NO₃)₂·6H₂O and 101.79 mg (0.748 mmoles) of CH₃COONa·3H₂O are dissolved in 12 mL of CH₃OH. To the mixture under reflux (about 65° C), 136.43 mg (0.374 mmoles) of ligand (**2_m** or **2_p**) are added, after about 30 minutes, 191 μL (1.87 mmoles) of 30% H₂O₂ are slowly introduced in the balloon. The mixture is left for 4 hours under reflux and stirring. After cooling to room temperature, the organic solvent is evaporated after removing the aqueous phase even if it is difficult distinguishing clearly. The obtained compound is washed with three aliquots of, one of H₂O and the last one of Et₂O again. The product is dried and weight. The yield is about 13 % for both **3_p** and **3_m**.

3_p)

¹H-NMR (DMSO-d₆; 300 MHz; δ, ppm): second order spectra, 2.1 (m, 2H), 2.3 (m, 2H), 3.2 (m, 2H), 8 (m, 13H), 10.3 (s, 1H).

ESI (FIA, flow: CH₃CN + HCOOH 0.1%, *m/z*): 1993,6; calculated: 1994.

FT-IR (KBr, cm^{-1}): 584, 633, 700, 762 (diagnostic of cubane structure), 841 (s), 1418 (s), 1509 (s), 1700, 3000. (s = strong).

CV (THF, 0,1 M TBAClO₄, 0,5 mM in **3_p**); (THF : B8 10 mM = 1 : 1, 0,5 mM in **3_p**)

UV-Vis (THF, nm): 340 nm c.a. (10^{-6} M), 640 nm c.a. (10^{-3} M)

Fluorescence (10^{-6} M, THF, nm): 370, 396, 410, 750, 790.

3_m)

¹H-NMR (DMSO-d₆; 200 MHz; δ , ppm): second order spectra, 2.2 (m, 4H), 3.2 (d, 2H), 8.2 (m, 13H), 10.1 (s, 1H).

ESI-MS (FIA, flow: CH₃CN + HCOOH 0.1%, m/z): 1993.30; calculated: 1994.00

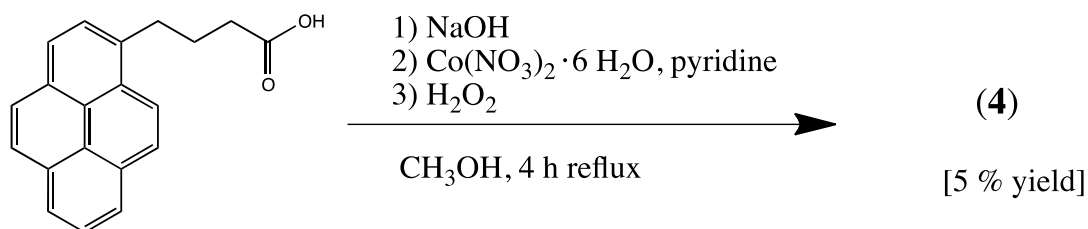
FT-IR (KBr, cm^{-1}): 584, 633, 700, 762 (diagnostic of cubane structure), 841 (s), 1418 (s), 1509 (s), 1700, 3000. (s = strong)

CV (THF, 0,1 M TBAClO₄, 0,5 mM in **3_m**); (THF: B8 10 mM = 1 : 1, 0,5 mM in **3_m**)

UV-Vis (THF, nm): 340 nm c.a. (10^{-6} M), 640 nm c.a. (10^{-3} M)

Fluorescence (10^{-6} M, THF, nm): 370, 396, 410, 750, 790.

6.1.5 Synthesis of Co₄(μ_3 -O)₄(4-(pyren-1-yl)butanoate)₄(py)₄ (4**)**



In 4 mL of NaOH 1 M, 1.44 g (5 mmoles) of pyrenbutirryc acid are dissolved to obtain the salt. Then, 727.57 mg (2.5 mmoles) of Co(NO₃)₂·6H₂O and CH₃OH (c.a. 25 mL) are added to the mixture with vigorous stirring because a foamy solution is obtained. After some stirring, 202.20 μ L (2.5 mmoles) of pyridine and slowly 1.28 mL (12.5 mmoles) of 30% H₂O₂ are introduced. Same temperature condition and stirring are maintained for 4 hours and then the mixture is brought to room temperature. CH₂Cl₂ is added to the solution in order to separate the organic phase, which is anhydrificated with Na₂SO₄ anhydrous and filtrated. When n-hexan is added, a suspension and a dark precipitate are obtained: the suspension is removed with centrifugation and from analysis

techniques turns out to be the desired product. The dark precipitate is the dirty product, which is washed with three aliquots of Et₂O, then with three of CH₃OH, checking the purity through TLC and UV lamp. The compound is washed a last time with H₂O obtaining the clear product. The yield is about 5 %.

¹H-NMR (CH₂Cl₂-d₂; 500 MHz; δ, ppm): second order spectra, 2.2(m, 2H), 2.5 (t, 2H), 3.4 (m, 2H), 7.9 (d, 2H, J = 10 Hz), c.a. 8.2 (m, 10H), 8.3 (d, 2H, J = 10 Hz) .

ESI-MS (FIA, flow: CH₃CN + HCOOH 0.1%, m/z): 1765; attended: 1765.

FT-IR (KBr, cm⁻¹): 588, 633, 691, 757 (diagnostic of cuban structure), 842 (s), 1182, 1213, 1311, 1399 (s), 1449, 1587, 1602, 2928, 3037, 3439. (s = strong).

CV (THF, 0,1 M TBAClO₄, 0,5mM in **4**); (THF : B8 10 mM = 1 : 1, 0,5 mM in **4**)

UV-Vis (CH₂Cl₂, nm): 345, 330, 277, 274, 244.

Fluorescence (10⁻⁵ M, CH₂Cl₂, nm): 703, 754, 793.

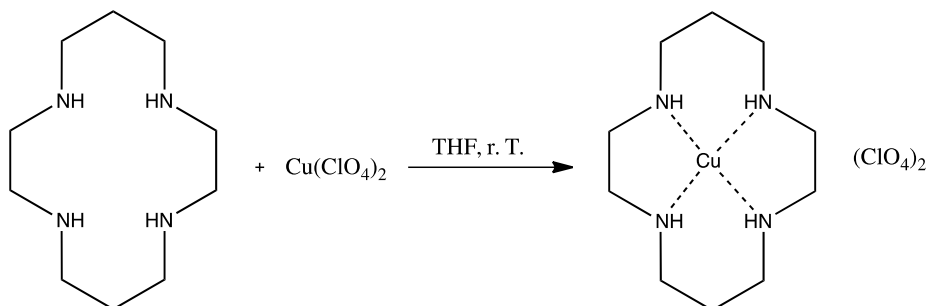
6.1.6 Synthesis of [Co₆(H₂O)₃₀{Co₉Cl₂(OH)₃(H₂O)₉(SiW₈O₃₁)₃}]⁵⁻ (Co₁₅)

Synthesis and characterization according to published procedures (a) Bassil et al. *Inorg Chem*, **2005**, *44*, 2659 and b) Keita et al. *Langmuir*, **2007**, *23*, 9531).

In a balloon, 1.00 g (0.36 mmoli) of K₈[γ-SiW₁₀O₃₆]⁸⁻ are added to a solution previously obtained dissolving 1.14 g (4.75 mmoli) of CoCl₂·6H₂O in 20 mL of NaCl 1 M. After completely reagents dissolution the mixture pH is adjusted to the value of 5 with NaOH 0.2 M and checked. The obtained solution is heated to 50°C for 30 minutes and after cooling to room temperature is filtrated with paper. By slowly evaporation of the clear red solution, the crystals of the product are obtained, then filtrated on gooch and washed with cool H₂O. About 350 mg of the product are obtained, with a total yield of about 10 %.

FT-IR (KBr, cm⁻¹): 1635, 991 (m), 938 (s), 891 (s), 853 (s), 804(m), 756 (s), 696 (s), 557 (w), 536 (w), 496 (w). (w = weak, m = medium, s = strong).

6.1.7 Synthesis of [Cu(1,4,8,11-Tetraazacyclotetradecane)](ClO₄)₂ (Cu-Cyclam)



Synthesis of Cucyclam was performed by a slight modification of literature procedure (Bosnich et al. *Inorg Chem*, **1965**, 4(8), 1102).

In a 100 mL becker, 200 mg (0.539 mmols) of $\text{Cu}(\text{ClO}_4)_2 \cdot 6 \text{H}_2\text{O}$ were dissolved in 30 mL of THF. Adding 108.12 mg (0.539 mmols) of 1,4,8,11-tetraazacyclotetradecane (Cyclam) the blue solution turns to pink. After two hours of stirring, the mixture is filtered and the solvent is evaporated. The pink compound is weighed and characterized (70 % yield).

ESI-MS (FIA, flow: $\text{CH}_3\text{CN} + \text{HCOOH}$ 0.1%, m/z): 362 [$\{\text{Cu}(\text{C}_{10}\text{H}_{24}\text{N}_4)\}\text{ClO}_4$]⁺.

FT-IR (KBr, cm^{-1}): 3240 (s), 3170 (m), 2930 (w), 2880 (w), 1430 (w), 1090 (vs), 998 (m), 883 (w), 625 (m). (vs = very strong, s = strong, m = medium, w = weak).

UV-Vis (NaOH at pH 12): $\lambda_{\text{max}} = 506 \text{ nm}$ ($\epsilon_{\text{max}} = 116.53 \text{ L mol}^{-1}\text{cm}^{-1}$).

6.2 Instrumentation

Electrochemistry:

In Chapter 2 the cyclic voltammeteries were represented with the old **convention** (negative values for anodic currents and increasing potential towards left) in order to compare easily our data with results from literature. While in Chapter 4 and 5 the new convention was applied (positive values for anodic currents and increasing potential towards right).

Padova: Cyclic voltammetry experiments were performed using a Cyclic voltammetry experiments were performed using a BAS EC-epsilon potentiostat

and an AMEL Potentiostat-Galvanostat, model 7050. A standard three-electrode electrochemical cell was used. Glassy carbon electrode (3 mm diameter, geometric surface area = 7 mm²) from BAS and a Pt wire were used respectively as working and auxiliary electrode. Potentials were referred to an Ag/AgCl/3 M NaCl reference electrode.

Electrolysis experiments were performed using an AMEL Potentiostat-Galvanostat, model 7050. A carbon crucible and a Pt wire were used respectively as working and auxiliary electrode. The auxiliary was separated from the solution with a frit. Potentials were measured to a Ag/AgCl/3 M NaCl reference electrode and then converted to the NHE scale values ($E_{\text{NHE}} = E_{\text{Ag/AgCl}} + 0.197 \text{ V}$).

Paris: Cyclic voltammetry experiments were performed using a Metrohm AUTOLAB instrument. A standard three-electrode electrochemical cell was used. Glassy carbon electrodes (3 mm diameter, geometric surface area = 7 mm²) from Tokai and a Pt wire were used respectively as working and auxiliary electrodes. Potentials were measured to an Ag/AgCl/3 M NaCl or a SCE KCl saturated reference electrode and then converted to the NHE scale values ($E_{\text{NHE}} = E_{\text{Ag/AgCl}} + 0.197 \text{ V}$; $E_{\text{NHE}} = E_{\text{SCE}} + 0.242 \text{ V}$).

Electrolysis experiments were performed using a Parstat 2273 potentiostat/galvanostat/FRA. A carbon crucible and a Pt grill were used respectively as working and auxiliary electrode. The auxiliary was separated from the solution with a frit. Potentials were measured to a SCE KCl saturated reference electrode and then converted to the NHE scale values ($E_{\text{NHE}} = E_{\text{SCE}} + 0.242 \text{ V}$).

Ring disk cyclic voltammetry experiments were performed with Pine Research Instrumentation model AFMSRCE: a MSR rotator used with a Glassy Carbon-Platinum rotated ring-disk (RRDE), a separate arbor and a rotating electrode speed controller. Pt wire was used as auxiliary electrode and a SCE KCl saturated as reference electrode.

UV-Vis: UV-Vis kinetic experiments were collected using a Varian Cary-100 Scan spectrophotometer.

¹H-NMR: ¹H-NMR spectra and kinetic experiments were recorded using Bruker AV300 instruments operating at 300 and 500 MHz.

FT-IR: FT-IR spectra were recorded on a Nicolet 5700 FT-IR instrument.

ESI-MS: Mass spectra were performed with an Agilent Technologies MSD SL Trap mass spectrometer with ESI source coupled with a 1100 Series HPLC system.

Light-driven water oxidation: In a typical experiment, about 15 mL of a buffered solution containing [Ru(bpy)₃]Cl₂·6H₂O (1 mM), Na₂S₂O₈ (5 mM) and the catalyst in several concentrations were introduced in a glass reactor (internal diameter 18 mm, total internal volume of 24 mL), deoxygenated with nitrogen and allowed to equilibrate at 25 °C under exclusion of light. Irradiation of the solution was then conducted in some cases with... and in other cases with one monochromatic LED emitting at 450 nm (LED450-06 from Roithner Lasertechnik GmbH); oxygen evolution was monitored with a FOXY-R-AF probe, inserted in the reaction headspace and interfaced with a Neofox Real-Time software for data collection; dissolved oxygen was assumed to be negligible. Quantum Yield for oxygen production (Φ_{O_2}) was determined by the following equation:

$$\Phi_{O_2} = \frac{\text{rate of } O_2 \text{ production (mol}\cdot\text{s}^{-1}\text{)}}{\text{absorbed photons per unit of time (einstein}\cdot\text{s}^{-1}\text{)}}$$

The rate of oxygen production was taken from the maximum slope of the kinetic O₂ evolution curves, between 10 and 20 minutes of irradiation. The number of absorbed photons was assumed to be equivalent to the number of incident photons, given the high Optical Density of the solution and the negligible loss of photons by reflection events.

7. CHAPTER

Conclusions and Perspectives: an overview

This thesis was focused on the development of new **catalytic, molecular systems** for the redox reactions in artificial photosynthesis, aimed at the production of renewable fuels with sunlight, by the water splitting into hydrogen and oxygen, or CO₂ reduction.

This work has mainly focused on the **water oxidation** reaction, since it was recognized as the major problem, or the bottleneck, in the development of a device for efficient water splitting. Actually, the literature scenario has changed a lot in the last few years. In 2008, T.J. Meyer was reporting that “*catalysts for water oxidation are so rare that the discovery of a new family is cause for celebration*”.⁽¹⁾ Since then, a lot of reports have been published, dealing with new molecular WOCs: X. Sala, A. Llobet et al. have recently reported that “*dWord did not find any entries for your table of contents.uring the last 5 years, there has been an explosion of reports in the field of water oxidation catalyzed by transition metals*”.⁽²⁾ Considerable results have been achieved, concerning stability and efficiency of WOCs. Unfortunately, this advancement is still not solving the problem: we believe that two fields in particular need a major in-depth analysis:

- 1) The understanding of the active species carrying on the catalysis, and their operating mechanism. Quoting X. Sala and A. Llobet: “*Despite its importance for biology and renewable energy, the **mechanism** of this reaction is not fully understood*”.⁽²⁾
- 2) The **interface of WOCs with light** systems, which is one of the target in a water splitting artificial device. Little is known about the light driven events that activate a WOC in the so called sacrificial systems. Moreover, despite their high activity, still few reports deal with the interface of molecular WOCs within a photoelectrode, with one key example reported by Sun et al.⁽³⁾

In this work, we have tried to consider also these open issues.

In **Chapter 2**, a **tetracobalt cubane** has been considered as a molecular WOC, mimicking the natural OEC structure and operating in a light activated system with $\text{Ru}(\text{bpy})_3^{2+}/\text{S}_2\text{O}_8^{2-}$. After characterization of the species through different techniques, tuning electronic substituents properties, we have investigated structure-activity correlations by means cyclic voltammetry and laser flash photolysis. The interesting results brought us to consider a synthetic approach in order to modify the catalyst structure and maximizing interactions in solution. The design of a no covalent dyad among moieties could be exploit to project devices for artificial photosynthesis. The real nature of the acting species in the catalytic process was recently discussed in the literature, and is still under investigation. Further insights in the role played by the tetracobalt cubane will likely contribute to better clarify the catalytic mechanism of water oxidation.

In **Chapter 3**, the potential of **high nuclearity, Cobalt based polyoxometalates** in water oxidation has been explored. In particular, one species has showed really interesting results in photoactivated system with high kinetic constant and multiple electron transfer to a photogenerated oxidant. From our studies, the multi-nuclearity, the polyanionic charge and the presence of water ligand on the Cobalt centres have appeared to be key features for the catalytic activity of these compounds.

In **Chapter 4**, a **single site Copper** species, with a tetraazamacrocyclic ligand is reported as a water oxidation catalyst. Single site catalysts often bare performances overcoming the multinuclear correspondings. They are appealing since structurally simpler, tuning their properties let to easier screening of activity, moreover they show possible linkage to several devices. The importance of single site catalysts has been recently recognized also by Hetterscheid et al. *“Mononuclear species may be the way to go in direct solar energy to fuel conversion applications”*.⁽⁴⁾

Indeed, we have studied a Copper based macrocyclic ligand as molecular WOC through electrochemical and photoelectrochemical systems. In particular we have found a low operating overpotential and interesting results interfacing for the first time a Cu-species with light. The catalyst activity has been explored in presence of hematite semiconductor as photoanode: in presence of light the Copper compound enhances the hematite at low potentials acting as a holes-capture for the semiconductor. The limit of this system consists in the evolution of the species into inactive products. Future perspectives will be focused on a deeper investigation of the system degradation and on the effect of the cyclam ligand functionalization among performance and stability.

Dealing with **CO₂ reduction**, the present scenario in literature includes few families of efficient catalysts, and the results are often complicated by issues of selectivity in the reduction products and by competitive proton reduction to hydrogen.

In **Chapter 5**, we have investigated the potential of polyoxometalates, the “molecular metal oxides”, in catalysing this reaction. In particular, we focused on **Copper based polyoxometalates**, being inspired by a recent work in the literature on a Copper(I) oxide as an efficient catalyst for CO₂ reduction. After a preliminary screening one compound has been selected and investigate through CO₂ reduction catalysis by means electrochemical techniques. However, a deeper electrochemical characterization revealed consumption of the species and metallic copper deposition onto the working electrode surface.

Finally, as already anticipate in the Introduction, our purpose is not to give a unique solution to the energy issue: we would like to suggest a method to achieve a better understanding through mechanistic insights and optimized experimental conditions. Indeed, with the right instruments we can think how to face the scientific fascinating challenge concerning energy issue.



¹ T. J. Meyer *Nature*, **2008**, *451*, 778

² X. Sala, S. Maji, R. Bofill, J. García-Antón, L. Escriche, A. Llobet *Acc Chem Res*, **2014**, *47*, 504

³ Y. Gao, X. Ding, J. Liu, L. Wang, Z. Lu, L. Li, L. Sun *J Am Chem Soc*, **2013**, *135*, 4219

⁴ D. G. H. Hetterscheid, J. N. H. Reek *Angew Chem Int Ed*, **2012**, *51*, 9740